Ruthenium-Rhenium and Ruthenium-Palladium Supramolecular Photocatalysts for Photoelectrocatalytic CO_2 and H^+ Reduction

Supporting Information

Joshua K. G. Karlsson[a], Florian J.R. Cerpentier[b], Ralte Lalrempuia[c], Owen Woodford,[a] Martin V. Appleby[d], James D. Shipp,[d] Dimitri Chekulaev,[d] Julia A. Weinstein[d], Mary T. Pryce[b*] and Elizabeth A. Gibson[a*]

[a]Energy Materials Laboratory, Chemistry, School of Natural and Environmental Sciences, Newcastle University, Newcastle upon Tyne, United Kingdom.
[b]School of Chemical Sciences, Dublin City University, Dublin, Ireland.
[c]Department of Chemistry, School of Physical Sciences, Mizoram University, Aizawl, India.
[d]Department of Chemistry, University of Sheffield, Sheffield, UK.

Contents:

S1 Experimental Section

Synthesis of Molecular Photocatalysts

3,5-di(pyridin-2-yl)-4H-1,2,4-triazole (Hbpt),[1] diethyl(2,2′-bipyridine)-4,4′-dicarboxylate (dceb),[2] $Ru(DMSO)_4Cl_2$[3] and $Ru(bpy)(DMSO)_2Cl_2$[4] were synthesized using reported procedures. All chemicals and solvents were purchased from Sigma Aldrich or Fluorochem and used without further purification.

$Ru(DMSO)_4Cl_2$[3]

2 g (7.65 mmol) of $RuCl_3.3H_2O$ was added to a 100 mL flask. 50 mL of ethanol was added and the solution was refluxed for 3 hours during which the brown solution turned a dark green colour. The solution was filtered to remove any unreacted ruthenium material and the ethanol was removed under reduced pressure. The green residue was dissolved in 8 mL of dimethylsulfoxide (DMSO) and stirred at 150 °C for 2 hours. The solution turned bright orange and yellow precipitate slowly appeared. The solution was cooled to room temperature and 60 mL acetone was added to complete precipitation of product. The yellow crystalline material was collected by filtration, washed with acetone and dried under air to yield $Ru(DMSO)_4Cl_2$ as a yellow crystalline material (3.21 g, 6.63 mmol, 86%). ^{1}H-NMR (600 MHz, D_2O): 2.74 (s, 6H), 3.40 (s, 6H), 3.49 (s, 6H), 3.51 (s, 6H).

$Ru(bpy)(DMSO)_2Cl_2$[4]

2 g (4 mmol) of $Ru(DMSO)_4Cl_2$ and 0.64 g(4 mmol) of 2,2'-bipyridine were added to a 100 mL flask. 36 mL of ethanol and 4 mL of DMSO were added and the solution was refluxed for 1 hour, after which the starting suspension had fully converted to a homogeneous orange solution. Further refluxing for at least 30 minutes resulted in the precipitation of an orange powder. The powder was collected by vacuum filtration, washed with 20 mL of ethanol and dried under air to yield $Ru(bpy)(DMSO)_2Cl_2$ as an orange powder (1.50 g, 3.08 mmol, 77%). ^{1}H-NMR (600 MHz, DMSO-d6): 2.28 (s, 3H), 2.99 (s, 3H), 3.36 (s, 3H), 3.40 (s, 3H), 7.62 (td, 1H), 7.78 (td, 1H), 8.11 (td, 1H), 8.23 (td, 1H), 8.61 (d, 1H), 8.66 (d, 1H), 9.56 (dd, 1H), 9.66 (dd, 1H).

$[Ru(dceb)(bpy)(bpt)](PF_6)$

0.2 g (0.41 mmol) of $Ru(bpy)(DMSO)_2Cl_2$ and 0.124 g (0.41 mmol) of diethyl(2,2′-bipyridine)-4,4′-dicarboxylate (dceb) were added to a 25 mL flask. 5 mL of ethanol and 5 mL of water were added and the solution was refluxed for 2 hours during which the solution changed from yellow to dark red. 0.092 g (0.41 mmol) of 3,5-di(pyridin-2-yl)-4H-1,2,4-triazole (Hbpt) was added to the solution and the solution was refluxed for a further 24 hours. The solution was allowed to cool to room temperature and the ethanol was removed under reduced pressure. An additional 10 mL of water was added

after which 0.301 g (1.64 mmol) of potassium hexafluorophosphate was added. The red precipitate was collected by vacuum filtration, washed with 10 mL of water and dried. The crude product was purified by column chromatography using SiO_2 as stationary phase. Unreacted starting material was removed using acetonitrile as mobile phase. The mobile phase was changed to 10:1:0.1 acetonitrile/water/10% KNO_3 (aq.) after which the product eluted as a red band. The acetonitrile was removed under reduced pressure and a small amount of potassium hexafluorophosphate was added to complete the precipitation of a dark red powder. The powder was collected by vacuum filtration, washed with 10 mL of water and dried under air to yield [Ru(dceb)(bpy)(bpt)](PF_6) as a dark red powder (0.143 g, 0.13 mmol, 33%). ^{1}H-NMR (600 Mhz, DMSO-d6): 1.33-1.39 (m, 6H), 4.40-4.48 (m, 4H), 7.44 (td, 1H), 7.52 (td, 1H), 7.55-7.63 (m, 2H), 7.76-7.81 (m, 1H), 7.85-7.98 (m, 2H), 8.04-8.21 (m, 6H), 8.32 (t, 1H), 8.60 (m, 1H), 8.77-8.83 (dd, 1H), 8.84 (dd, 1H).

Mass spectrometry (ESI mode): $[Ru(dceb)(bpy)(bpt)]^{1+}$ calculated *m/z* = 780.162, found = 780.163. $[Ru(dceb)(bpy)(Hbpt)]^{2+}$ calculated *m/z* = 390.585, found 390.585.

[Ru(dcb)(bpy)(Hbpt)](PF_6)$_2$ (PC3)

0.27 g (0.25 mmol) of [Ru(dceb)(bpy)(bpt)](PF_6) and 0.06 g (2.5 mmol, 10 eq.) of anhydrous lithium hydroxide were added to a 25 mL flask. The flask was cooled to 0 °C and 6 mL of THF and 1.5 mL of water were added. The solution was stirred overnight while being allowed to heat up to room temperature slowly. The THF was removed under reduced pressure and the solution was acidified to pH 3 using 0.1 M HCl solution. 0.184 g (1 mmol, 4 eq.) of potassium hexafluorophosphate was added resulting in the precipitation of the product as a red powder. The precipitate was collected by vacuum filtration, washed with 20 mL of water and dried under air to yield [Ru(dcb)(bpy)(Hbpt)](PF_6)$_2$ as a dark red powder (0.214 g, 0.21 mmol, 84%). ^{1}H-NMR (600 MHz, DMSO-d6): 7.38 (m, 1H), 7.44 (m, 1H), 7.49 (m, 1H), 7.65 (m, 1H), 7.75 (m, 1H), 7.78-7.97 (m, 4H), 8.00-8.20 (m, 5H), 8.41-8.58 (m, 5H), 8.66 (t, 1H), 8.93-9.08 (m, 2H).

Mass spectrometry (ESI mode): $[Ru(dcb)(bpy)(Hbpt)]^{2+}$ calculated m/z = 362.555, found = 362.554. $[Ru(dcb)(bpy)(bpt)]^{+}$ calculated m/z = 724.100, found = 724.100.

[Ru(dceb)(bpy)(bpt)Re(CO)$_3$Cl](PF)$_6$

0.1 g (0.115 mmol) of **[Ru(dceb)(bpy)(bpt)](PF_6)**, 0.032 g (0.130 mmol, 1.2 eq.) of $Re(CO)_5Cl$ and 3 mL of methanol were added to a 10 mL flask. The resulting red solution was refluxed overnight resulting in precipitation of the product. The precipitate was collected by vacuum filtration, washed with cold ethanol and ether and airdried to yield **[Ru(dceb)(bpy)(bpt)Re(CO)$_3$Cl](PF)$_6$** as a dark red solid (0.71 g, 0.058 mmol, 50%). ^{1}H-NMR (600 MHz, DMSO-d6): 1.31-1.38 (m, 6H), 4.39-4.69 (m, 4H), 7.40-7.45 (m, 2H), 7.50-7.54 (m, 1H), 7.57-7.73 (m, 3H), 7.79-7.88 (m, 3H), 7.93-7.97 (m, 1H), 8.01 (t, 1H), 8.06-8.22 (m, 5H), 8.27-8.35 (m, 1H), 8.55-8.62 (dd, 1H), 8.78-8.86 (m, 2H), 8.95-8.99 (m, 1H), 9.20-9.26 (m, 2H).

Mass spectrometry (ESI mode): [Ru(dceb)(bpy)(bpt)Re(CO)$_3$Cl-H]$^{-1}$ calculated *m/z* 1230.027 found 1230.1179

[Ru(dcb)(bpy)(bpt)Re(CO)$_3$Cl](PF$_6$) (PC1)

0.05 g (0.041 mmol) of **[Ru(dceb)(bpy)(bpt)Re(CO)$_3$Cl](PF)$_6$** and 0.01 g of LiOH (0.39 mmol, 10 eq.) were dissolved in 5 mL of a 4:1 THF:water mixture. The mixture was stirred on ice and slowly allowed to heat to room temperature overnight while stirring. The THF was removed under reduced pressure and the solution was acidified to pH 3 with 0.1 M HCl solution. The complex was precipitated from the aqueous solution by addition of 0.025 g (0.16 mmol, 4 eq.) NH_4PF_6. The precipitate was collected by vacuum filtration, washed with water and diethyl ether and dried under air to yield **[Ru(dcb)(bpy)(bpt)Re(CO)$_3$Cl](PF$_6$)** as a red solid (0.039 g, 0.034 mmol, 82%). ^{1}H-NMR (600 MHz, DMSO-d6): 7.36-7.64 (m, 5H), 7.75-7.95 (m, 4H), 8.00-8.21 (m, 7H), 8.32-8.35 (1H), 8.59-8.65 (m, 1H), 8.76-8.82 (dd, 1H), 8.82-8.87 (m, 1H), 9.18-9.26 (dd, 2H) 14.2 (br, 1H, COOH). FTIR ($CHCl_2$) 2021, 1912, 1895, 1716 cm^{-1}.

Mass spectrometry (ESI mode): [Ru(dcb)(bpy)(bpt)Re(CO)$_3$Cl]$^{1+}$ calculated *m/z* = 1030.0083, found = 1030.0142. [Ru(dcb-2H$^+$)(bpy)(bpt)Re(CO)3Cl] + 2 Na$^+$] calculated m/z = 1218.938, found = 1218.0245

[Ru(dceb)(bpy)(bpt)PdCl$_2$](PF$_6$)

0.1 g (0.115 mmol) of **[Ru(dceb)(bpy)(bpt)](PF$_6$)**, 0.046 g (0.138 mmol, 1.2 eq.) of Pd(DMSO)$_2$Cl$_2$ and 5 mL of methanol were added to a 10 mL flask. The resulting red solution was refluxed overnight resulting in a precipitate to form. The precipitate was collected via filtration, washed with cold ethanol and diethyl ether and air dried yielding **[Ru(dceb)(bpy)(bpt)PdCl$_2$)](PF$_6$)** as a red solid (0.088 g, 0.068 mmol, 59%). ^{1}H-NMR (600 MHz, DMSO-d6): 1.37-1.43 (m, 6H), 4.41-4.47 (m, 4H), 7.22-7.41 (m, 2H), 7.43-7.49 (m, 2H), 7.53-7.73 (m, 3H), 7.76-7.87 (m, 3H), 7.91-8.10 (m, 6H), 8.44-8.52 (m, 2H), 8.95-9.07 (m, 3H)9.9 (t, 1H).

Mass spectrometry (ESI mode): [Ru(dceb)(bpy)(bpt)PdCl$_2$]$^{1+}$ calculated *m/z* = 956.003, found = 956.008.

[Ru(dcb)(bpy)(bpt)PdCl$_2$](PF$_6$) (PC2)

0.05 g (0.039 mmol) of **[Ru(dceb)(bpy)(bpt)PdCl(dmso)](PF)$_6$** and 0.01 g of LiOH (0.39 mmol, 10 eq.) were dissolved in 5 mL of a 4:1 THF:water mixture. The mixture was stirred on ice and slowly allowed to heat to room temperature overnight while stirring. The THF was removed under reduced pressure and the solution was acidified to pH 3 with 0.1 M HCl solution. The complex was precipitated from the aqueous solution by addition of 0.025 g (0.16 mmol, 4 eq.) NH_4PF_6. The precipitate was collected by vacuum filtration, washed with water and diethyl ether and dried under air to yield **[Ru(dcb)(bpy)(bpt)PdCl$_2$](PF$_6$)** as a red solid (0.037 g, 0.030 mmol, 77%). ^{1}H-NMR (600

MHz, DMSO-d6): 1.37-1.43 (m, 6H), 4.41-4.47 (m, 4H), 7.22-7.41 (m, 2H), 7.43-7.49 (m, 2H), 7.53-7.73 (m, 3H), 7.76-7.87 (m, 3H), 7.91-8.10 (m, 6H), 8.44-8.52 (m, 2H), 8.95-9.07 (m, 3H)9.9 (t, 1H). FTIR (CH_2Cl_2) 1697 cm^{-1}.

Mass spectrometry (ESI mode): $[Ru(dcb)(bpy)(bpt)PdCl_2]^{1+}$ calculated *m/z* = 899.941 found 899.946

Analytical Methods

UV-visible absorption measurements were obtained on either an Ocean Optics USB 2000+ or Hitachi U3310 spectrophotometer. Steady-state fluorescence spectra were interrogated with a Hitachi F4500 instrument. Spectrophotometric grade solvents were used for all measurements and fluorescence spectra were obtained using optically thin samples. Cyclic voltammetry (CV) for PC1-3 was performed in acetonitrile with 0.1 M tetrabutylammonium hexafluorophosphate as the supporting electrolyte, glassy carbon working electrode, platinum wire counter electrode and $Ag/AgNO_3$ reference electrode and calibrated against ferrocene (Fc). Gas chromatography measurements were performed with a Shimadzu GC-2014 instrument where a thermal conductivity detector at 200 ^oC (TCD) and flame-ionisation detector (FID) at 250 ^oC operated in tandem. A Restek ShinCarbon ST 80/100 packed column (2 metre, 2 mm ID) was used where argon was the carrier gas. The oven temperature was 50 ^oC with a temperature ramp to 200 ^oC (after an initial period of 2 mins at 50 ^oC) at a rate of 15 ^oC min^{-1}, followed by a final hold time of 10 mins.

XPS data was acquired using a Kratos Axis SUPRA using monochromated Al kα (1486.69 eV) X-rays at 15 mA emission and 12 kV HT (180W) and a spot size/analysis area of 700 x 300 μm. The instrument was calibrated to gold metal Au 4f (83.95 eV) and dispersion adjusted give a binding energy (BE) of 932.6 eV for the Cu 2p3/2 line of metallic copper. Ag $3d_{5/2}$ line FWHM at 10 eV pass energy was 0.544 eV. Source resolution for monochromatic Al Kα X-rays is ~0.3 eV. The instrumental resolution was determined to be 0.29 eV at 10 eV pass energy using the Fermi edge of the valence band for metallic silver. Resolution with charge compensation system on <1.33 eV FWHM on PTFE. High resolution spectra were obtained using a pass energy of 20 eV, step size of 0.1 eV and sweep time of 60 s, resulting in a line width of 0.696 eV for Au $4f_{7/2}$. Survey spectra were obtained using a pass energy of 160 eV. Charge neutralisation was achieved using an electron flood gun with filament current = 0.38 A, charge balance = 2 V, filament bias = 4.2 V. Successful neutralisation was adjudged by analysing the C 1s region wherein a sharp peak with no lower BE structure was obtained. Spectra have been charge corrected to the main line of the carbon 1s spectrum (adventitious carbon) set to 284.8 eV. All data was recorded at a base pressure of below 9 x 10^{-9} Torr and a room temperature of 294 K. Data was analysed using CasaXPS v2.3.19PR1.0. Peaks were fit with a Shirley background prior to component analysis. Spectra are calibrated energy of all regions to the position of Au4f core level. Samples were examined at three random spot before and after photocatalysis.

Photoelectrochemical Cell

The design of the cell used for photoelectrocatalysis are outlined in Figure S1. In the static cell, a three-electrode setup was integrated into a gas-tight glass assembly, where gaseous products can be sampled by headspace injection via a septum. The working electrode was a 2 × 2 cm TEC15 (NSG) conductive glass slide with a 0.79 cm^2 area covered in mesoporous NiO, soaked in a dye bath solution (approx. 3 mM dye in dry acetonitrile) with the appropriate photocatalyst for 12 hours prior to the experiment. The counter-electrode was platinum wire and the reference was Ag/AgCl (3M KCl). The assembled cell was filled with a fixed amount of the desired electrolyte and bubbled with research grade CO_2 (BOC) for at least 15 minutes before commencing a photoelectrocatalysis experiment. A PalmSens EmStat3 Blue potentiostat was used to apply bias and record the current throughout the experiment. The face of the working electrode was illuminated by AM 1.5 filtered light from a Xe-arc lamp calibrated to an intensity of 1 sun (100 mW cm^{-2}). Light chopping was accomplished with an electronic shutter.

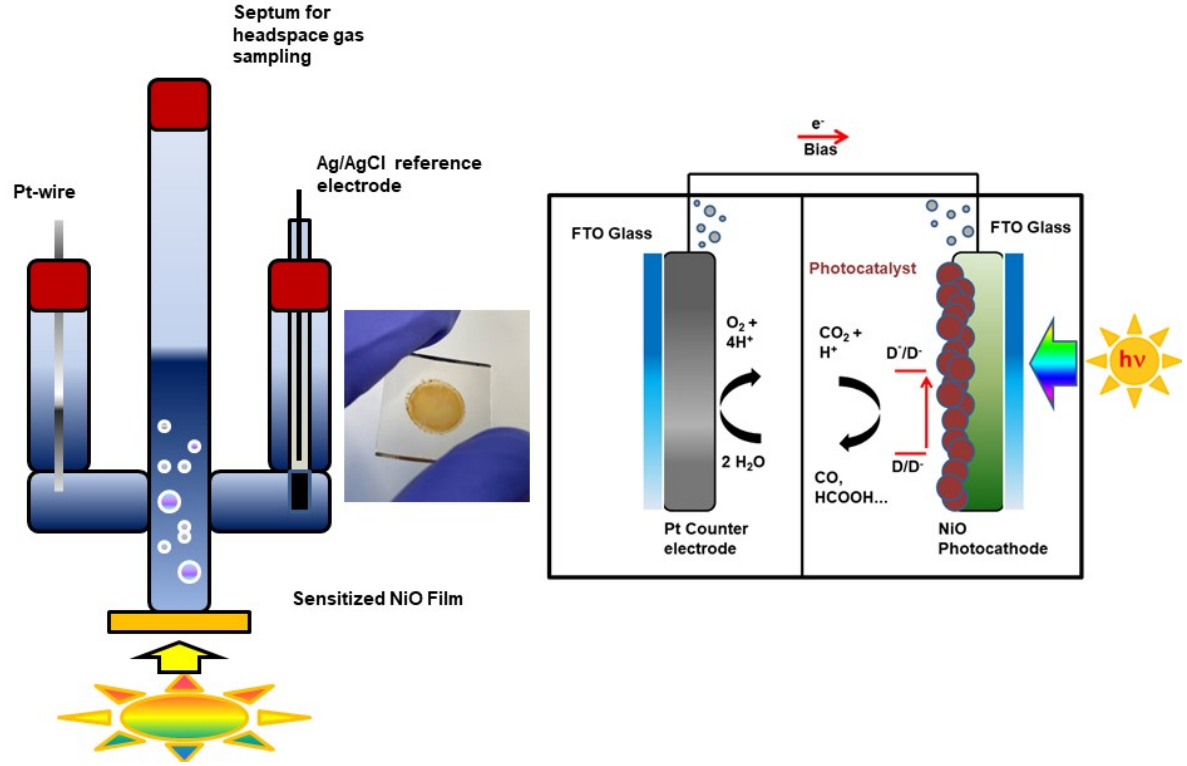

Figure S 1. Illustration of the reaction cells used for photoelectrocatalysis.

Preparation of the Photocathode

The working electrode for all systems in this study was a mesoporous NiO semiconductor thin film on conductive glass (TEC 15 FTO, Pilkington) for photoelectrochemical experiments or polished

CaF_2 windows for time-resolved infrared spectroscopy. The procedure for producing the NiO layer by doctor blading NiO sol-gel solution has been described elsewhere.[5] NiO sol-gel precursor solution was prepared by adding anhydrous $NiCl_2$ (1 g, Sigma) and tri-block co-polymer F108 (poly (ethylene glycol)-block-poly (propylene glycol)-block-poly (ethylene glycol)) (1g, Sigma) to ethanol (6 ml) and ultrapure water (5 ml). The solution was left to age in a vial for two weeks and aliquots centrifuged prior to use. The NiO films have an average thickness of 1.5 μm by doctor-blading a total of three layers (annealing each layer at 450^{O}C for 30 mins). Thickness of the thin film was determined with a Dektak^{3}ST Surface Profile Measuring System.

Transient Absorption Spectroscopy and Time-resolved Infrared Spectroscopy

UV-visible transient absorption (TA) experiments were performed using a Helios spectrometer (HE-VIS-NIR-3200, Ultrafast Systems) at the University of Sheffield, Lord Porter laser laboratory. Briefly, a Ti:Sapphire regenerative amplifier (Spitfire ACE PA-40, Spectra-Physics) provided 800 nm pulses (40 fs FWHM, 10 KHz, 1.2 mJ). The amplifier was seeded by a Ti:Sapphire oscillator (Mai Tai, Spectra-Physics), providing 800 nm pulses (25 fs FWHM, 84 MHz). 400 nm excitation pulses were obtained by frequency-doubling the 800-nm pulse. 500 nm pump pulses (80 fs FWHM, 2.5 KHz, 0.4 μJ) were generated by a TOPAS prime, Light Conversion, which was pumped by the 800 nm (40 fs, 10 KHz, 0.5 mJ) output of the spitfire ACE. The pump pulse was passed through a mechanical chopper with a frequency of 2.5 KHz, to allow for the probing of both pumped and unpumped sample. The pump pulse was depolarized prior to sample excitation. The pump pulses were focused onto the sample cell (fused silica with an internal path length of 2 mm), to a spot diameter of ≤ 0.3 mm. Solutions were stirred using a magnetic stirrer bar. Global fitting of transient absorption data was performed with the OPTIMUS software package using a sequential model to extract the species associated spectra and corresponding lifetimes.[6] This approach simultaneously analyses the multiple kinetic traces for the different wavelengths using a sum of exponentials function. We used the minimum number of components required to give a good fit (i.e. minimisation of residuals).

In all experiments the cell was rastered in the two dimensions orthogonal to the direction of beam propagation to minimize localized sample decomposition. Care was taken to ensure the absorption signals measured fell with the linear region of pump laser intensity.

S2. Characterization Data for Photocatalysts

NMR spectroscopy and mass spectrometry

[Ru(bpy)(dceb)(bpt)](PF$_6$)

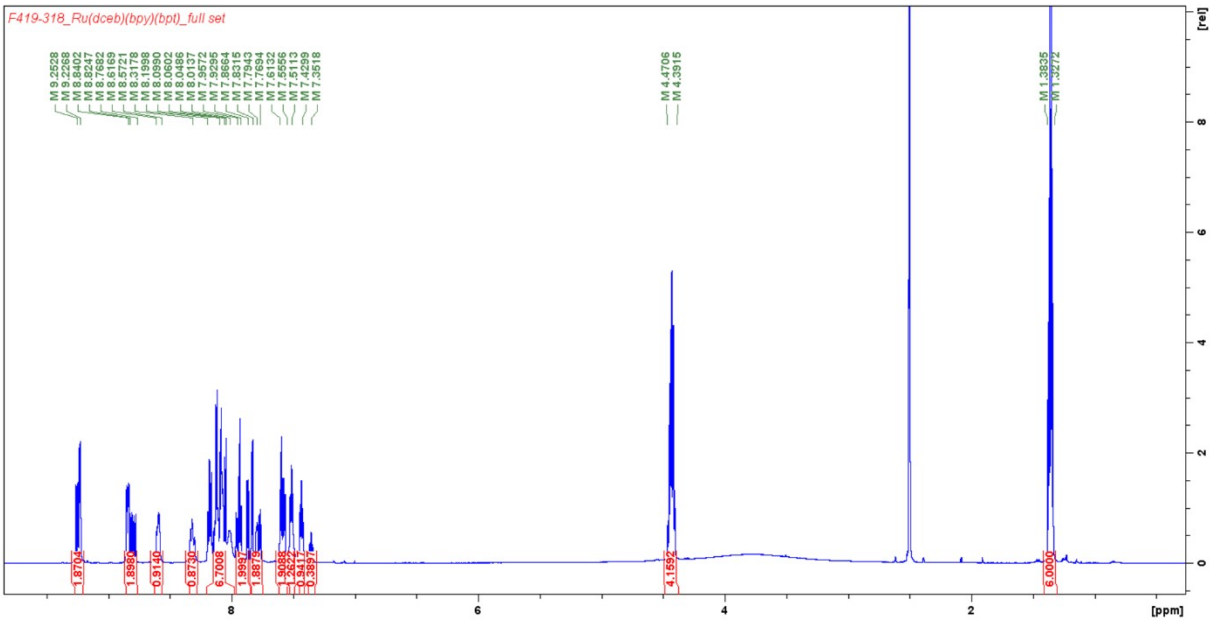

Figure S 2. ^{1}H-NMR spectrum of **[Ru(dceb)(bpy)(bpt)](PF$_6$)** in dmso-d$_6$.

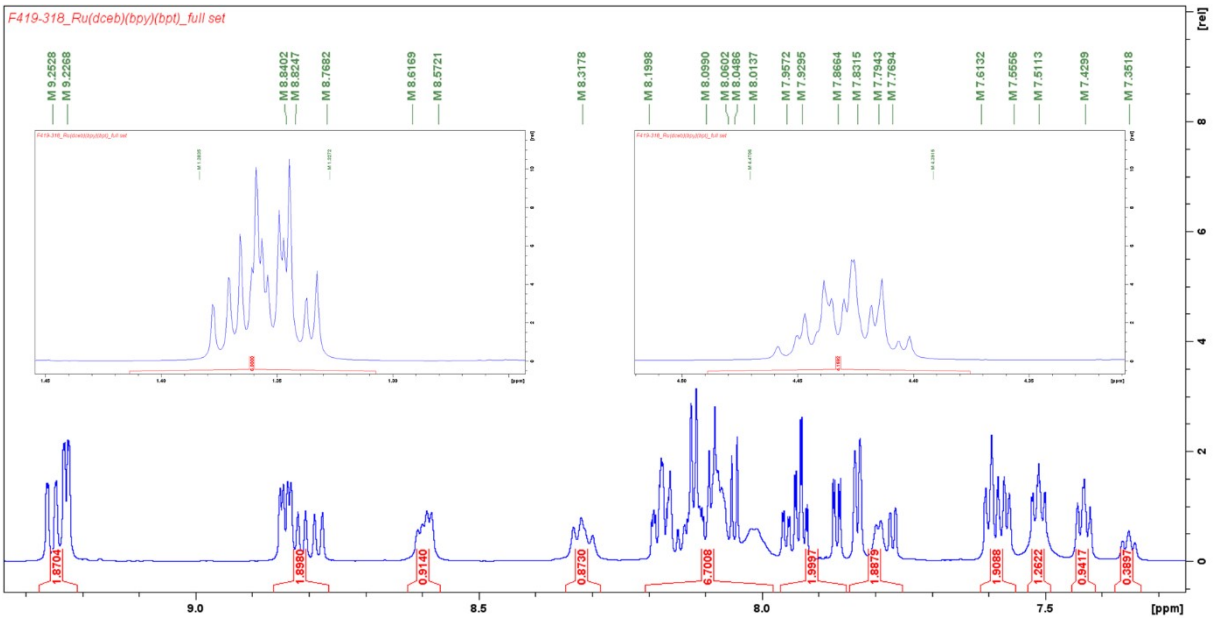

Figure S 3. ^{1}H-NMR spectrum of **[Ru(dceb)(bpy)(bpt)](PF$_6$)** in dmso-d$_6$. The signals for the ester moieties are shown in the insets.

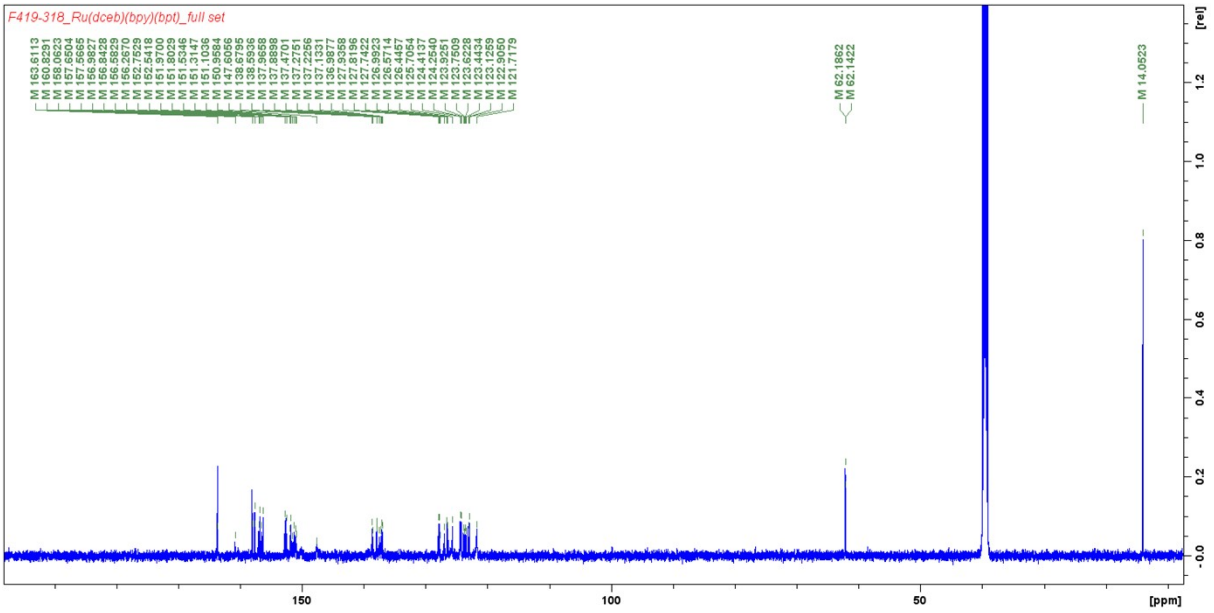

Figure S 4. ^{13}C-NMR spectrum of **[Ru(dceb)(bpy)(bpt)](PF$_6$)** in dmso-d$_6$.

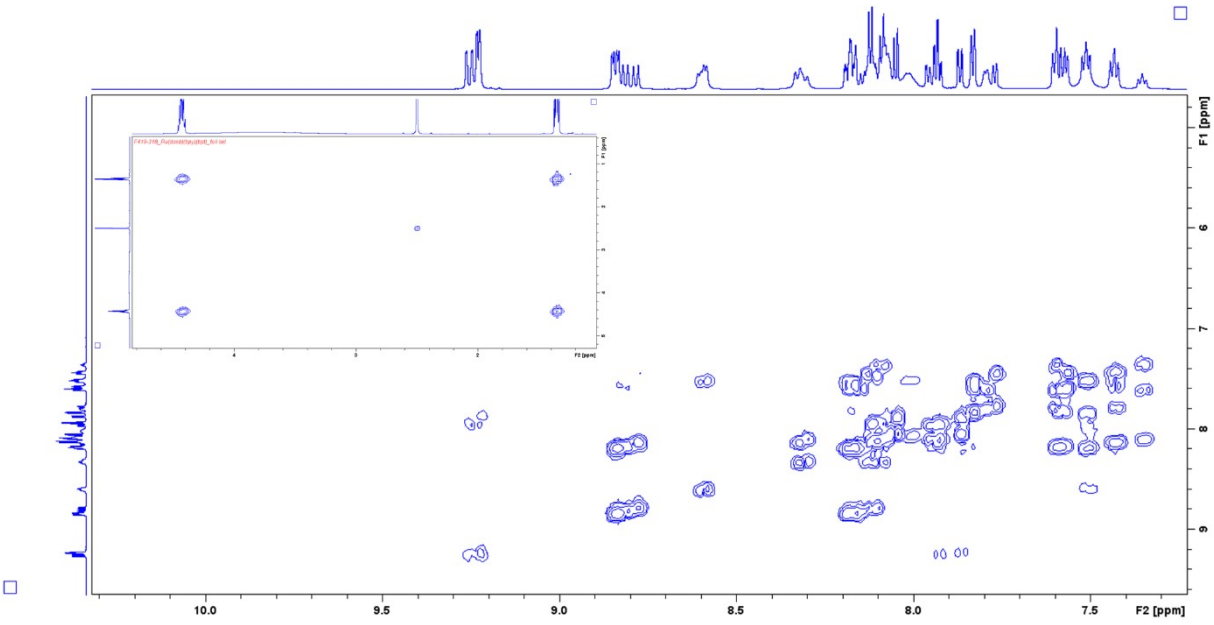

Figure S 5. COSY spectrum of **[Ru(dceb)(bpy)(bpt)](PF$_6$)** in dmso-d$_6$. The aliphatic region with the signals for the ester moiety is shown in the inset.

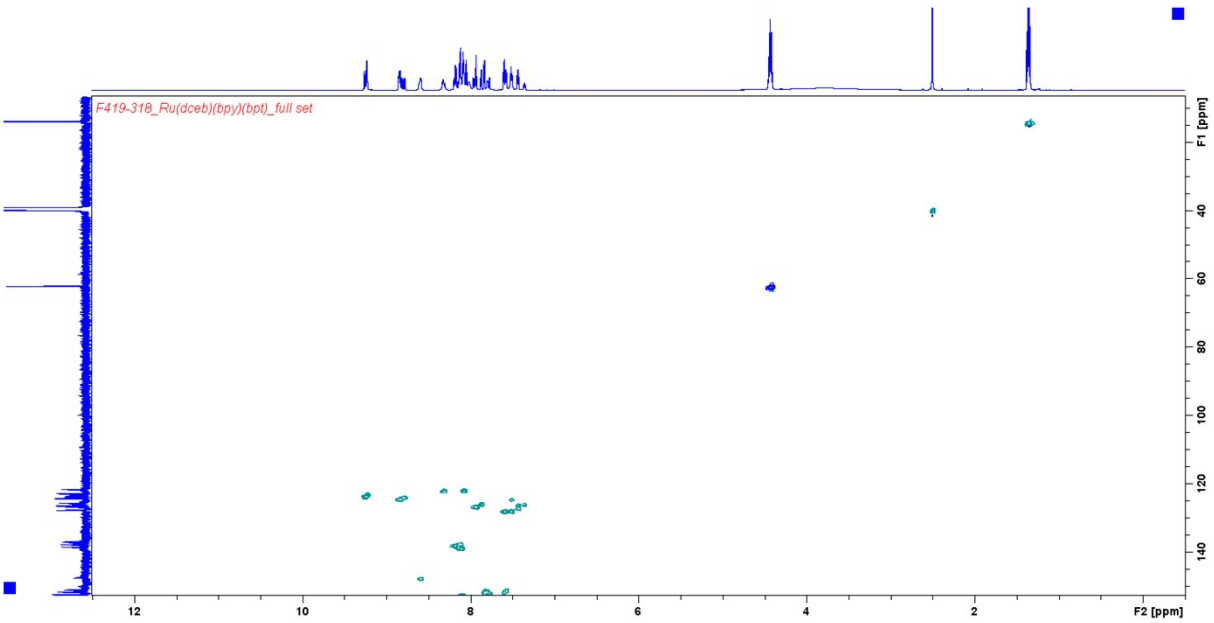

Figure S 6. HSQC spectrum of **[Ru(dceb)(bpy)(bpt)](PF$_6$)** in dmso-d$_6$.

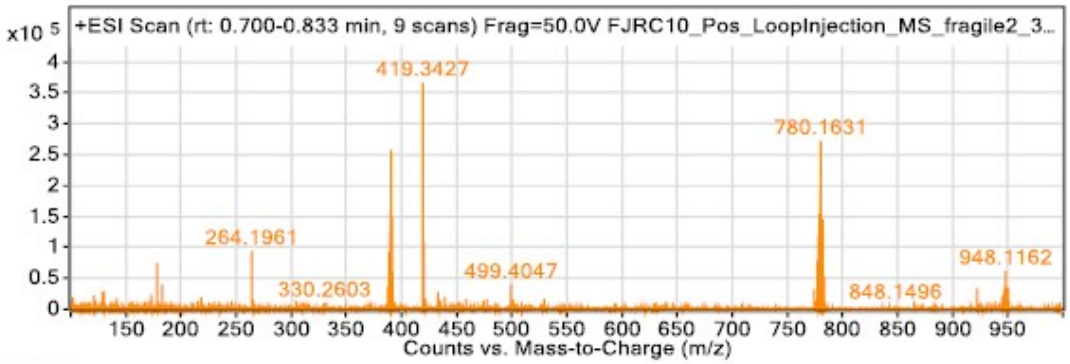

Figure S 7. Mass spectrogram for **[Ru(dceb)(bpy)(bpt)](PF$_6$).** [Ru(dceb)(bpy)(bpt)]$^{1+}$ calculated m/z = 780.162, found = 780.163. [Ru(dceb)(bpy)(Hbpt)]$^{2+}$, calculated m/z = 390.585, found 390.585

[Ru(bpy)(dcb)(Hbpt)](PF$_6$)$_2$ (PC3)

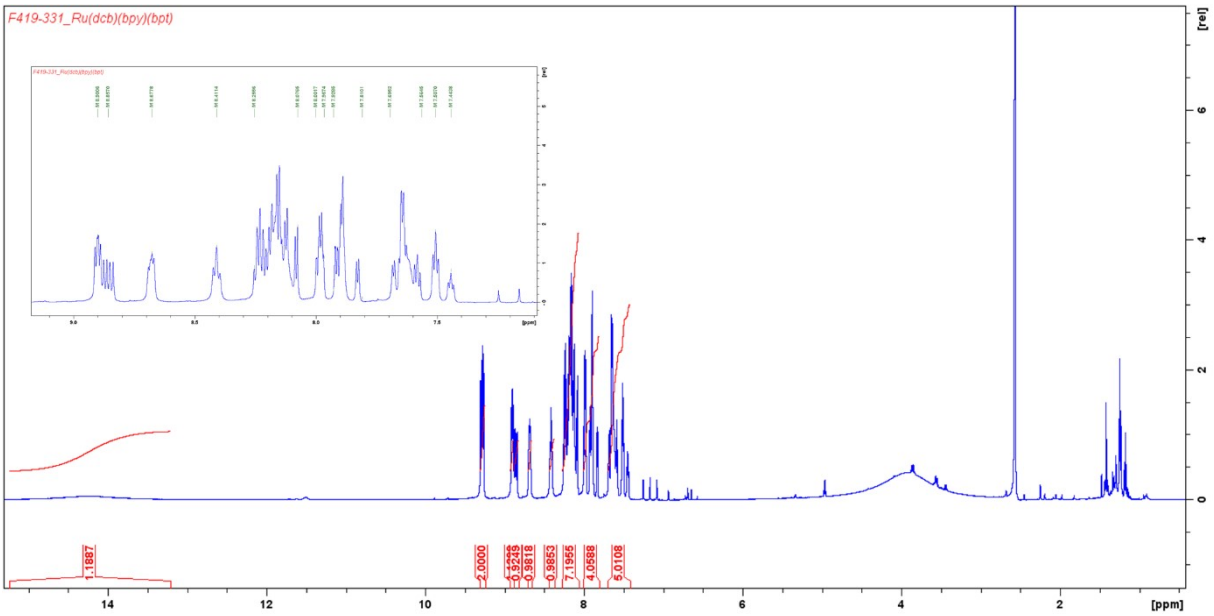

Figure S 8. ^{1}H-NMR spectrum of **[Ru(bpy)(dcb)(Hbpt)](PF$_6$)$_2$** in dmso-d$_6$. Inset the aromatic region expanded.

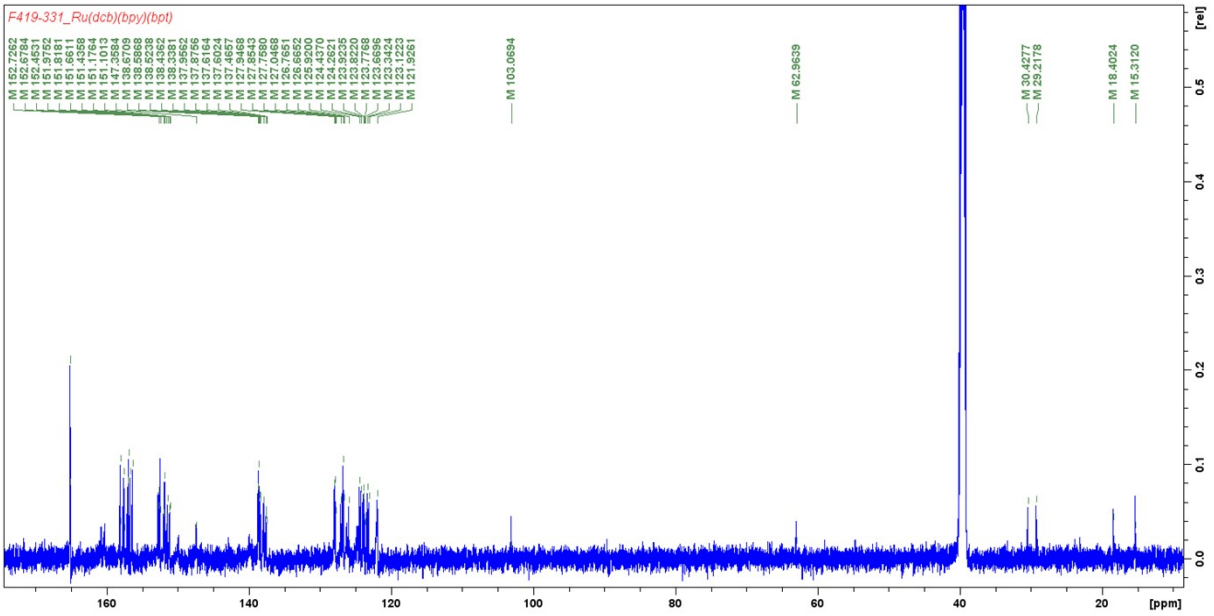

Figure S 9. ^{13}C-NMR spectrum of **[Ru(bpy)(dcb)(Hbpt)](PF$_6$)$_2$** in dmso-d$_6$.

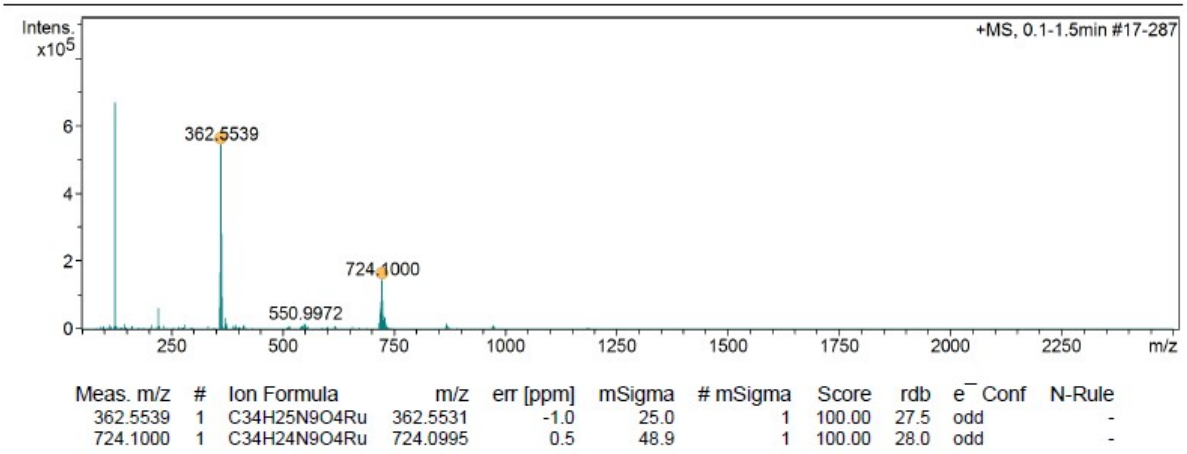

Meas. m/z	#	Ion Formula	m/z	err [ppm]	mSigma	# mSigma	Score	rdb	e⁻ Conf	N-Rule
362.5539	1	C34H25N9O4Ru	362.5531	-1.0	25.0	1	100.00	27.5	odd	-
724.1000	1	C34H24N9O4Ru	724.0995	0.5	48.9	1	100.00	28.0	odd	-

Figure S 10. Mass spectrogram for **Ru(dcb)(bpy)(Hbpt)](PF$_6$)$_2$**. [Ru(dcb)(bpy)(Hbpt)]$^{2+}$ calculated m/z = 362.555, found = 362.554. [Ru(dcb)(bpy)(bpt)]$^{+}$ calculated m/z = 724.100, found = 724.100

[Ru(bpy)(dceb)(bpt)Re(CO)$_3$Cl](PF$_6$)

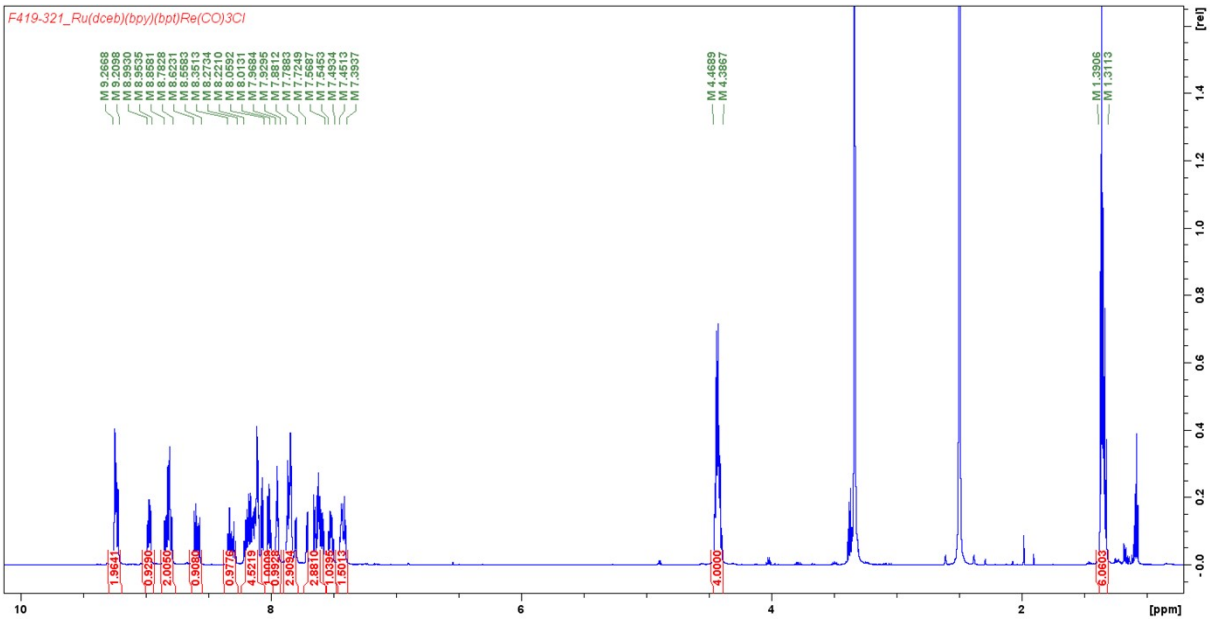

Figure S 11. ^{1}H-NMR of **[Ru(bpy)(dceb)(bpt)Re(CO)$_3$Cl](PF$_6$)** in dmso-d$_6$. Some residual ether was observed at 1.084 and 3.375 ppm.

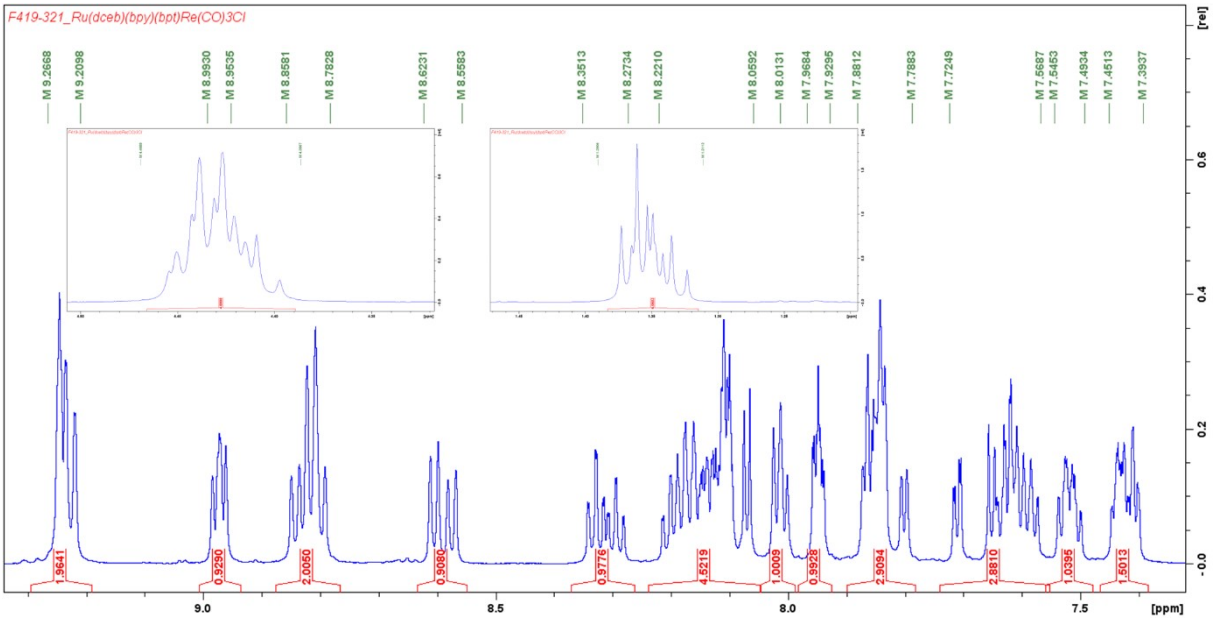

Figure S 12. ^{1}H-NMR spectrum of **[Ru(bpy)(dceb)(bpt)Re(CO)$_3$Cl](PF$_6$)** in dmso-d$_6$. The ester moieties are shown in the insets.

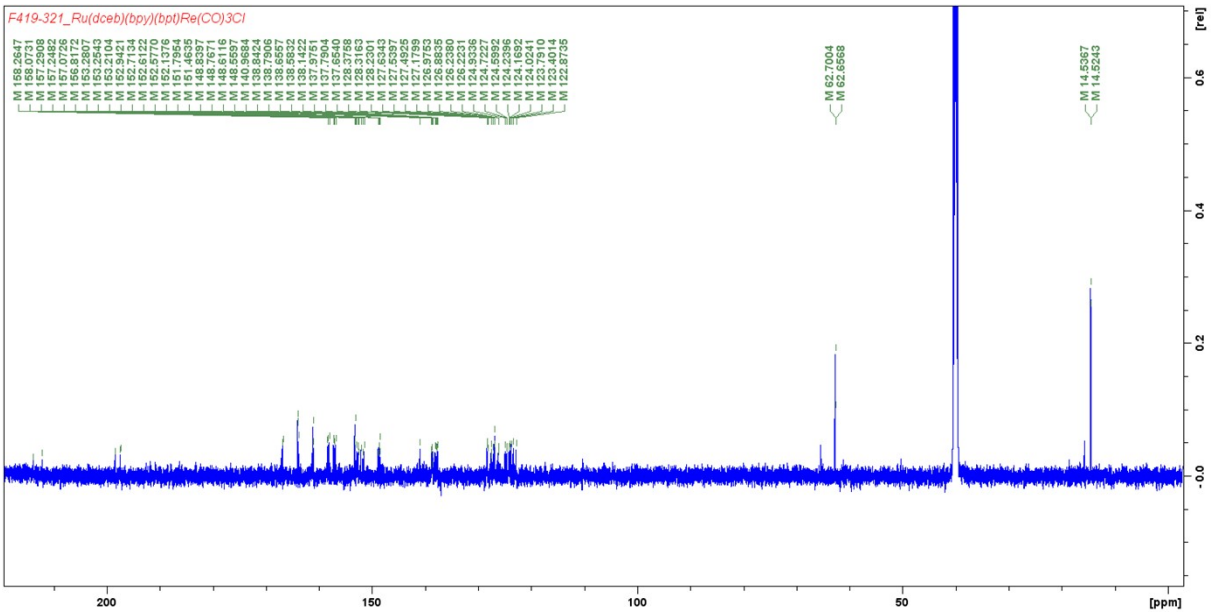

Figure S 13. ^{13}C-NMR of **[Ru(bpy)(dceb)(bpt)Re(CO)$_3$Cl](PF$_6$)** in dmso-d$_6$.

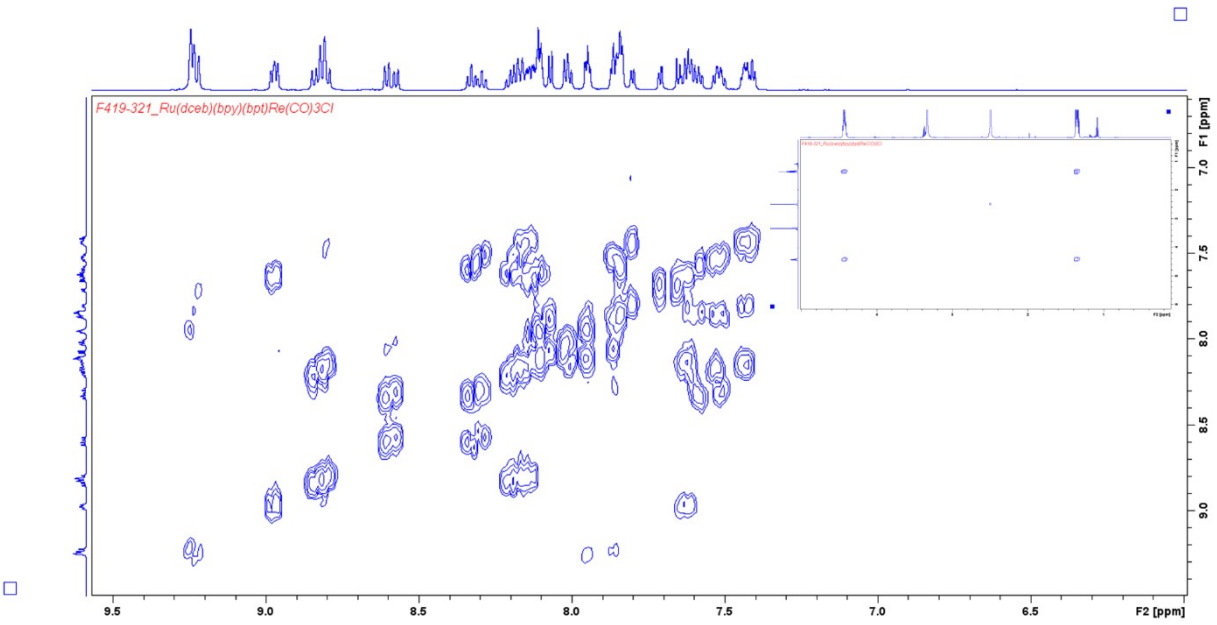

Figure S 14. COSY spectrum for **[Ru(bpy)(dceb)(bpt)Re(CO)$_3$Cl](PF$_6$)** in dmso-d$_6$.

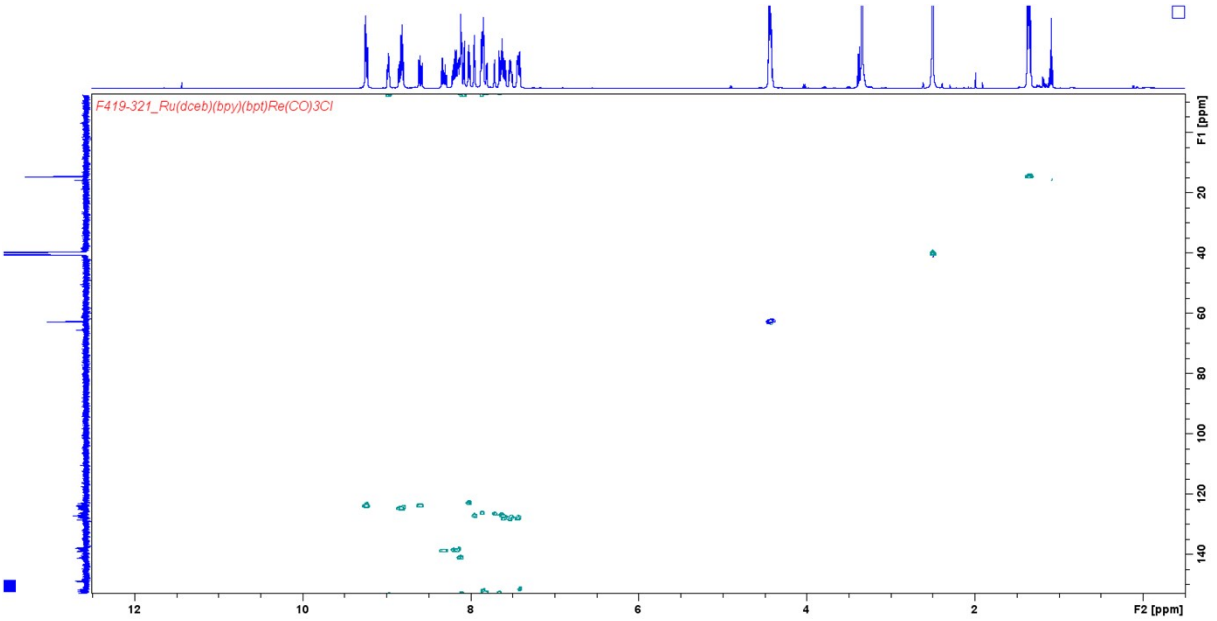

Figure S 15. HSQC spectrum of **[Ru(bpy)(dceb)(bpt)Re(CO)$_3$Cl](PF$_6$)** in dmso-d$_6$.

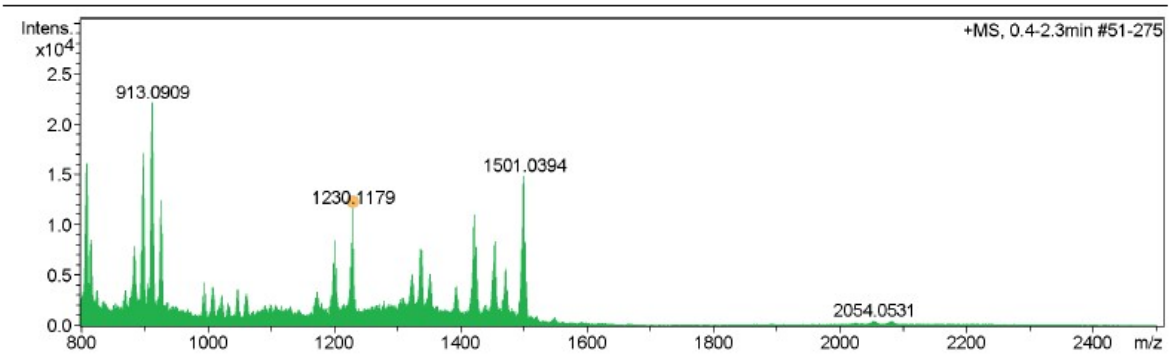

Meas. m/z	#	Ion Formula	m/z	err [ppm]	mSigma	# mSigma	Score	rdb	e⁻ Conf	N-Rule
1230.1179	1	C41H33ClF6N9O7PReRu	1232.0429	-61.4	254.9	1	-1.#J	28.5	even	ok

Figure S 16. Mass spectrogram for **[Ru(bpy)(dceb)(bpt)Re(CO)$_3$Cl](PF$_6$).**
[Ru(dceb)(bpy)(bpt)Re(CO)$_3$Cl-H]$^{-1}$ calculated m/z 1230.027 found 1230.1179

[Ru(bpy)(dcb)(bpt)Re(CO)$_3$Cl](PF$_6$) (PC1)

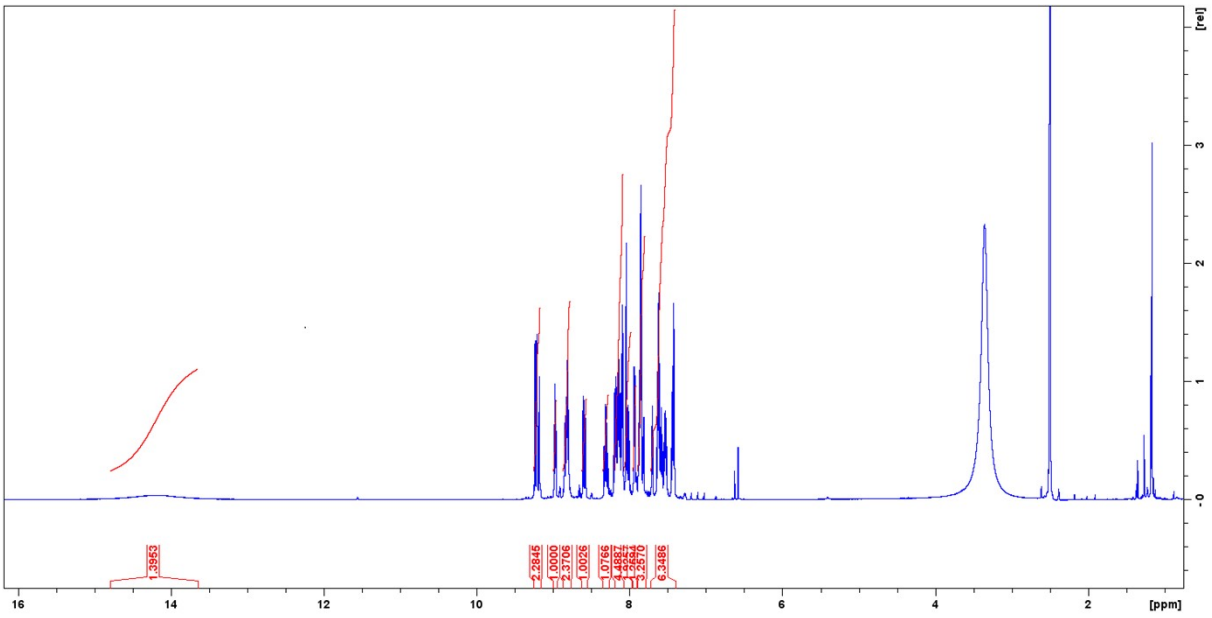

Figure S 17. ^{1}H-NMR of **[Ru(bpy)(dcb)(bpt)Re(CO)$_3$Cl](PF$_6$)** in dmso-d$_6$.

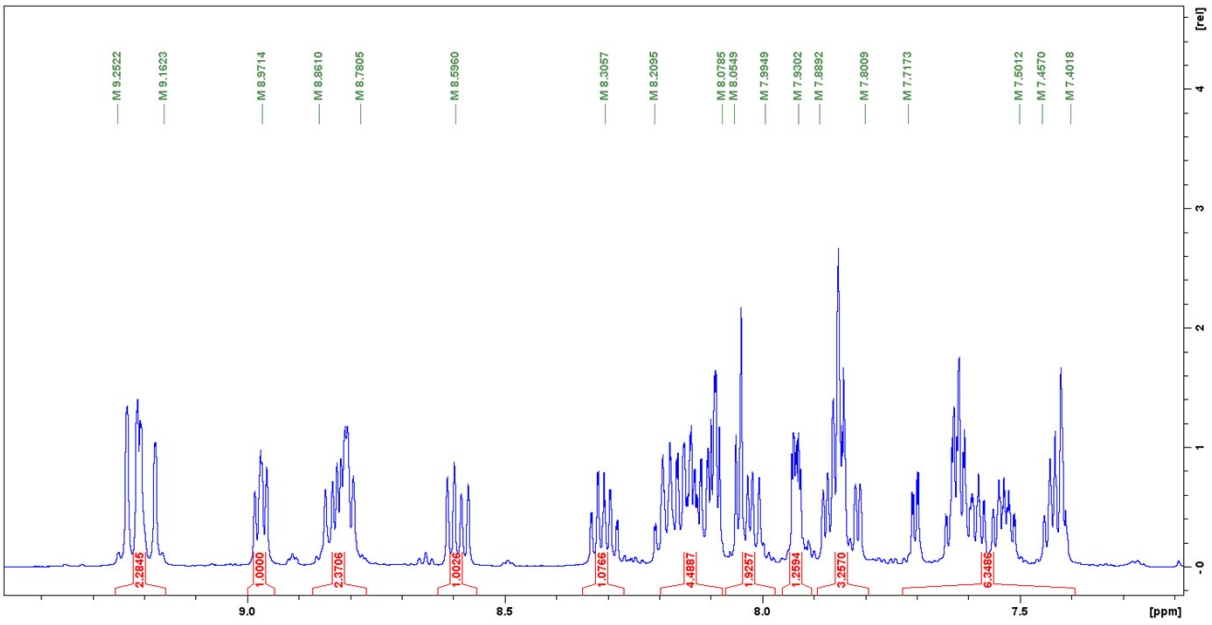

Figure S 18. ^{1}H-NMR of **[Ru(bpy)(dcb)(bpt)Re(CO)$_3$Cl](PF$_6$)** in dmso-d$_6$. Close up of the aromatic region.

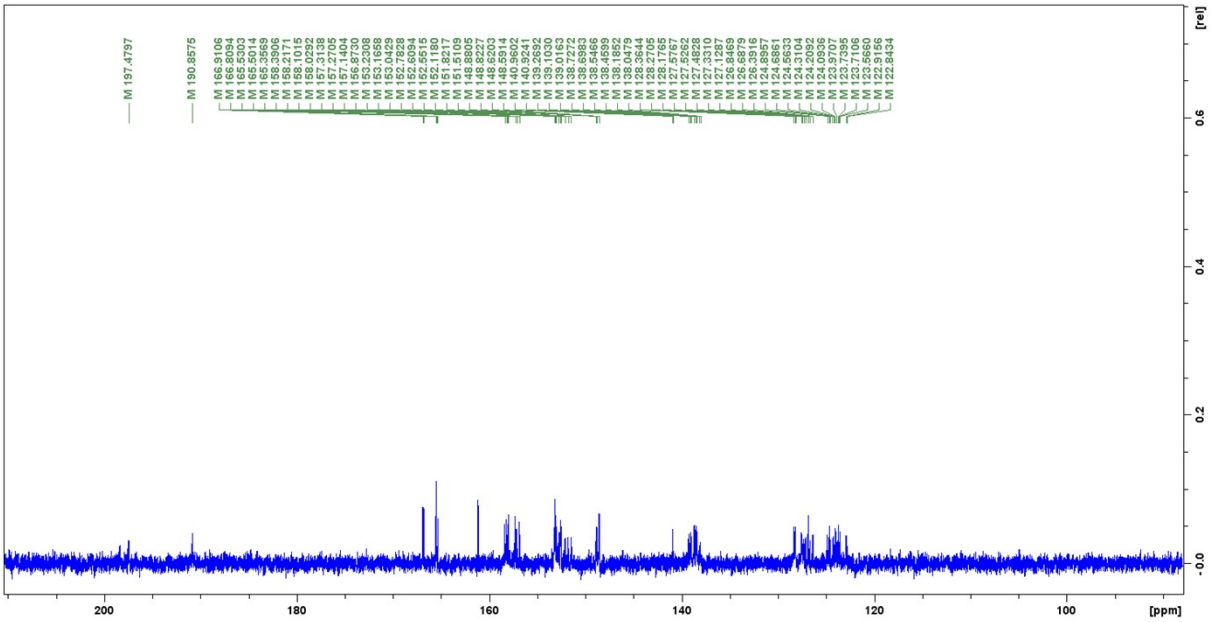

Figure S 19. ^{13}C-NMR of **[Ru(bpy)(dcb)(bpt)Re(CO)$_3$Cl](PF$_6$)** in dmso-d$_6$.

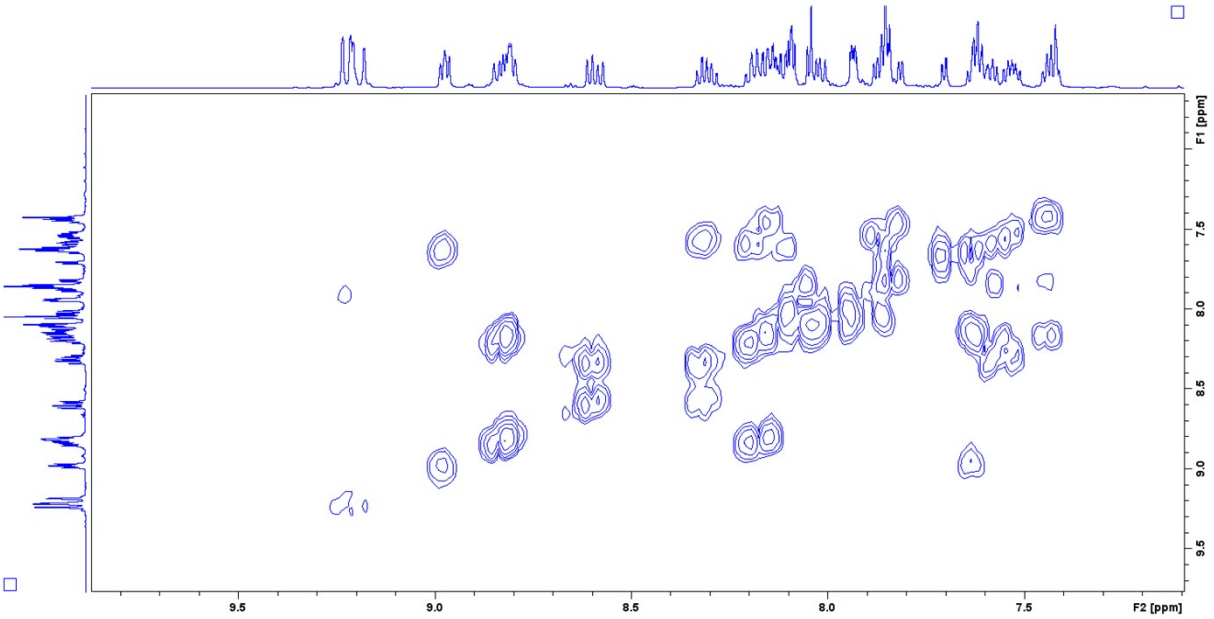

Figure S 20. COSY spectrum of **[Ru(bpy)(dcb)(bpt)Re(CO)$_3$Cl](PF$_6$)** in dmso-d$_6$.

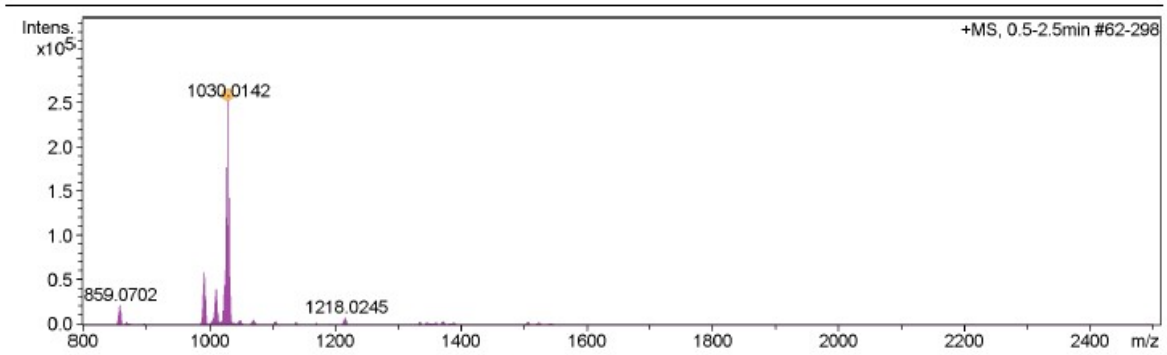

Meas. m/z	#	Ion Formula	m/z	err [ppm]	mSigma	# mSigma	Score	rdb	e¯ Conf	N-Rule
1030.0142	1	C37H24ClN9O7ReRu	1030.0083	-6.0	16.6	1	100.00	31.5	even	ok

Figure S 21. Mass spectrogram for **[Ru(bpy)(dcb)(bpt)Re(CO)$_3$Cl](PF$_6$)**. [Ru(dcb)(bpy)(bpt)Re(CO)$_3$Cl]$^{1+}$ calculated *m/z* = 1030.0083, found = 1030.0142. [Ru(dcb-2H$^+$)(bpy)(bpt)Re(CO)$_3$Cl] +2 Na$^+$] calculated *m/z* = 1218.938, found = 1218.0245

[Ru(bpy)(dceb)(bpt)PdCl$_2$](PF$_6$)

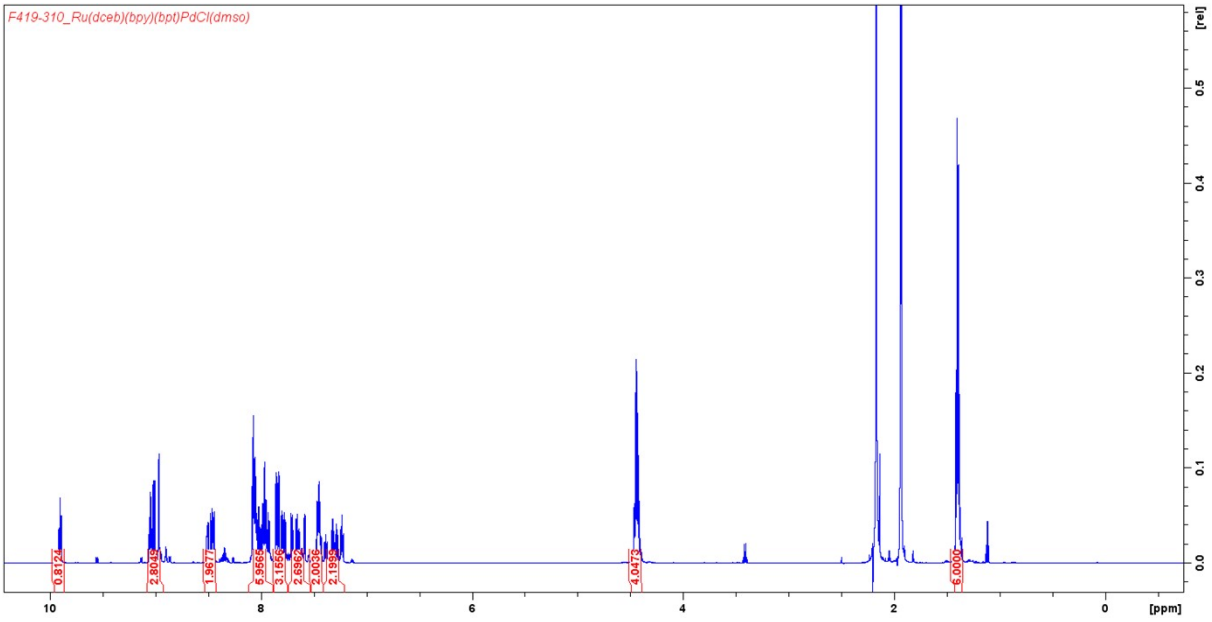

Figure S 22. ^{1}H-NMR spectrum of **[Ru(bpy)(dceb)(bpt)PdCl$_2$](PF$_6$)** in acetonitrile-d$_3$.

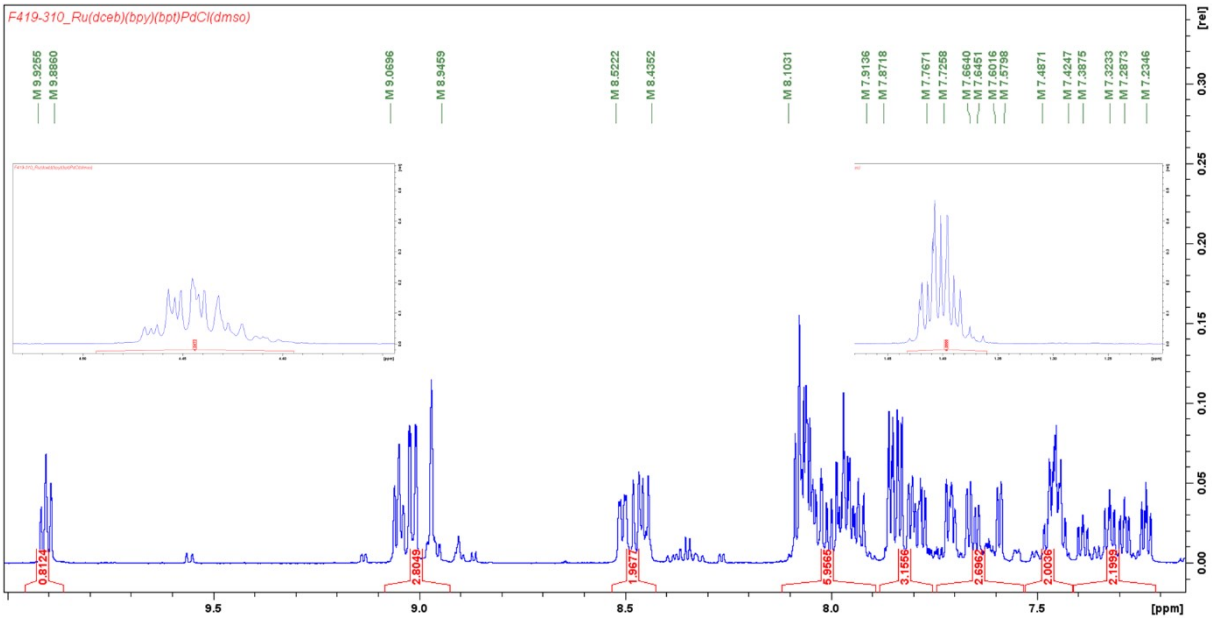

Figure S 23. ^{1}H-NMR of **[Ru(bpy)(dceb)(bpt)PdCl$_2$](PF$_6$)** in acetonitrile-d$_3$. Insert of the ester moieties.

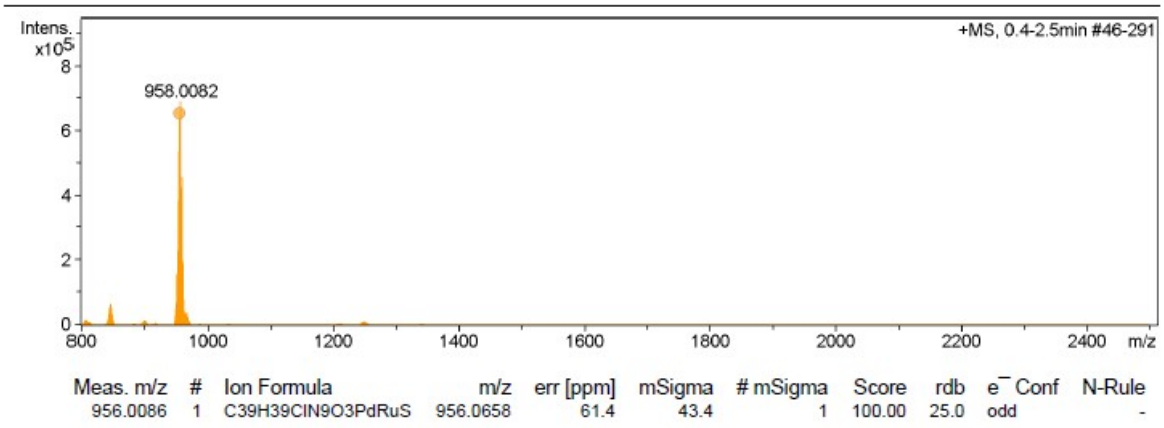

Figure S 24. Mass spectrogram for **[Ru(dceb)(bpy)(bpt)PdCl$_2$](PF$_6$)**. [Ru(dceb)(bpy)(bpt)PdCl$_2$]$^{1+}$ calculated m/z = 956.003, found = 956.008.

[Ru(bpy)(dcb)(bpt)Pd(dmso)Cl](PF$_6$)$_2$ (PC2)

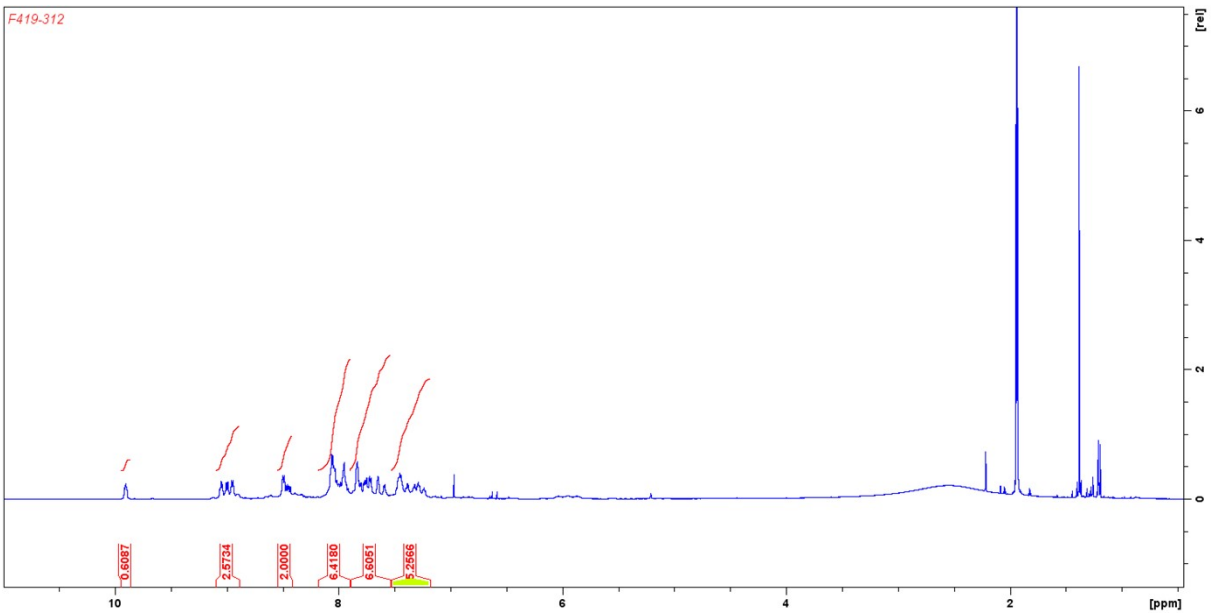

Figure S 25. ^{1}H-NMR of **[Ru(bpy)(dcb)(bpt)PdCl$_2$](PF$_6$)** in acetonitrile-d$_3$

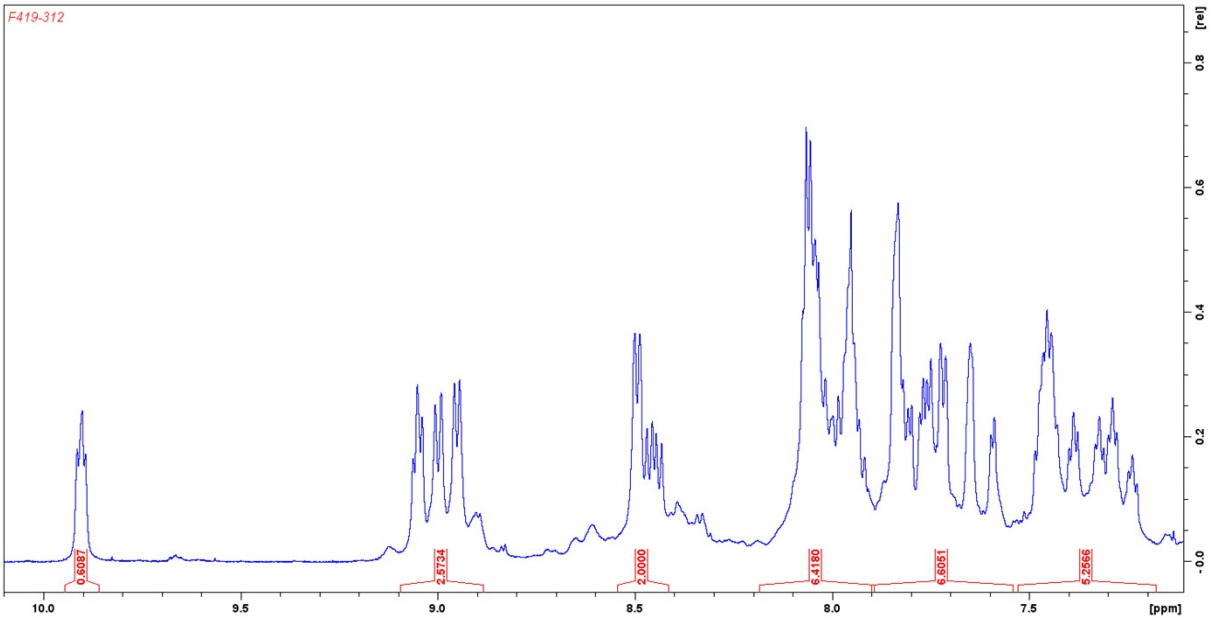

Figure S 26. ^{1}H-NMR of **[Ru(bpy)(dcb)(bpt)PdCl$_2$](PF$_6$)** in acetonitrile-d$_3$.Zoom in of the aromatic region.

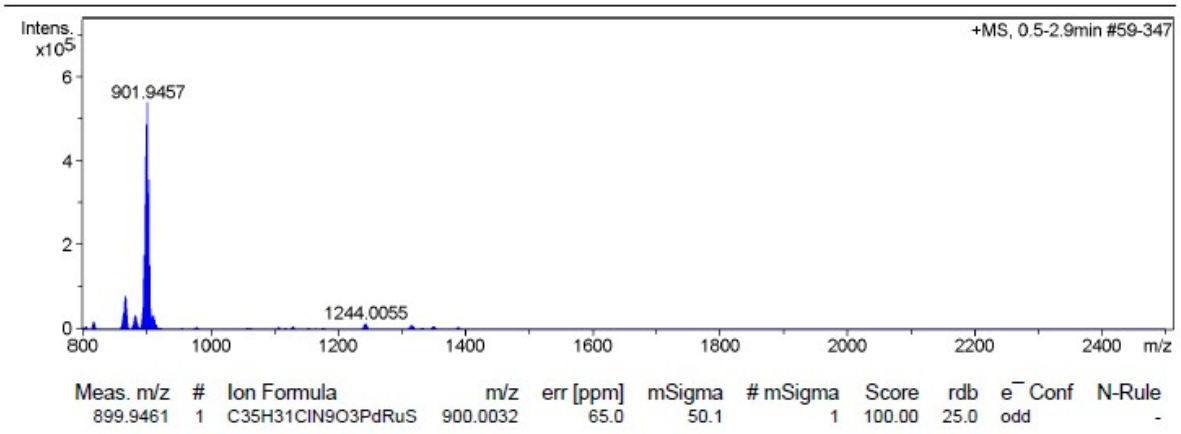

Figure S 27. Mass spectrogram for [Ru(dceb)(bpy)(bpt)PdCl$_2$](PF$_6$). [Ru(dcb)(bpy)(bpt)PdCl$_2$]$^{1+}$ calculated m/z = 899.941 found 899.946.

FTIR Spectra

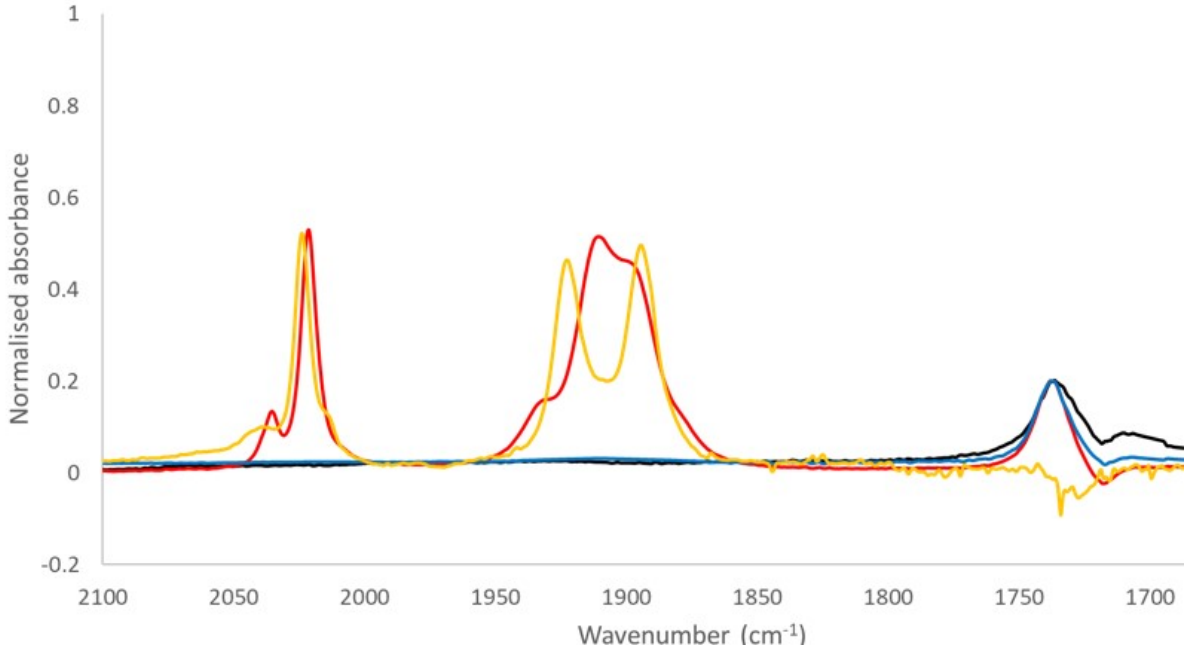

Figure S 28. FTIR spectra of $[Ru(dcb)(bpy)(Hbpt)](PF_6)_2$ (black), $[Ru(dcb)(bpy)(bpt)Re(CO)_3Cl](PF_6)$ (red), $[Ru(dcb)(bpy)(bpt)PdCl_2](PF_6)$ (blue) and the model complex $Re(Hbt)(CO)_3Cl$ complex in THF (yellow). Due to low solubility of this complex the FTIR spectrum was recorded in THF instead of MeCN.

UV-visible Absorption Spectroscopy

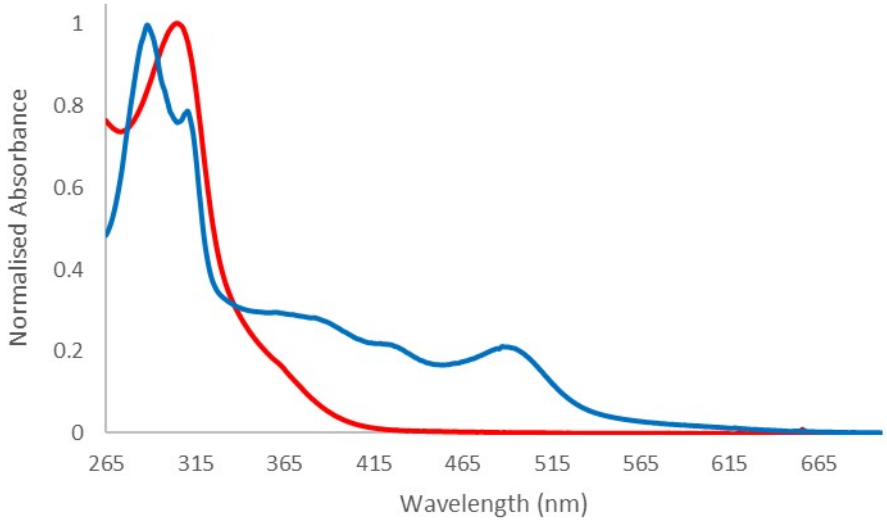

Figure S 29. Normalised UV-Vis spectra for PC1 (blue) and $Re(Hbpt)(CO)_3Cl$ (red) in acetonitrile.

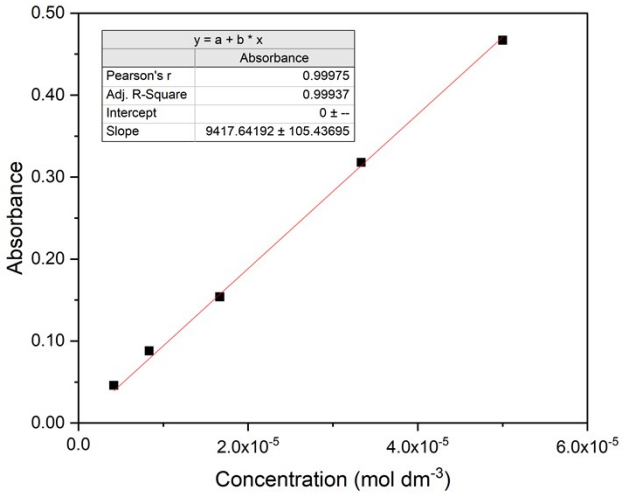

Figure S 30. Beer-Lambert plot for PC1 in acetonitrile solution recorded at 470 nm.

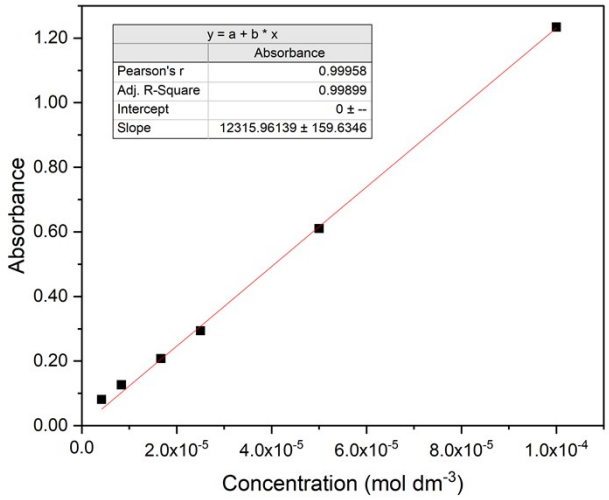

Figure S 31. Beer-Lambert plot for PC2 in acetonitrile solution recorded at 474 nm.

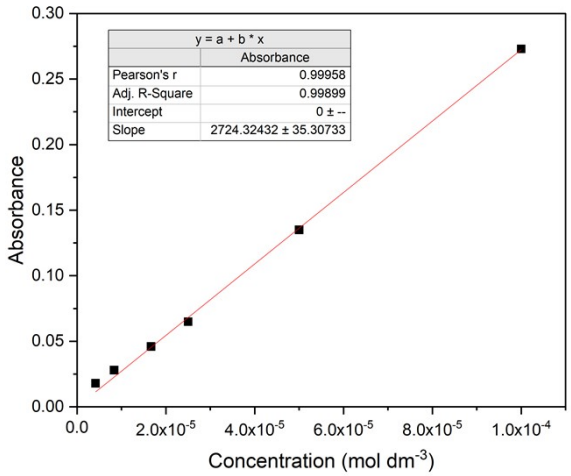

Figure S 32. Beer-Lambert plot for PC3 in acetonitrile solution recorded at 490 nm.

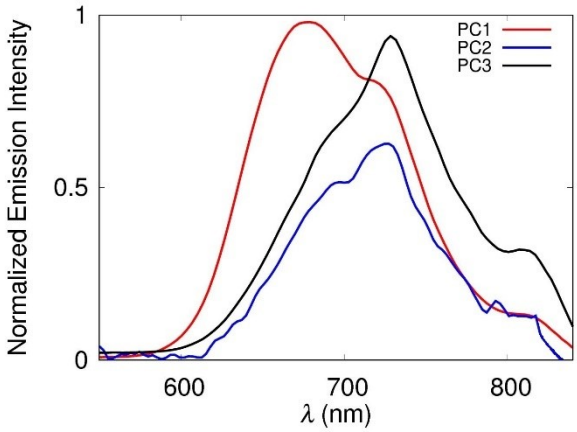

Figure S 33. Emission spectra for the photocatalysts in optically thin (<0.1 abs at excitation wavelength) acetonitrile solution following illumination at 460 nm. Emission spectra were recorded with a Hitachi F-4500 spectrophotometer.

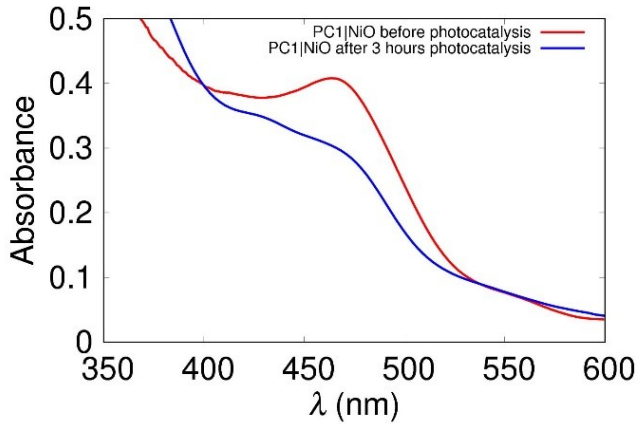

Figure S 34. UV-visible absorption spectrum of photocatalyst PC1|NiO before and after three hours 1 sun irradiation with AM 1.5 filtered light in a photoelectrochemical cell saturated with CO_2 and an applied external bias of -0.5 V vs Ag/AgCl, in a 0.1 M pH 5 acetate buffer.

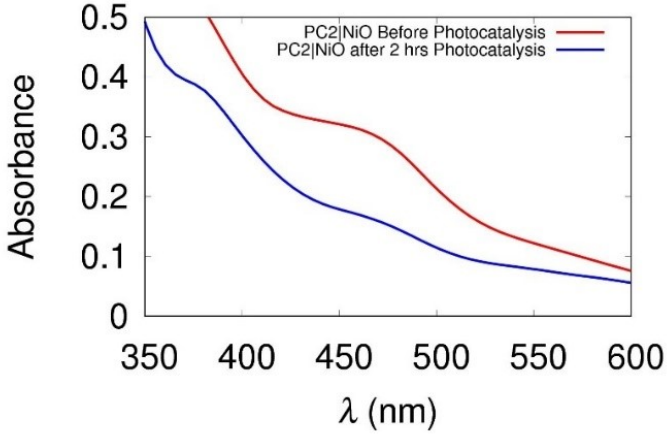

Figure S 35. UV-visible absorption spectrum of photocatalyst PC2|NiO before and after two hours 1 sun irradiation with AM 1.5 filtered light in a photoelectrochemical cell saturated with Ar and an applied external bias of -0.5 V vs Ag/AgCl, in a 0.1 M pH 5 acetate buffer.

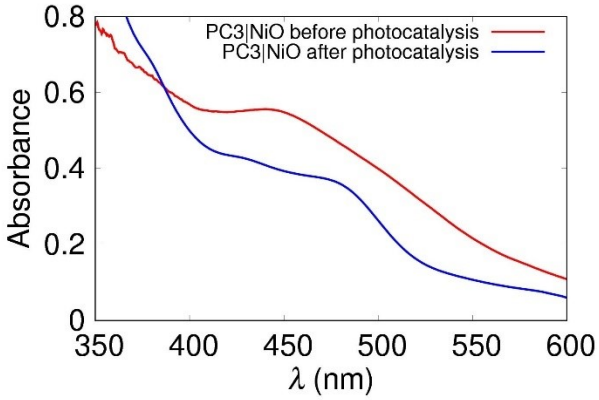

Figure S 36. UV-visible absorption spectrum of photocatalyst PC3|NiO before and after three hours 1 sun irradiation with AM 1.5 filtered light in a photoelectrochemical cell saturated with CO_2 and an applied external bias of -0.5 V vs Ag/AgCl in a 0.1 M pH 5 acetate buffer.

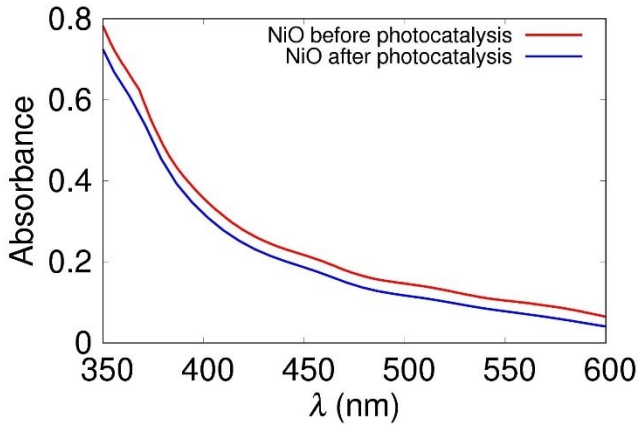

Figure S 37. UV-visible absorption spectrum of an unsensitized NiO film before and after three hours 1 sun irradiation with AM 1.5 filtered light in a photoelectrochemical cell saturated with CO_2 and an applied external bias of -0.5 V vs Ag/AgCl in a 0.1 M pH 5 acetate buffer.

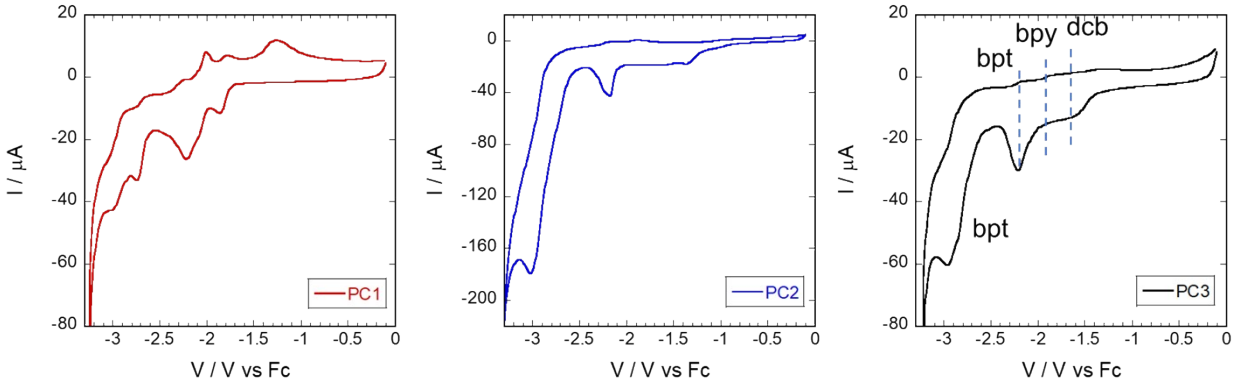

Figure S 38. Cyclic voltammogram for PC1-3 in acetonitrile with 0.1 M tetrabutylammonium hexafluorophosphate as supporting electrolyte, 100 mV s^{-1} scan rate.

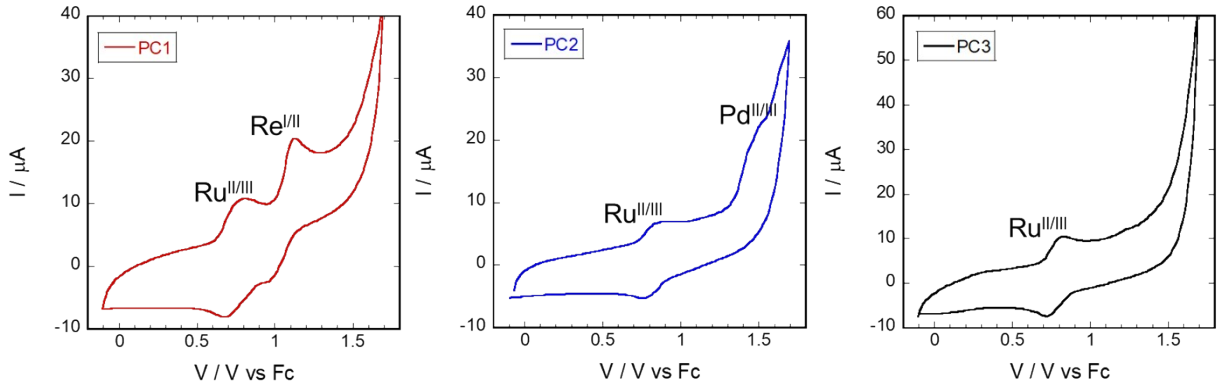

Figure S 39. Cyclic voltammogram for PC1-3 in acetonitrile with 0.1 M tetrabutylammonium hexafluorophosphate as supporting electrolyte, 100 mV s^{-1} scan rate.

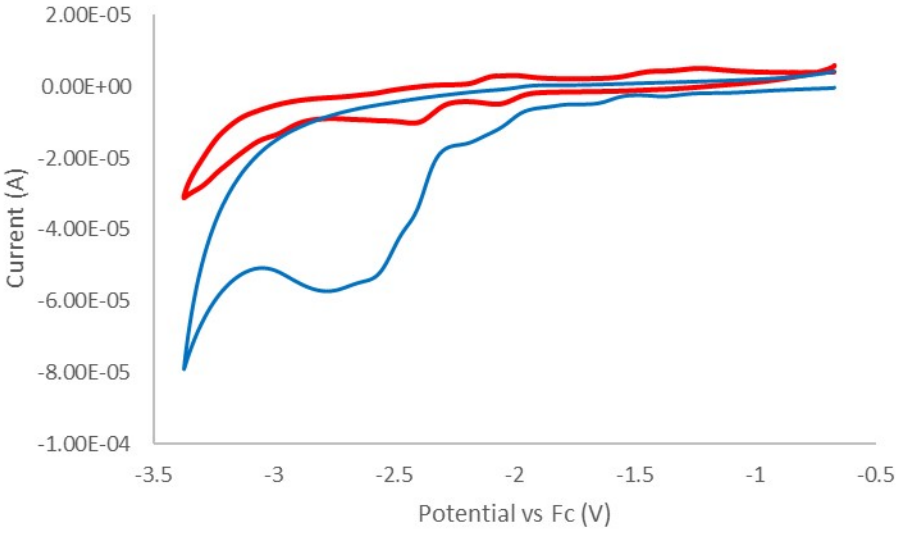

Figure S 40. Cyclic voltammogram of **PC1** in DMF with 0.1 M $TBAPF_6$ as supporting electrolyte following bubbling with N_2 (red) and CO_2 (blue).

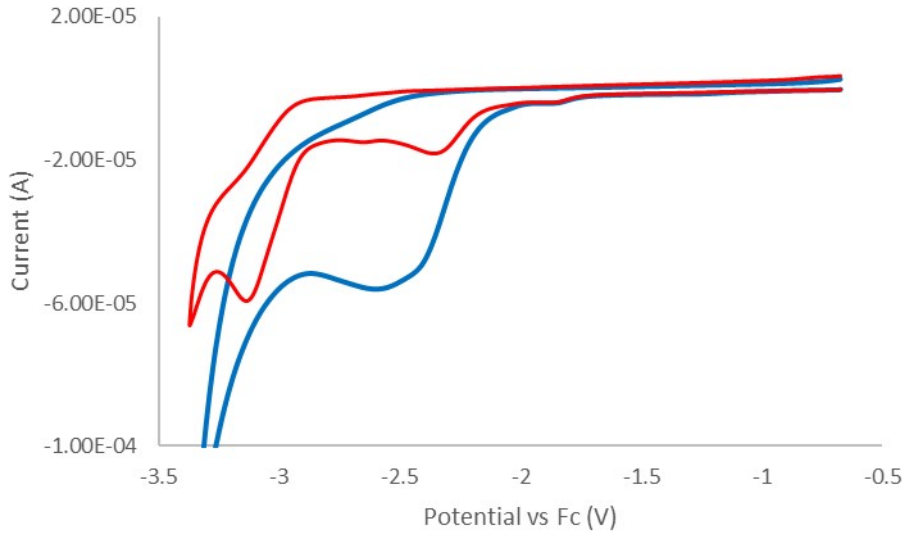

Figure S 41. Cyclic voltammogram of **Re(HBpt)(CO)$_3$Cl** in DMF with 0.1 M TBAPF$_6$ as supporting electrolyte following bubbling with N_2 (red) and CO_2 (blue).

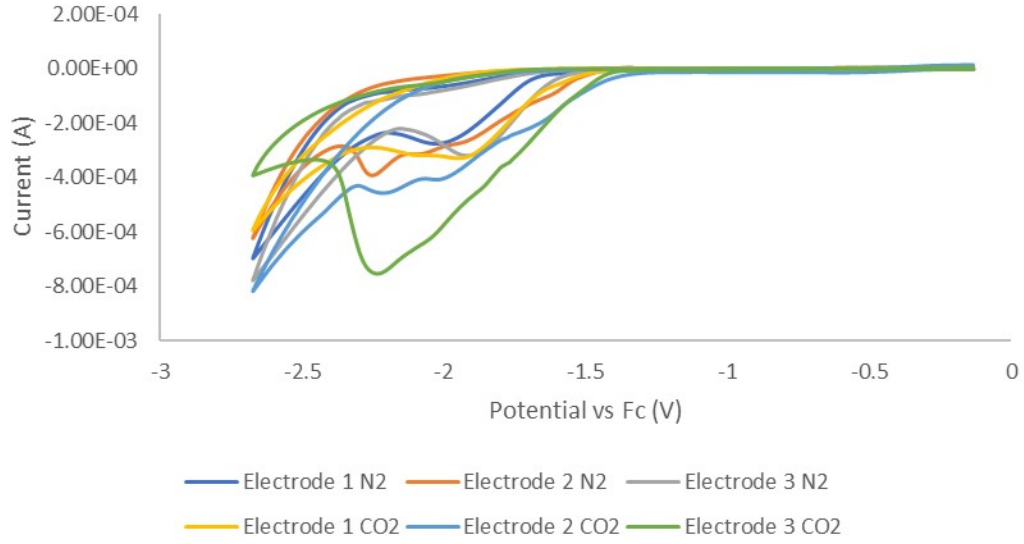

Figure S 42. Cyclic voltammograms of RuRe dropcast on glassy carbon electrodes.

We attempted to mimic the photoelectrochemical experimental setup by dropcasting 10 mM solutions of PC1 in DMSO on glassy carbon electrodes. The electrodes were left to dry over night to form a homogeneous film of the catalyst on the electrode surface. The electrodes were tested in pH 5 buffered solutions of acetic acid/sodium acetate bubbled with nitrogen or carbon dioxide, identical to the experiments conducted for the photoelectrochemical studies on NiO. Unfortunately, rapid desorption of the catalyst layer was observed when the electrocatalysis was started. This rapid desorption made accurate determination of CO_2 reduction by a thin film of catalyst impossible. As seen in the main text, desorption of the catalyst did not occur as readily for the NiO surfaces. Potentially, the stronger interaction including covalent bonding through pendant hydroxyl moieties on the NiO result in a stronger interaction between the catalyst and the NiO surface compared to

that between the catalyst and the glassy carbon surface. Furthermore, the potentials required to reduce CO_2 electrochemically in these dropcast experiments are significantly higher than those employed for the photoelectrochemical studies on NiO. During the dropcast experiment, hydrogen formation was observed catalysed by the glassy carbon electrode, and H_2 bubble formation likely accelerated desorption of the catalyst layer from the electrode.

S3. Transient Optical and Infrared Spectroscopy

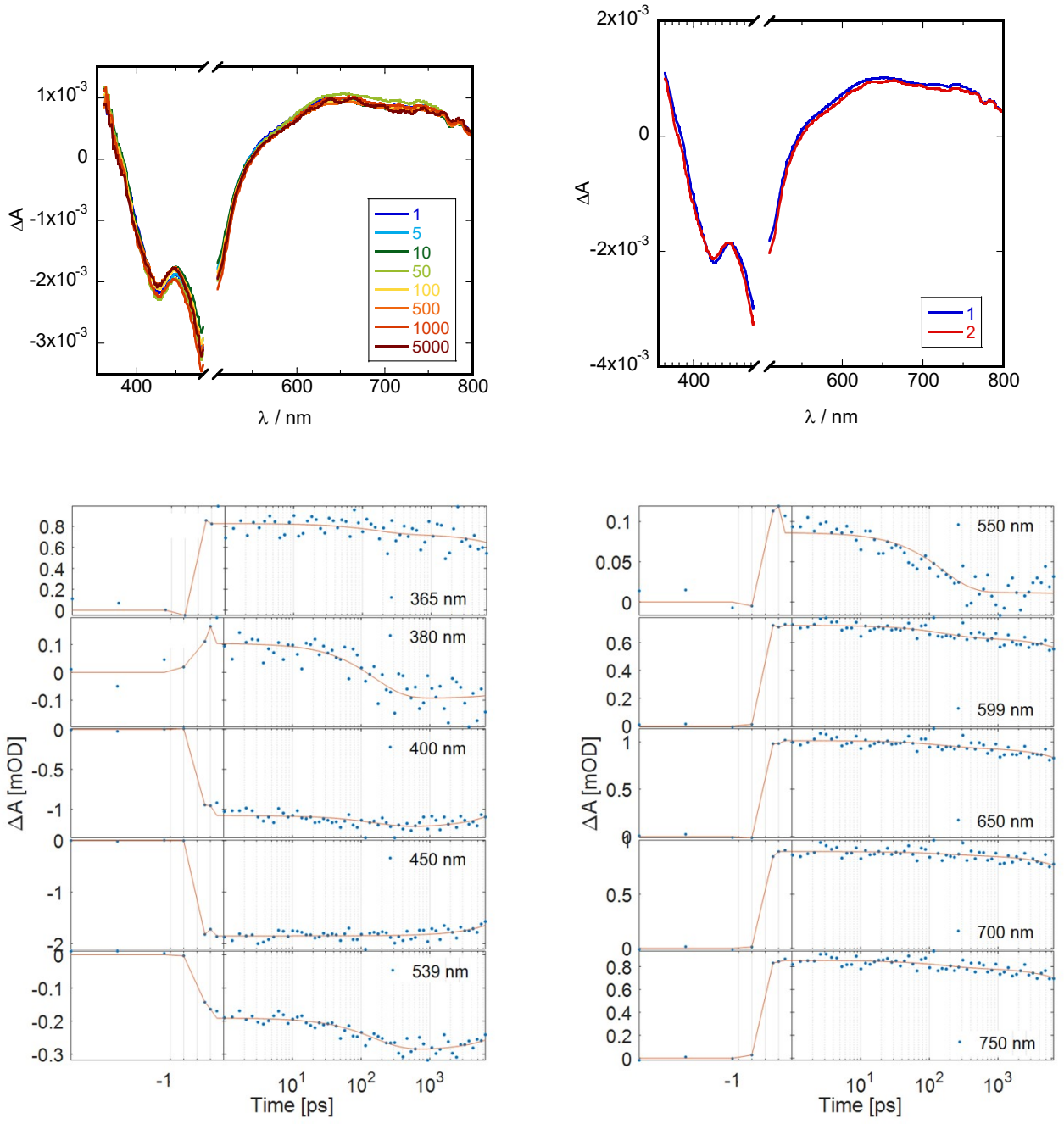

Figure S 43. Transient absorption spectra for PC1 in acetonitrile solution with corresponding delay times in picoseconds (top left); the species associated spectra from global fitting where the

numbers correspond to 1 = τ_1 = 160 ps, and 2 = τ_2 >>1 ns (top right); kinetic traces for selected wavelengths (bottom) with fits (orange line). The excitation wavelength was 500 nm.

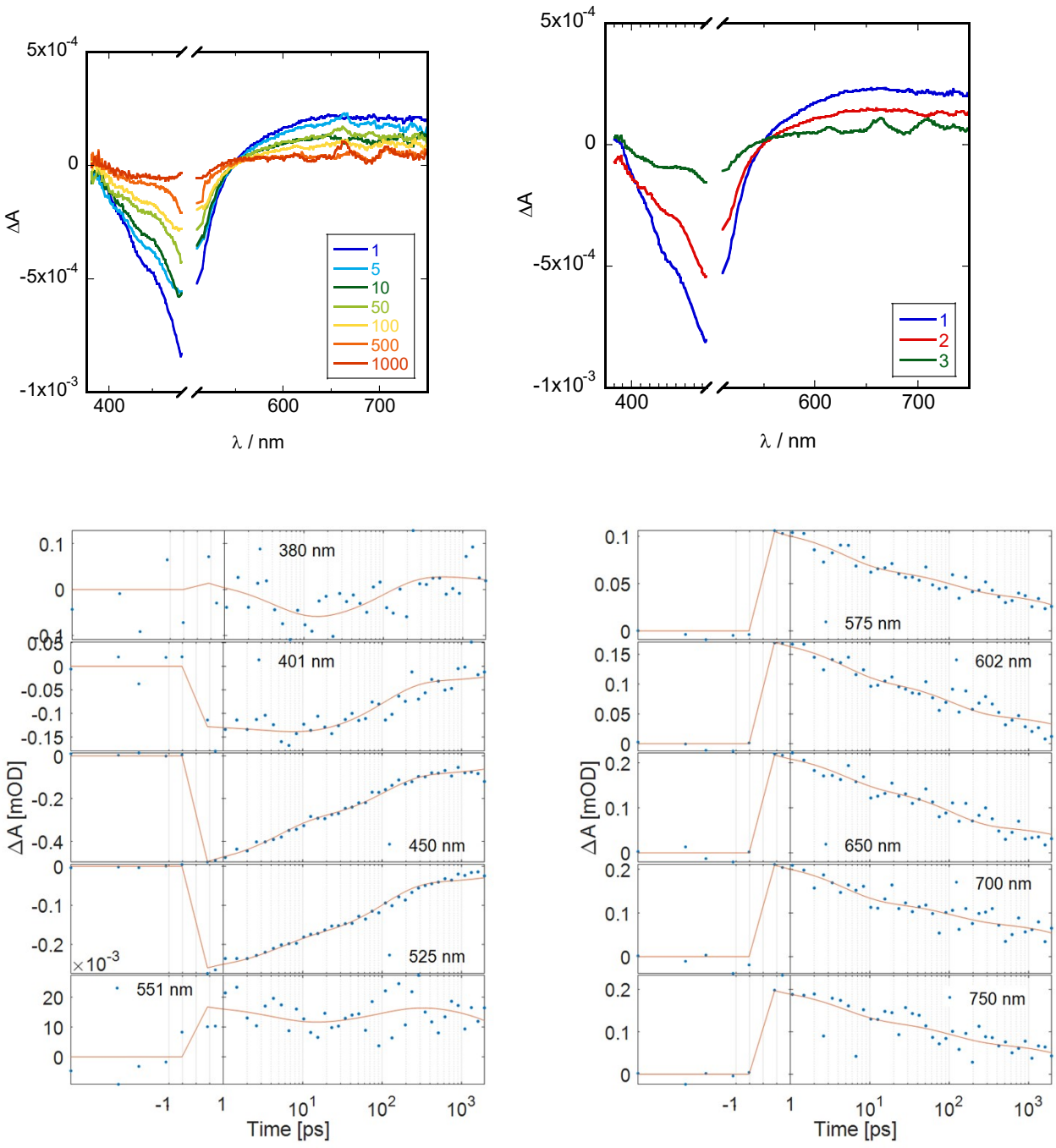

Figure S 44 Transient absorption spectra for PC1|NiO with corresponding delay times in picoseconds (top left); the species associated spectra from global fitting where the numbers correspond to 1 = τ_1 = 4.6 ps, 2 = τ_2 = 110 ps, and 3 = τ_3 ~ 5.1 ns (top right); kinetic traces for selected wavelengths (bottom) with fits (orange line). The excitation wavelength was 500 nm.

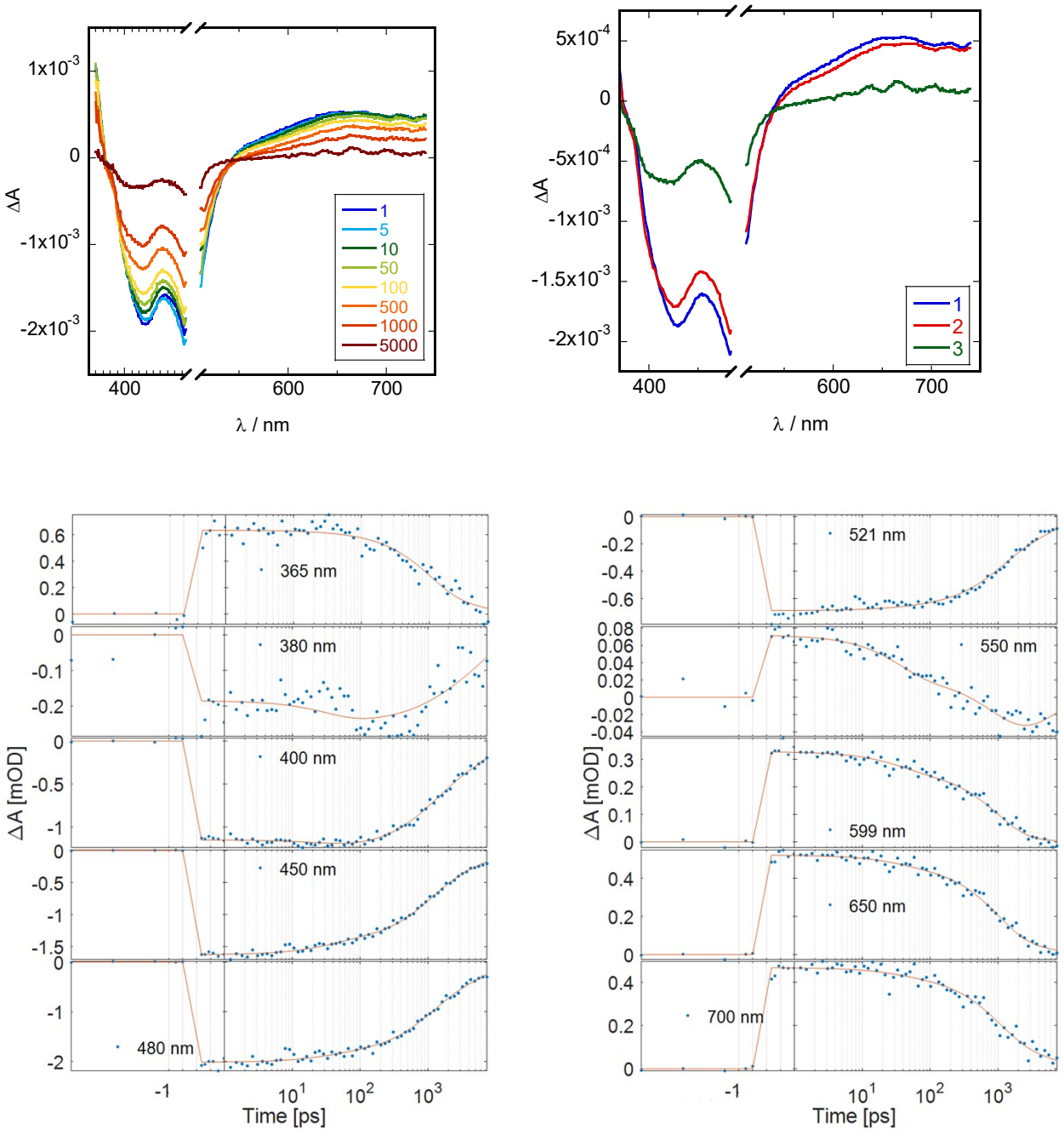

Figure S 45. Transient absorption spectra for PC2 in acetonitrile solution with corresponding delay times in picoseconds (top left); the species associated spectra from global fitting where the numbers correspond to 1 = τ_1 = 35 ps, and 2 = τ_2 = 980 ps, 3 = τ_3 >>1 ns (top right); kinetic traces for selected wavelengths (bottom) with fits (orange line). The excitation wavelength was 500 nm.

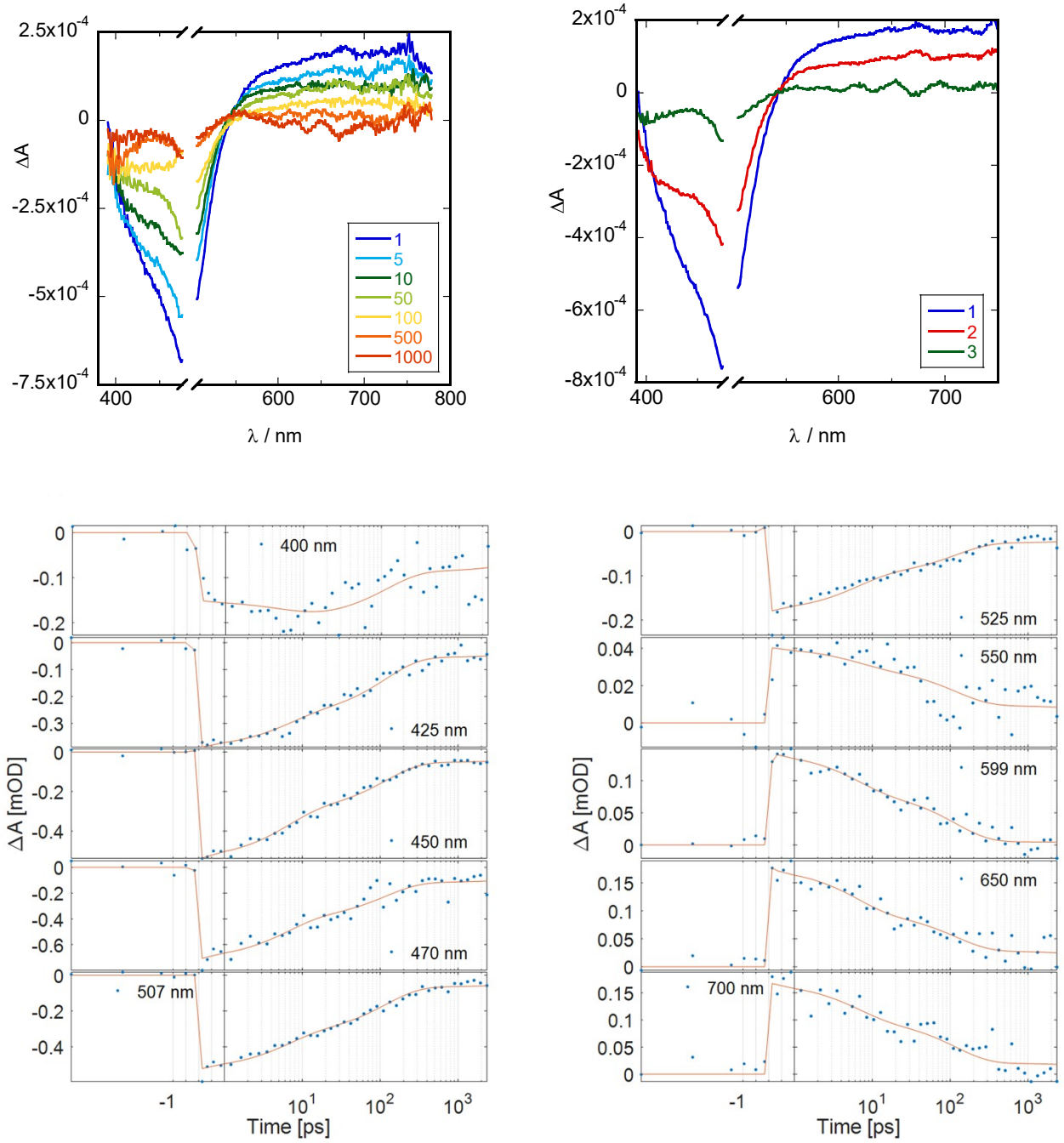

Figure S 46. Transient absorption spectra for PC2|NiO with corresponding delay times in picoseconds (top left); the species associated spectra from global fitting where the numbers correspond to 1 = τ_1 = 6.0 ps, 2 = τ_2 = 120 ps, and 3 = τ_3 >> 1 ns (top right); kinetic traces for selected wavelengths (bottom) with fits (orange line). The excitation wavelength was 490 nm.

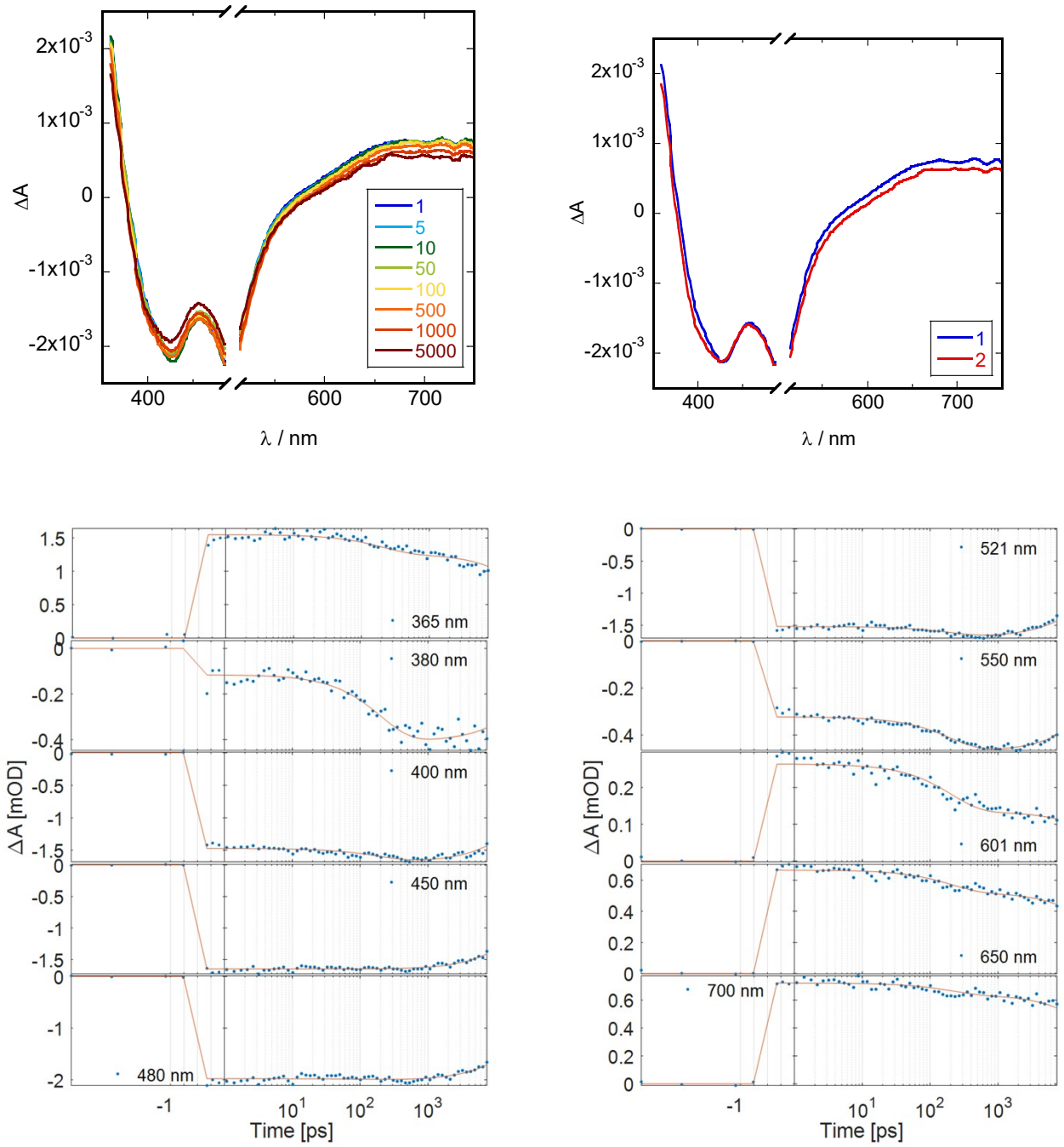

Figure S 47. Transient absorption spectra for PC3 in acetonitrile solution with corresponding delay times in picoseconds (top left); the species associated spectra from global fitting where the numbers correspond to 1 = τ_1 = 200 ps, and 2 = τ_2 >>1 ns (top right); kinetic traces for selected wavelengths (bottom) with fits (orange line). The excitation wavelength was 500 nm.

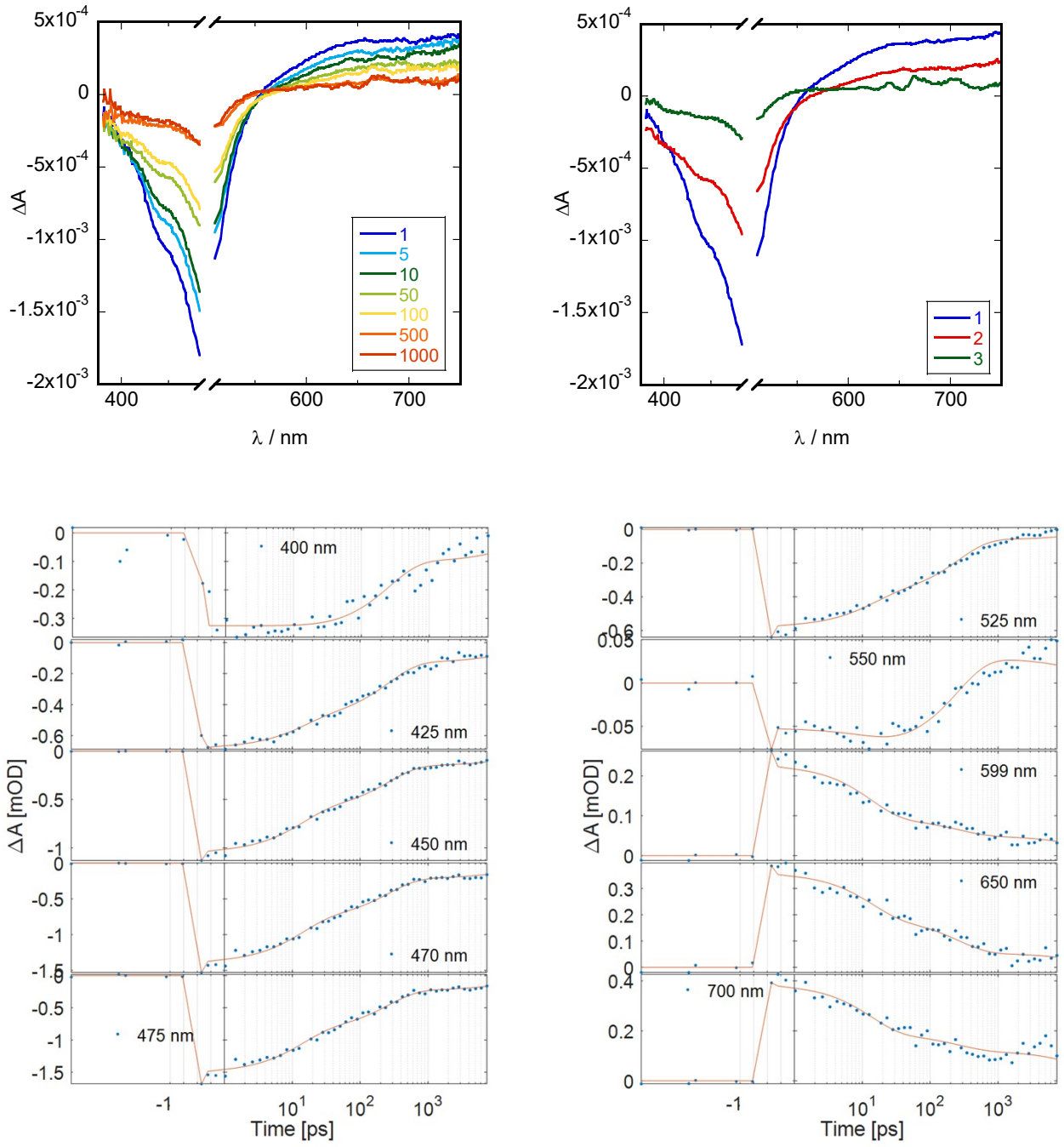

Figure S 48. Transient absorption spectra for PC3|NiO with corresponding delay times in picoseconds (top left); the species associated spectra from global fitting where the numbers correspond to 1 = τ_1 = 13 ps, 2 = τ_2 = 260, and 3 = τ_3 >>1 ns (top right); kinetic traces for selected wavelengths (bottom) with fits (orange line). The excitation wavelength was 500 nm.

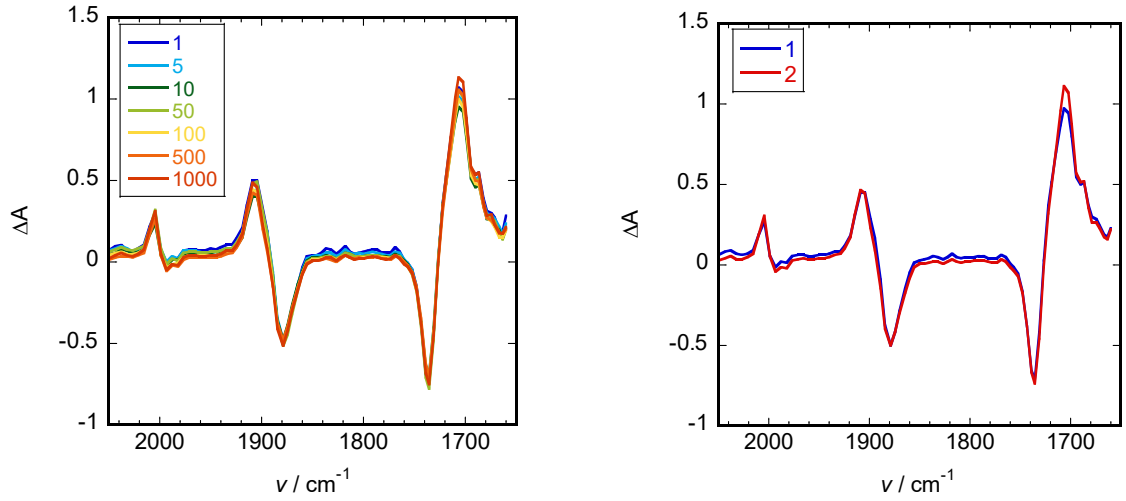

Figure S 49. Time-resolved infrared spectra for PC1 in acetonitrile with delay times in picoseconds (left); the species associated spectra from global fitting where the numbers correspond to 1 = τ_1 = 130 ps, and 2 = τ_2 >>1 ns (right). The excitation wavelength was 500 nm.

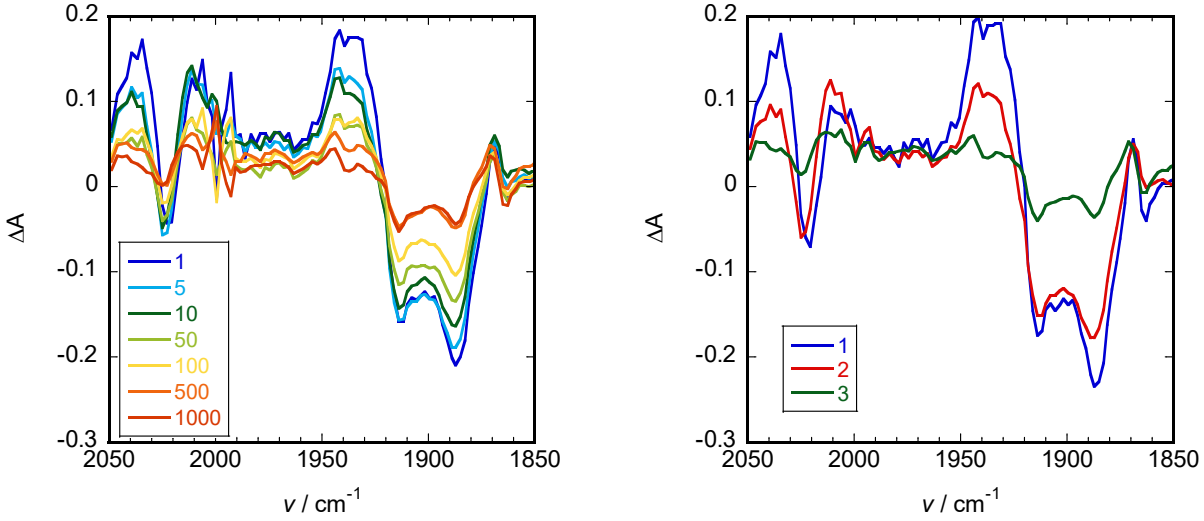

Figure S 50. Time-resolved infrared spectra for PC1|NiO with delay times in picoseconds (left); the species associated spectra from global fitting where the numbers correspond to 1 = τ_1 = 2.4 ps, 2 = τ_2 = 150 ps, and 3 = τ_3 >>1 ns (right). The excitation wavelength was 500 nm.

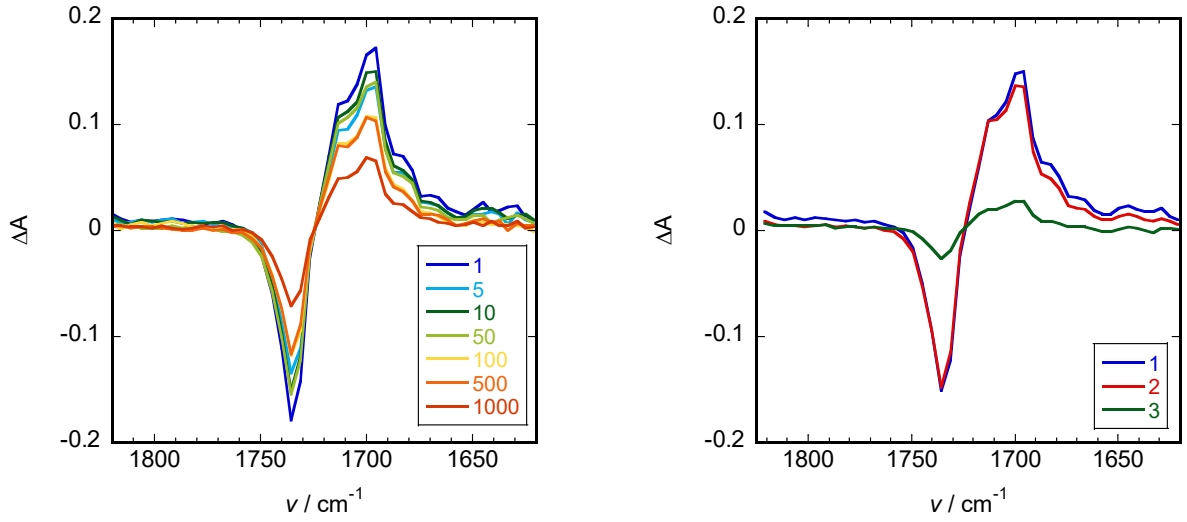

Figure S 51. Transient infrared spectra (left) for PC2 in acetonitrile with delay times in picoseconds (left); the species associated spectra from global fitting where the numbers correspond to 1 = τ_1 = 22 ps, and 2 = τ_2 = 1.2 ns, 3 = τ_3 >>1 ns (right). The excitation wavelength was 500 nm.

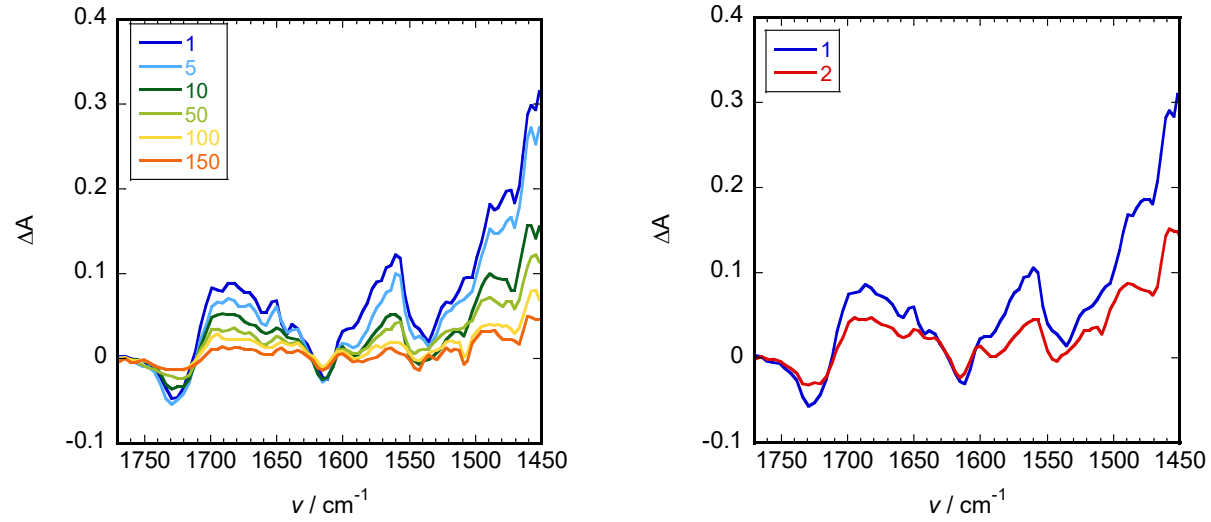

Figure S 52. Transient infrared spectra (left) for PC2|NiO with delay times in picoseconds (left); the species associated spectra from global fitting where the numbers correspond to 1 = τ_1 = 7.0 ps, 2 = τ_2 = 120 ps, and 3 = τ_3 >> 1 ns (right). The excitation wavelength was 500 nm.

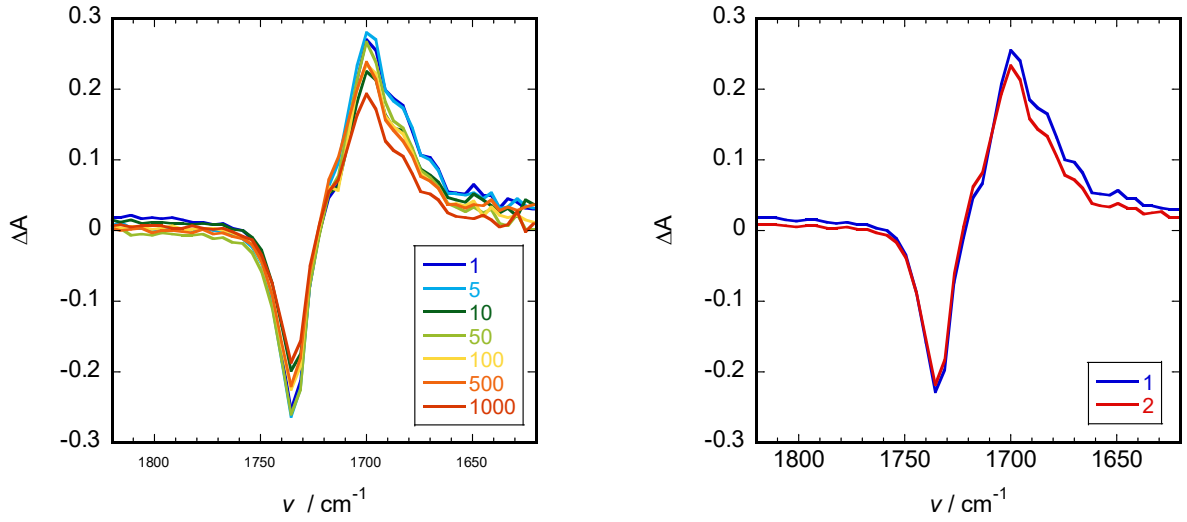

Figure S 53. Transient infrared spectra (left) for PC3 in acetonitrile with delay times in picoseconds (left); the species associated spectra from global fitting where the numbers correspond to 1 = τ_1 = 14 ps, and 2 = τ_2 >>1 ns (right). The excitation wavelength was 500 nm.

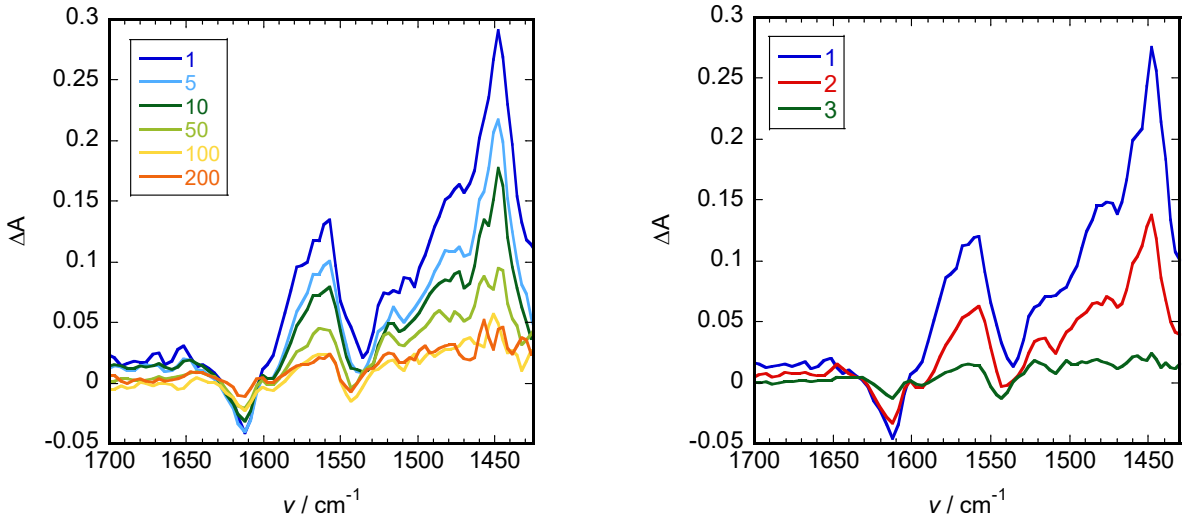

Figure S 54. Transient infrared spectra (left) for PC3|NiO with delay times in picoseconds (left); the species associated spectra from global fitting where the numbers correspond to 1 = τ_1 = 7 ps, 2 = τ_2 = 81, and 3 = τ_3 >>1 ns (right). The excitation wavelength was 500 nm.

S4. Photoelectrochemical Data

All electrochemical measurements were completed in a three-electrode setup containing a platinum counter electrode, Ag/AgCl reference electrode and a sensitized NiO film as a working electrode. Irradiation was provided by a Xe-arc lamp set at 1 sun intensity (100 mW cm^{-2}) and filtered with an AM 1.5 reference filter to simulate the solar spectrum.

The following aqueous buffer (made up in deionised water) solutions were used:

0.1 M pH 5 acetate buffer (0.07 M sodium acetate + 0.03 M acetic acid, adjusted with concentrated HCl)

0.1 M pH 8 phosphate buffer (0.0935 M K_2HPO_4 + 0.0065 M K_2HPO_4)

0.1 M pH 9.2 carbonate buffer (0.091 M sodium bicarbonate + 0.009 M sodium carbonate)

50 mM sodium hydrogen carbonate solution adjusted to pH 6.6 with concentrated HCl.

Components of the buffer solutions were obtained from Sigma-Aldrich and used as received.

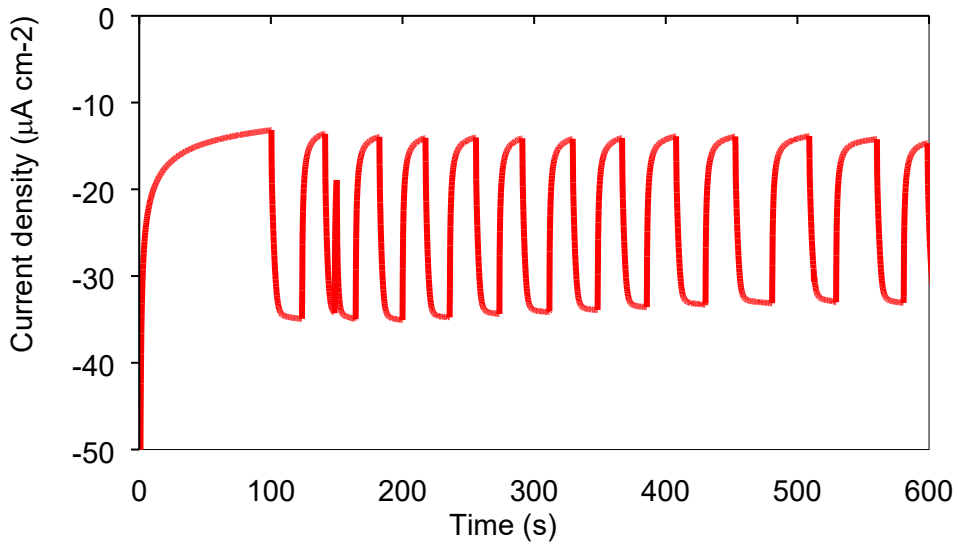

Figure S 55. Photocurrent density of PC1|NiO with an applied external bias of -0.5 Volts vs Ag/AgCl in pH 5 acetate buffer in the presence of 10 mM tris(ethyldiamine)cobalt(III) as an electron acceptor, under chopped 1 sun AM 1.5, (100 mW cm^{-2}) irradiation.

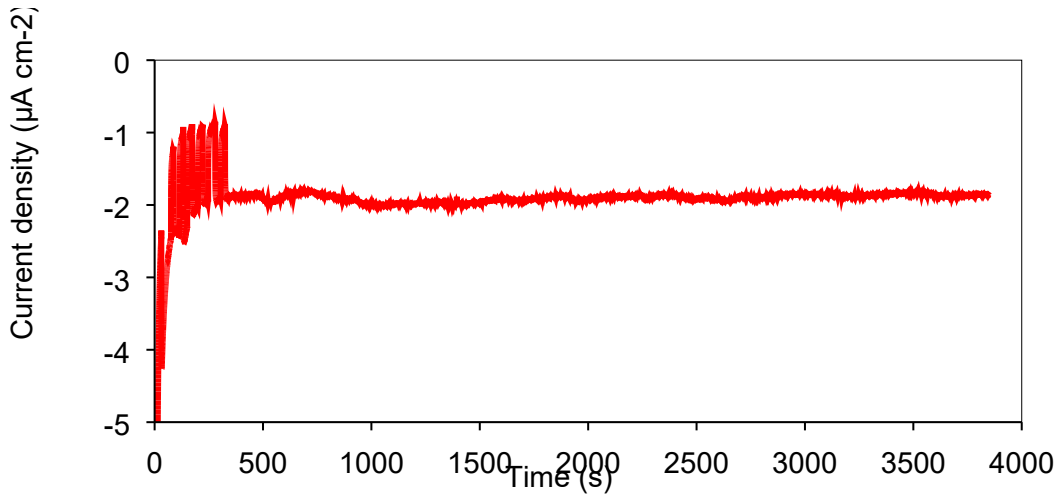

Figure S 56. Chronoamperometry data for an unsensitized NiO in pH 5 acetate buffer (saturated with CO_2) irradiated under 1 sun AM 1.5, (100 mW cm^{-2}) irradiation. The light output was chopped at the beginning of the experiment. Applied bias is -0.5 V vs Ag/AgCl.

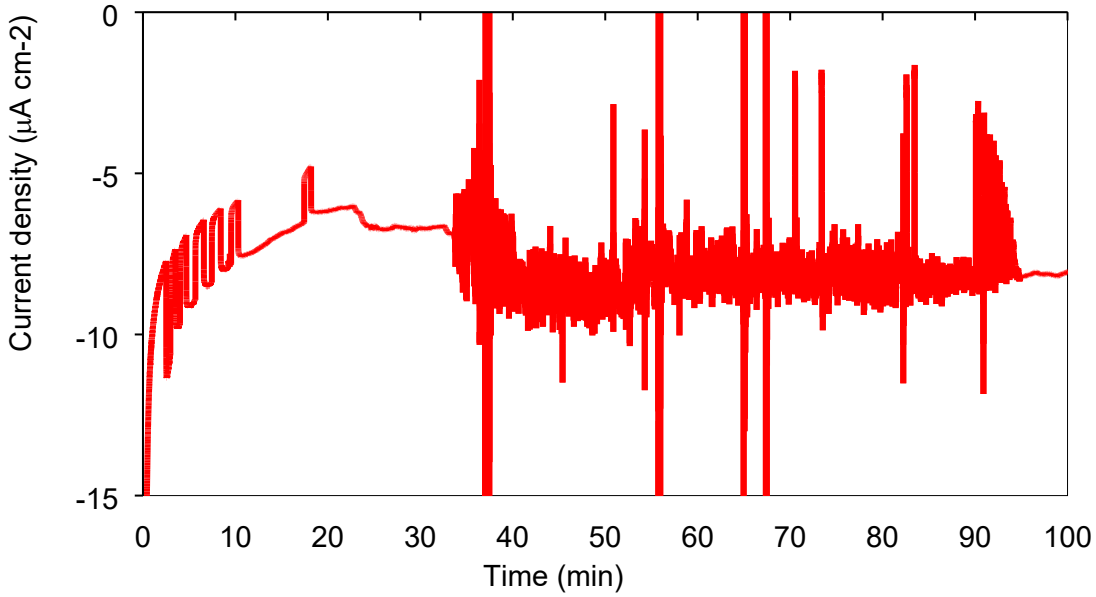

Figure S 57. Photocurrent density of PC1|NiO with an applied external bias of -0.5 V vs Ag/AgCl in pH 5 acetate buffer under an extended period 1 sun AM 1.5, (100 mW cm^{-2}) irradiation. The signal noise after 30 minutes is associated with the formation of gas bubbles on the working electrode.

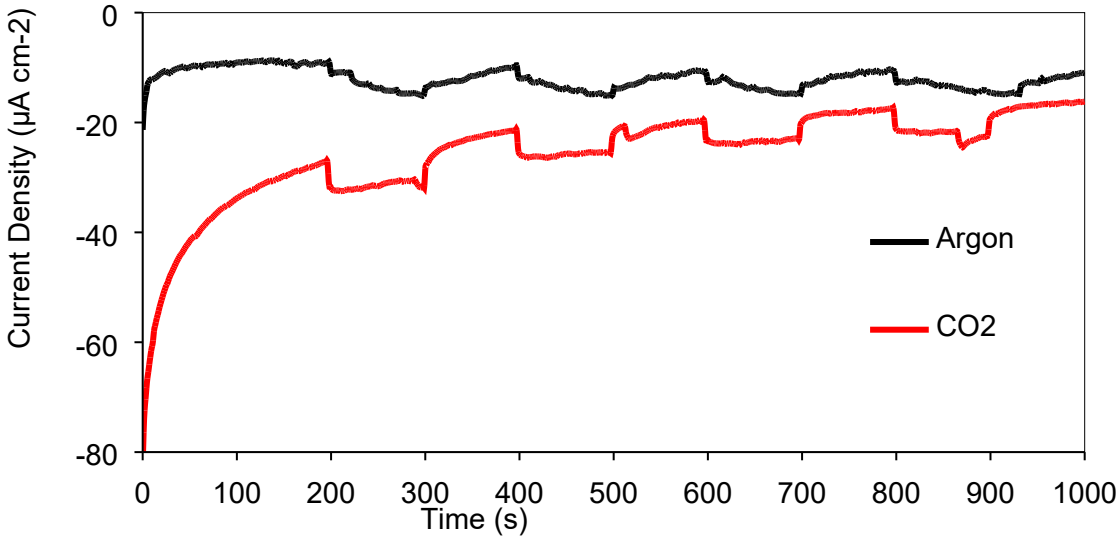

Figure S 58. Chronoamperometry data for PC1|NiO in pH 5 acetate buffer under 1 sun AM 1.5, (100 mW cm^{-2}) irradiation. The applied bias was -0.5 V vs Ag/AgCl both in the presence of argon and CO_2.

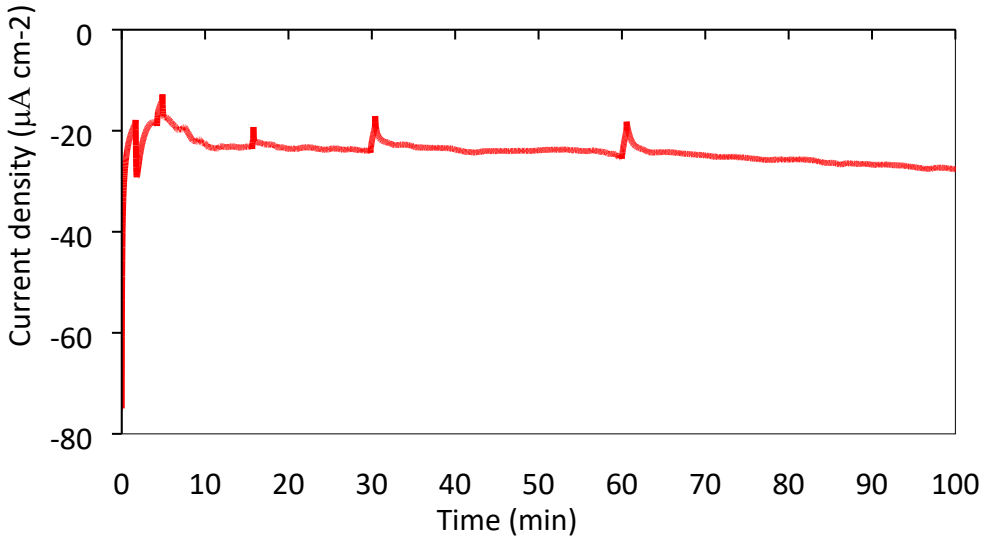

Figure S 59. Chronoamperometry data for PC2|NiO in pH 5 acetate buffer saturated with argon and irradiated under 1 sun AM 1.5, (100 mW cm^{-2}) irradiation. The applied bias was -0.5 V vs Ag/AgCl.

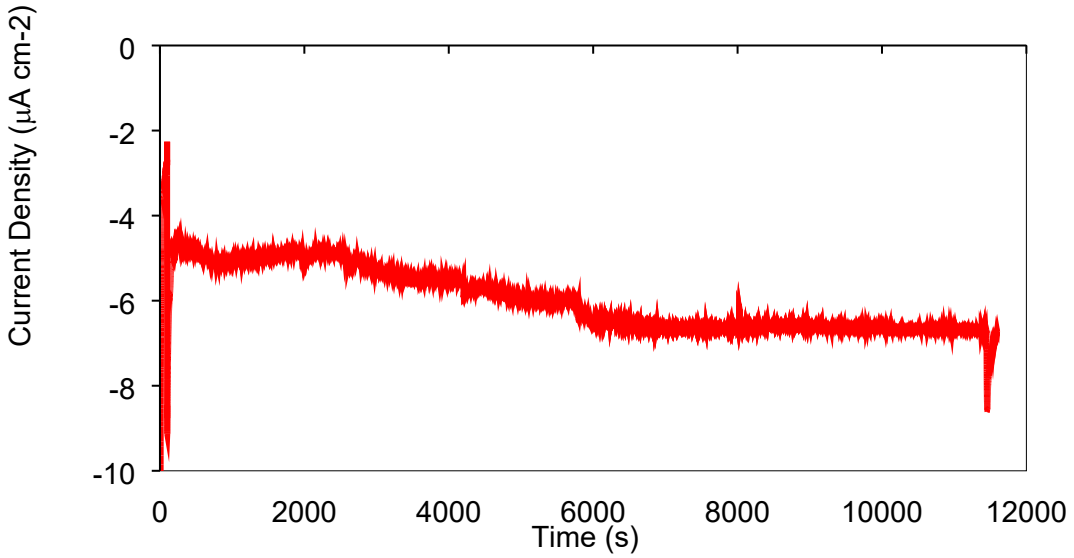

Figure S 60. Chronoamperometry data for PC3|NiO in pH 5 acetate buffer (saturated with CO_2) under 1 sun AM 1.5, (100 mW cm^{-2}) irradiation. Applied bias: -0.5 V vs Ag/AgCl.

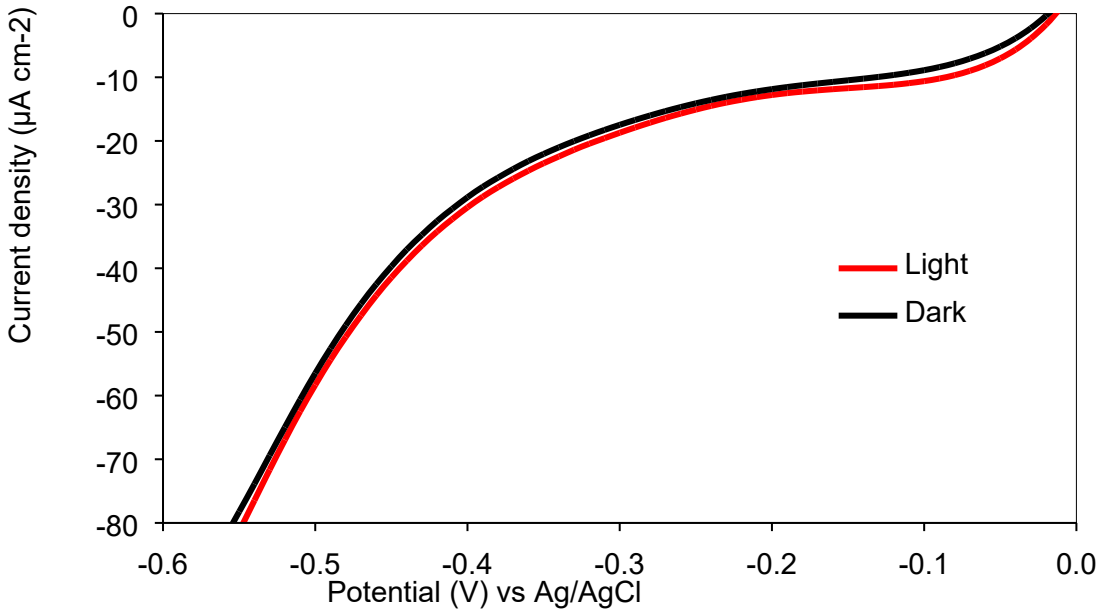

Figure S 61. Linear sweep measurements of a bare NiO film in pH 5 acetate buffer. The light measurement was under 1 sun AM 1.5, (100 mW cm^{-2}) irradiation. The cell was saturated with argon and the scan rate was 0.1 Vs^{-1}.

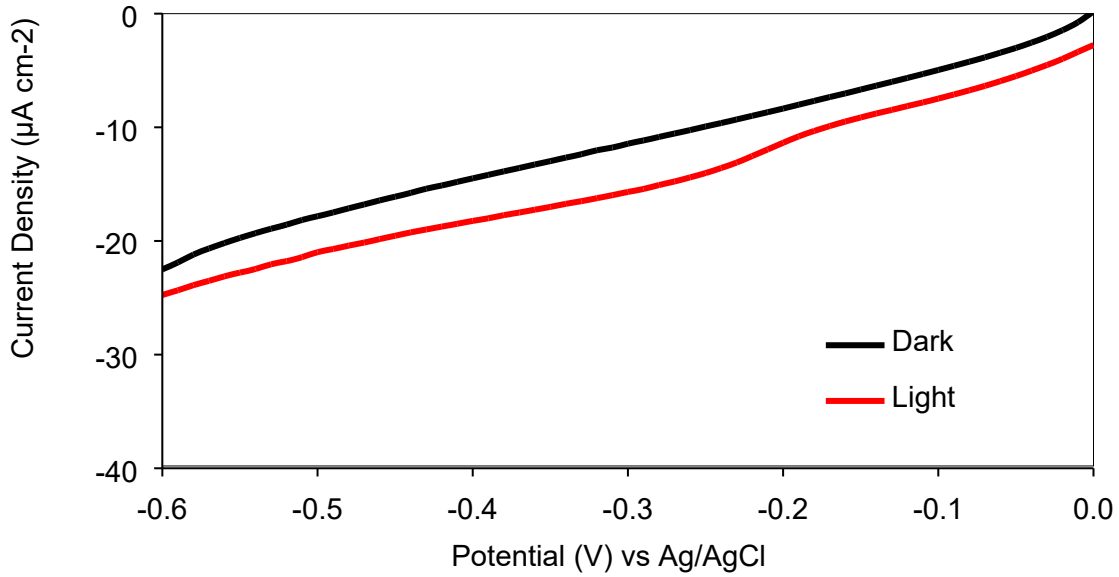

Figure S 62. Linear sweep measurements of PC1|NiO in pH 5 acetate buffer. The light measurement was under 1 sun AM 1.5 (100 mW cm^{-2}) illumination. The scan rate was 0.1 V s^{-1}. The cell was saturated with CO_2.

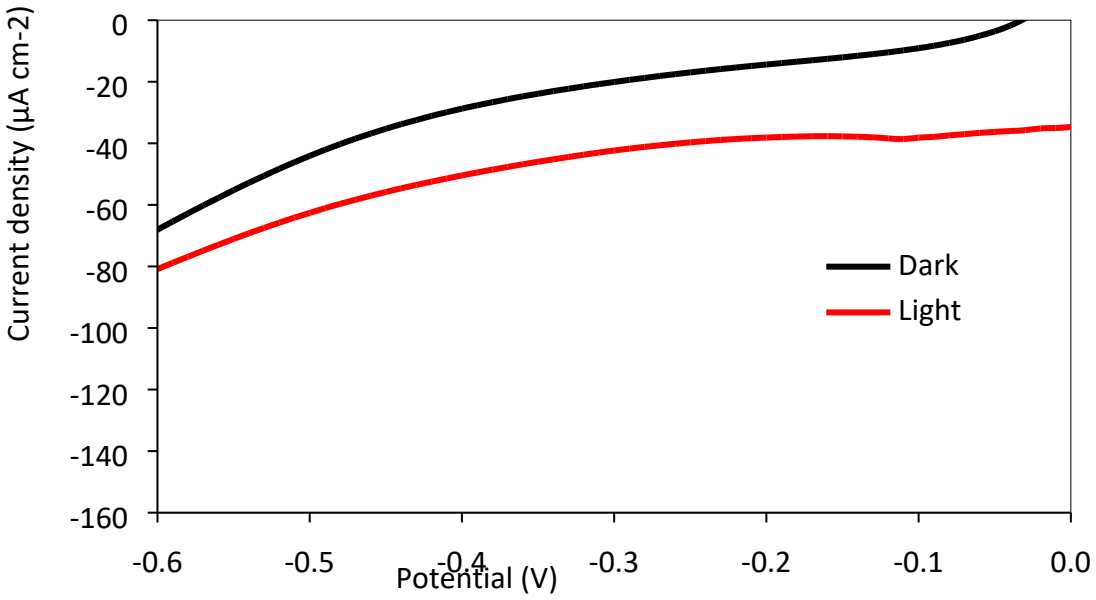

Figure S 63. Linear sweep measurements of PC2|NiO in pH 5 acetate buffer. The light measurement was under 1 sun AM 1.5 (100 mW cm^{-2}) illumination. The scan rate was 0.1 V s^{-1}. The cell was saturated with Ar.

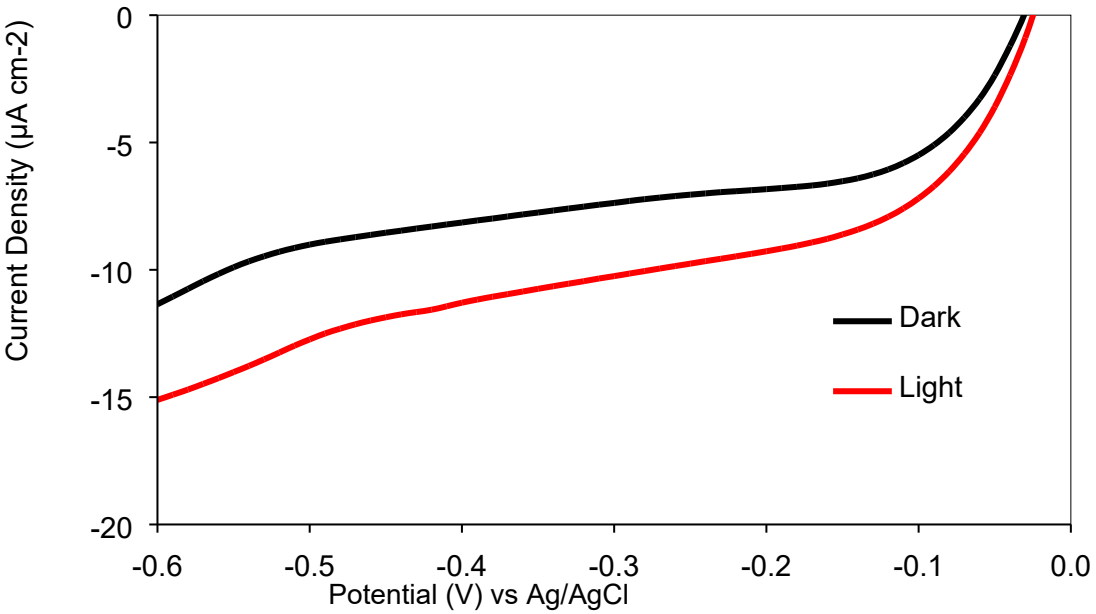

Figure S 64. Linear sweep measurements of PC3|NiO in pH 5 acetate buffer. The light measurement was under 1 sun AM 1.5 (100 mW cm^{-2}) illumination. The scan rate was 0.1 V s^{-1}. The cell was saturated with CO_2.

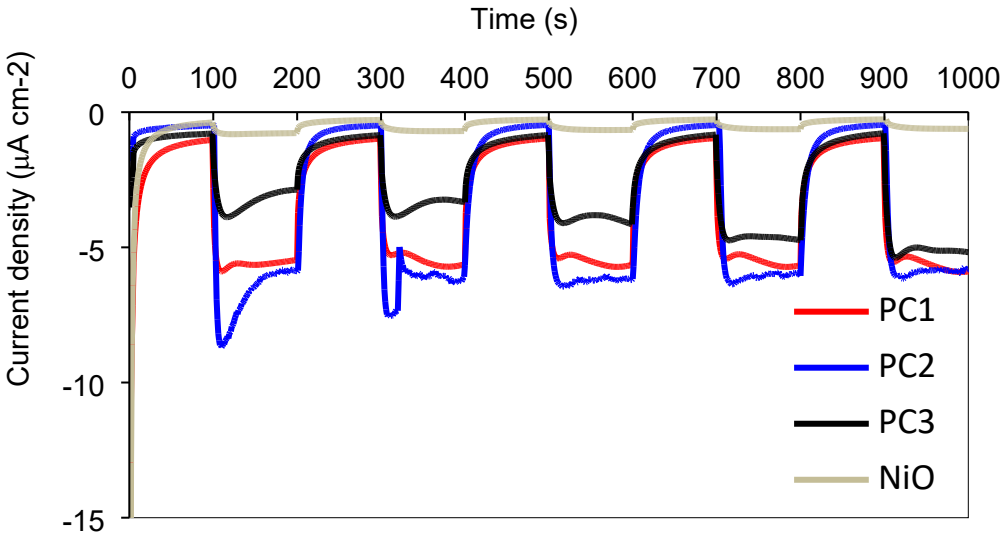

Figure S 65. Representative example of photocurrent densities from photoelectrocatalysis experiments of NiO films sensitized with photocatalysts in 0.1 M pH 5 acetate buffer under chopped 1 sun AM 1.5, (100 mW cm^{-2}) irradiation. The applied bias was -0.2 V vs Ag/AgCl. The reaction cell was saturated with CO_2 for unsensitized NiO, PC1|NiO and PC3|NiO. In the case of PC2|NiO, the cell was saturated with Ar. Bubbles at the surface caused the noisy photocurrent signal recorded.

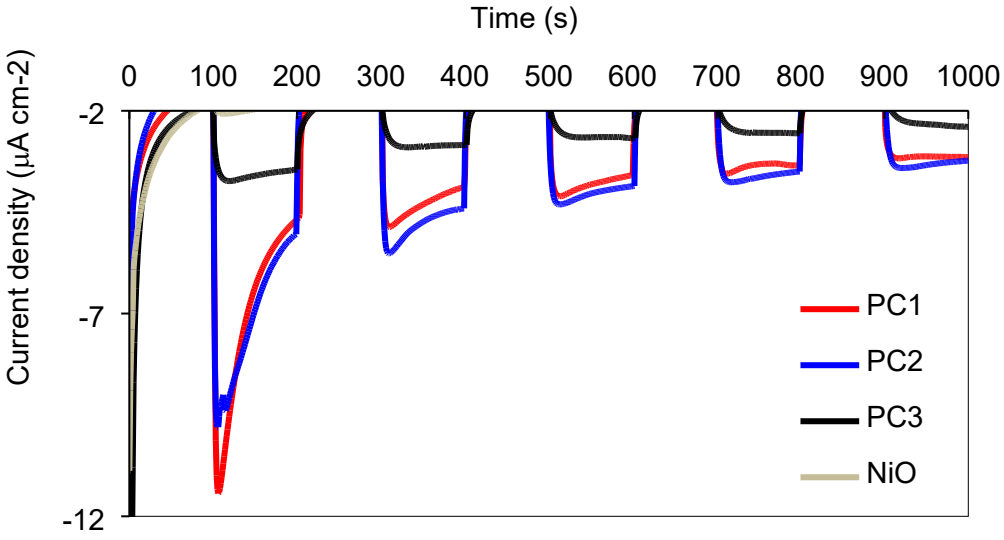

Figure S 66. Representative example of photocurrent densities from photoelectrocatalysis experiments of NiO films sensitized with photocatalysts in 50 mM pH 6.6 $NaHCO_2$ solution under chopped 1 sun AM 1.5, (100 mW cm^{-2}) irradiation. The applied bias was -0.2 V vs Ag/AgCl. The reaction cell was saturated with CO_2 for unsensitized NiO, PC1|NiO and PC3|NiO. In the case of PC2|NiO, the cell was saturated with Ar.

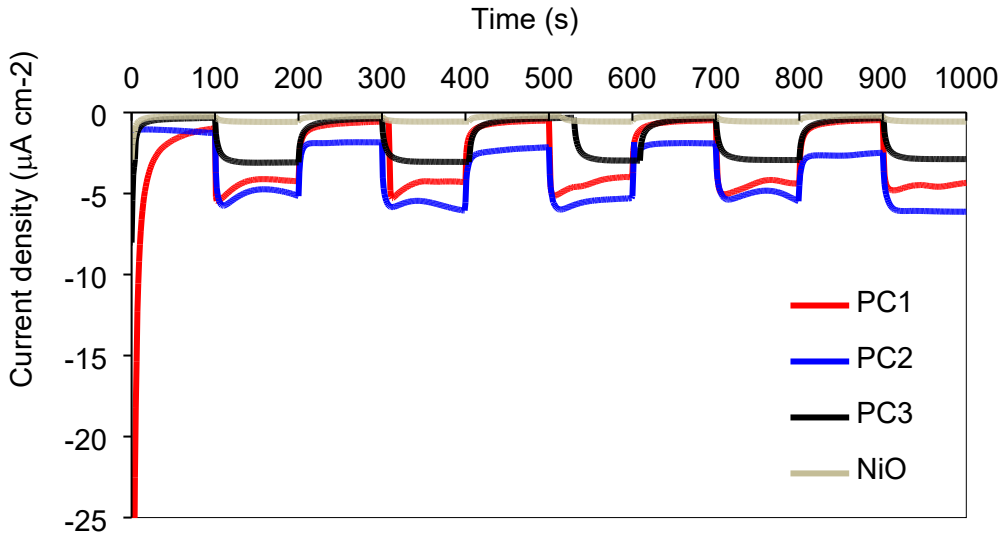

Figure S 67. Representative example of photocurrent from photoelectrocatalysis experiments of NiO films sensitized with photocatalysts in 0.1 M pH 8 phosphate buffer under chopped 1 sun AM 1.5, (100 mW cm^{-2}) irradiation. The applied bias was -0.2 V vs Ag/AgCl. The reaction cell was saturated with CO_2 for unsensitized NiO, PC1|NiO and PC3|NiO. In the case of PC2|NiO, the cell was saturated with Ar.

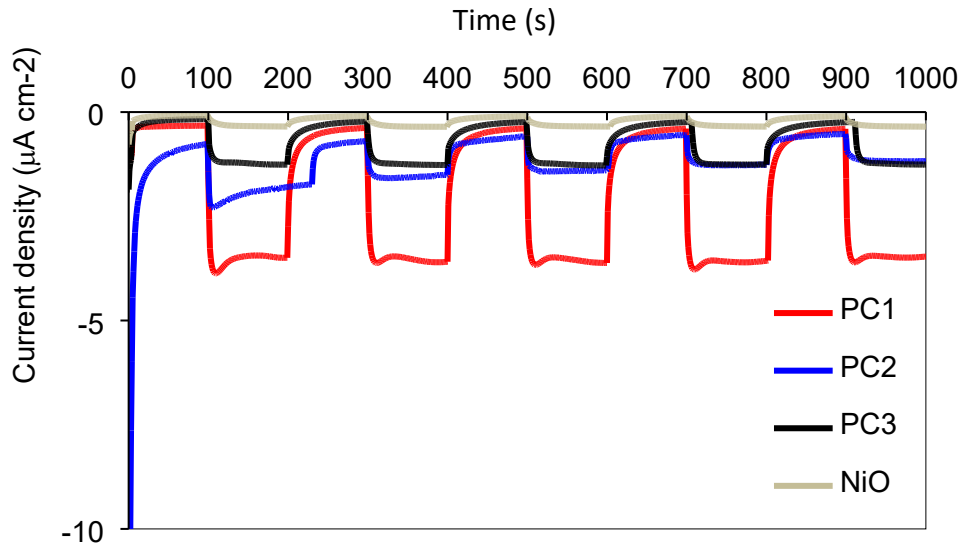

Figure S 68. Representative example of photocurrent densities from photoelectrocatalysis experiments of NiO films sensitized with photocatalysts in 0.1 M pH 9.2 carbonate buffer under chopped 1 sun AM 1.5, (100 mW cm^{-2}) irradiation. The applied bias was -0.2 V vs Ag/AgCl. The reaction cell was saturated with CO_2 for unsensitized NiO, PC1|NiO and PC3|NiO. In the case of PC2|NiO, the cell was saturated with Ar.

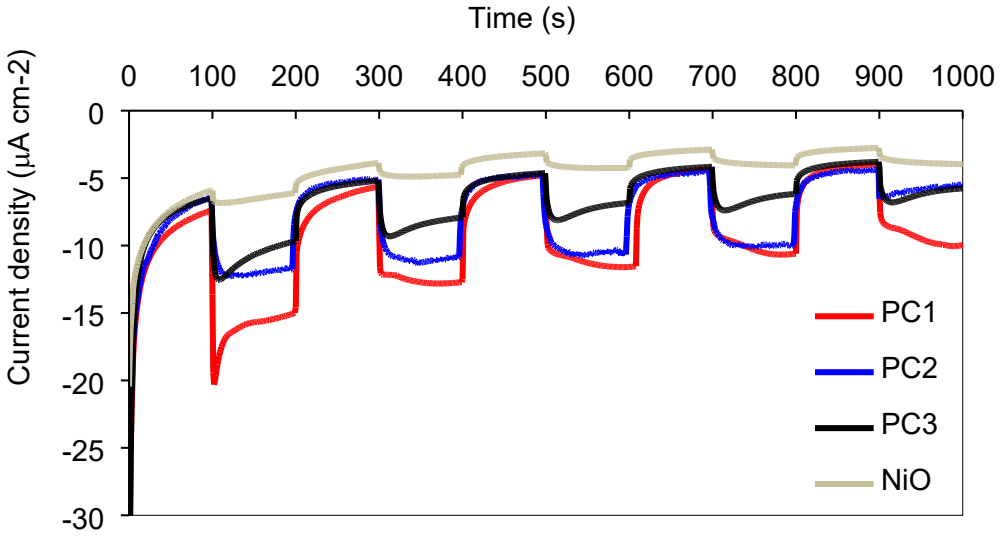

Figure S 69. Representative example of photocurrent from photoelectrocatalysis experiments of NiO films sensitized with photocatalysts in 0.1 M pH 5 acetate buffer under chopped 1 sun AM 1.5, (100 mW cm^{-2}) irradiation. The applied bias was -0.5 V vs Ag/AgCl. The reaction cell was saturated

with CO_2 for unsensitized NiO, PC1|NiO and PC3|NiO. In the case of PC2|NiO, the cell was saturated with Ar.

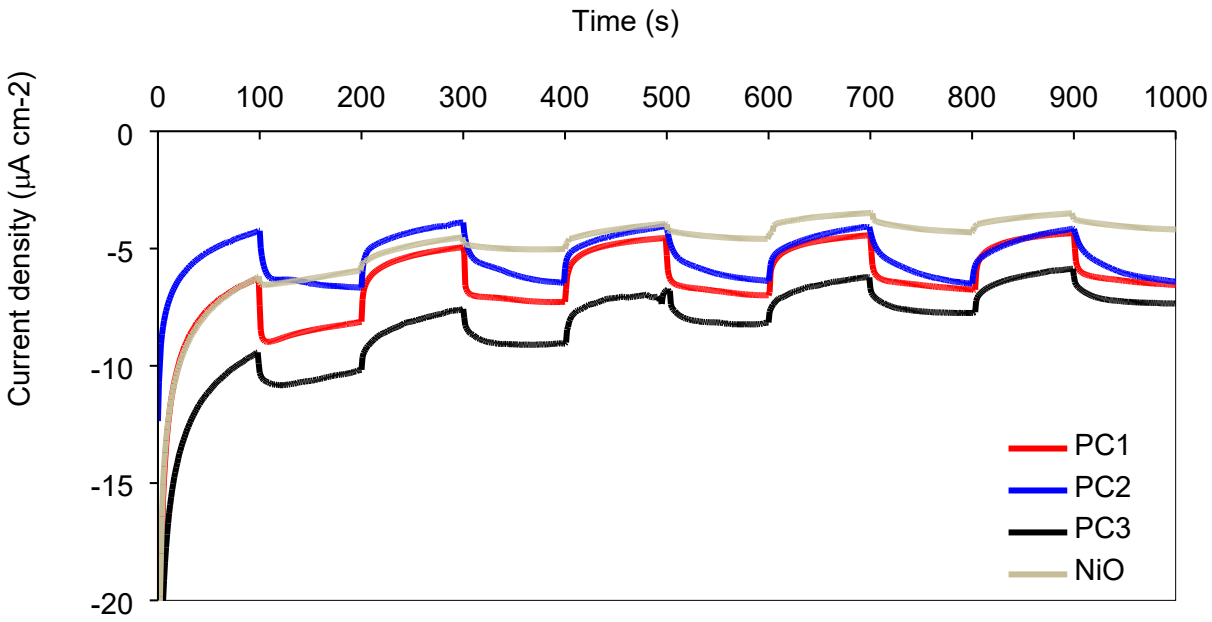

Figure S 70. Representative example of photocurrent densities from photoelectrocatalysis experiments of NiO films sensitized with photocatalysts in 50 µM pH 6.6 $NaHCO_2$ solution under chopped 1 sun AM 1.5, (100 mW cm^{-2}) irradiation. The applied bias was -0.5 V vs Ag/AgCl. The reaction cell was saturated with CO_2 for unsensitized NiO, PC1|NiO and PC3|NiO. In the case of PC2|NiO, the cell was saturated with Ar. Bubbles at the surface caused the noisy photocurrent signal recorded.

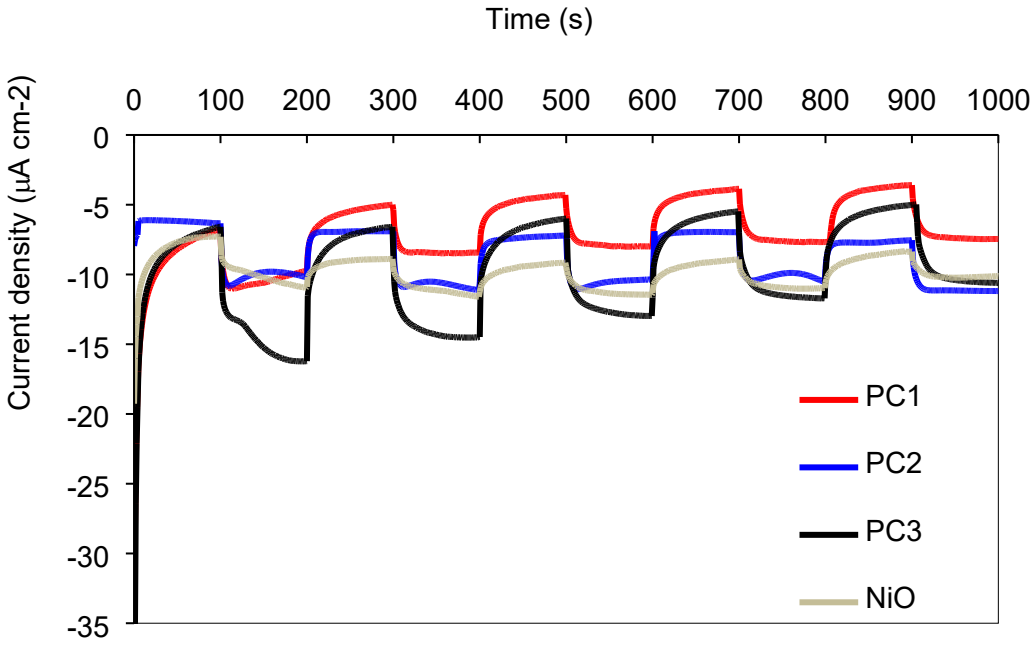

Figure S 71. Representative example of photocurrent from photoelectrocatalysis experiments of NiO films sensitized with photocatalysts in 0.1 M pH 8 phosphate buffer under chopped 1 sun AM 1.5, (100 mW cm^{-2}) irradiation. The applied bias was -0.5 V vs Ag/AgCl. The reaction cell was saturated with CO_2 for unsensitized NiO, PC1|NiO and PC3|NiO. In the case of PC2|NiO, the cell was saturated with Ar.

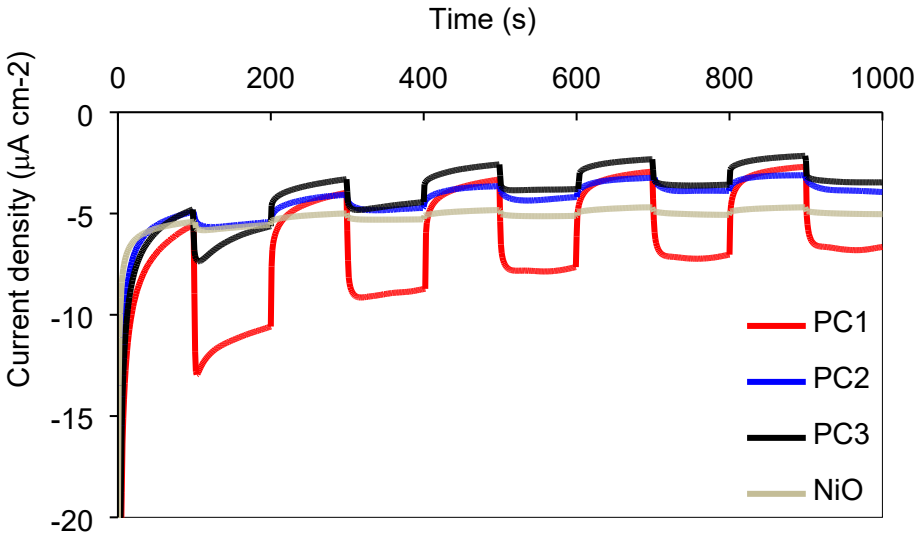

Figure S 72. Representative example of photocurrent from photoelectrocatalysis experiments of NiO films sensitized with photocatalysts in 0.1 M pH 9.2 carbonate buffer under chopped 1 sun AM 1.5, (100 mW cm^{-2}) irradiation. The applied bias was -0.5 V vs Ag/AgCl. The reaction cell was saturated with CO_2 for unsensitized NiO, PC1|NiO and PC3|NiO. In the case of PC2|NiO, the cell was saturated with Ar.

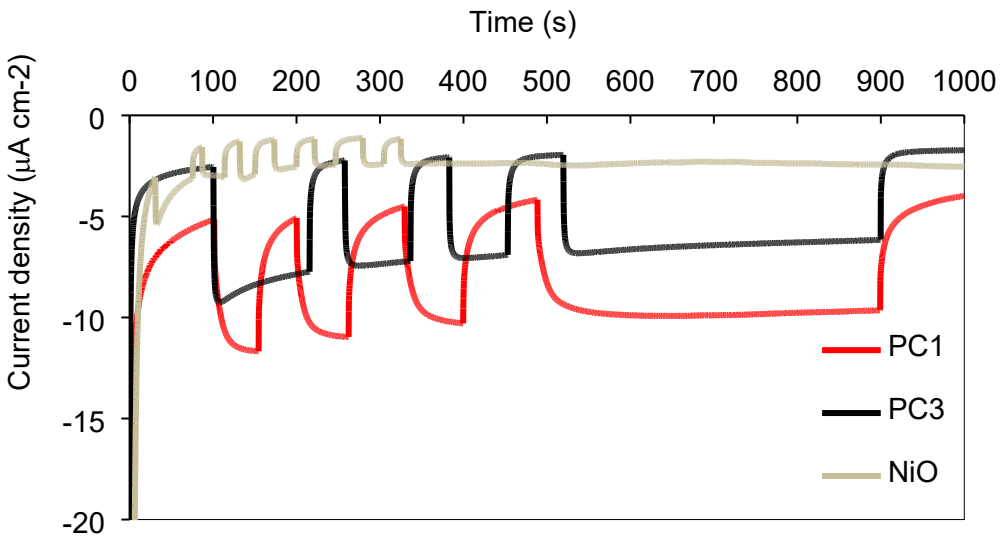

Figure S 73. Representative example of photocurrent from photoelectrocatalysis experiments of NiO films sensitized with photocatalysts in 1-ethyl-3-methylimidazolium bis(trifluoromethylsulfonyl)imide under 1 sun AM 1.5, (100 mW cm^{-2}) irradiation. The applied bias was -0.5 V vs Ag/AgCl. The cell was saturated with CO_2 in each case.

Table S1. Summary of average photocurrent densities obtained under chopped 1 sun AM 1.5, (100 mW cm^{-2}) irradiation for photocatalysts systems under different conditions where the applied external bias -0.2 Volts vs Ag/AgCl. The information here is obtained from a 15 minute experiment, extracting the average.

Photocatalyst	Current density / pH 5 (μA cm^{-2})	Current density / pH 6.6 (μA cm^{-2})	Current density / pH 8 (μA cm^{-2})	Current density / pH 9.2 (μA cm^{-2})	Current density / Ionic liquid * (μA cm^{-2})
PC1	4.6	2.9	3.8	3.1	3.3
PC2	5.7	3.5	3.7	0.9	X
PC3	4.1	1.4	6.8	1.0	3.7

*Note the ionic liquid is 1-ethyl-3-methylimidazolium bis(trifluoromethylsulfonyl)imide.

Table S2. Summary of average photocurrent densities obtained under chopped 1 sun AM 1.5, (100 mW cm^{-2}) irradiation for photocatalysts systems under different conditions where the applied external bias -0.5 V vs Ag/AgCl. The information here is obtained from a 15 minute experiment, extracting the average.

Photocatalyst	Current density / pH 5 ($\mu A\ cm^{-2}$)	Current density / pH 6.6 ($\mu A\ cm^{-2}$)	Current density / pH 8 ($\mu A\ cm^{-2}$)	Current density / pH 9.2 ($\mu A\ cm^{-2}$)	Current density / Ionic liquid * ($\mu A\ cm^{-2}$)
PC1	6.80	2.6	3.70	4.73	6.50
PC2	5.88	2.3	3.9	2.7	X
PC3	3.20	1.4	3.90	1.90	5.30

*1-ethyl-3-methylimidazolium bis(trifluoromethylsulfonyl)imide.

S5. Gas Chromatography

GC Method (as described in the experimental section):

Gas chromatography (GC) measurements were performed with a Shimadzu GC-2014 instrument where a thermal conductivity detector at 200 ^{o}C (TCD) and flame-ionisation detector (FID) at 250 ^{o}C operated in tandem. A Restek ShinCarbon ST 80/100 packed column (2 metre, 2 mm ID) was used with argon as the carrier gas. The initial oven temperature was 50 ^{o}C with a temperature ramp to 200 ^{o}C (after an initial period of 2 mins at 50 ^{o}C) at a rate of 15 ^{o}C min^{-1}, followed by a final hold time of 10 mins.

In the selection below are results for gas analysis of photocatalysis products under various conditions. For all gas chromatography measurements the injection volume was 0.5 ml. We estimate the error from gas chromatography measurements at 4 % from repeats of calibration gas standard samples. Note that carbon monoxide is detected with an FID and hydrogen is determined using a TCD.

Calculation of Faradaic Efficiency and Turnover Frequencies:

Where the quantity of evolved gaseous products was measured for a photoelectrocatalytic experiment by means of gas chromatography (either hydrogen or carbon monoxide in this case), faradaic efficiencies were determined by the method outlined below for the following reactions.

$$CO_2 + 2H^+ + 2e^- \rightarrow CO + H_2O$$

or

$$4H^+ + 4e^- \rightarrow 2H_2$$

The faradaic efficiency $\eta_{far} = \frac{Q_{exp}}{Q_{theo}}$ where Q_{exp} reflects the number of moles of gaseous product and Q_{theo} the overall charge passed in the photoelectrocatalytic experiment. Q_{theo} is obtained directly from experimental data, integrating current over the duration of the experiment. Q_{exp} = n x F x moles product where n is the number of electrons involved in the reaction and F is Faraday's constant.

The turnover frequency $TOF = \frac{n_{product}}{n_{catalyst}\, x\, t}$ where $n_{product}$ is the number of moles of evolved gaseous product and $n_{catalyst}$ is the number of moles photocatalyst (estimated from the dye-loading on NiO), and t is the time of the experiment.

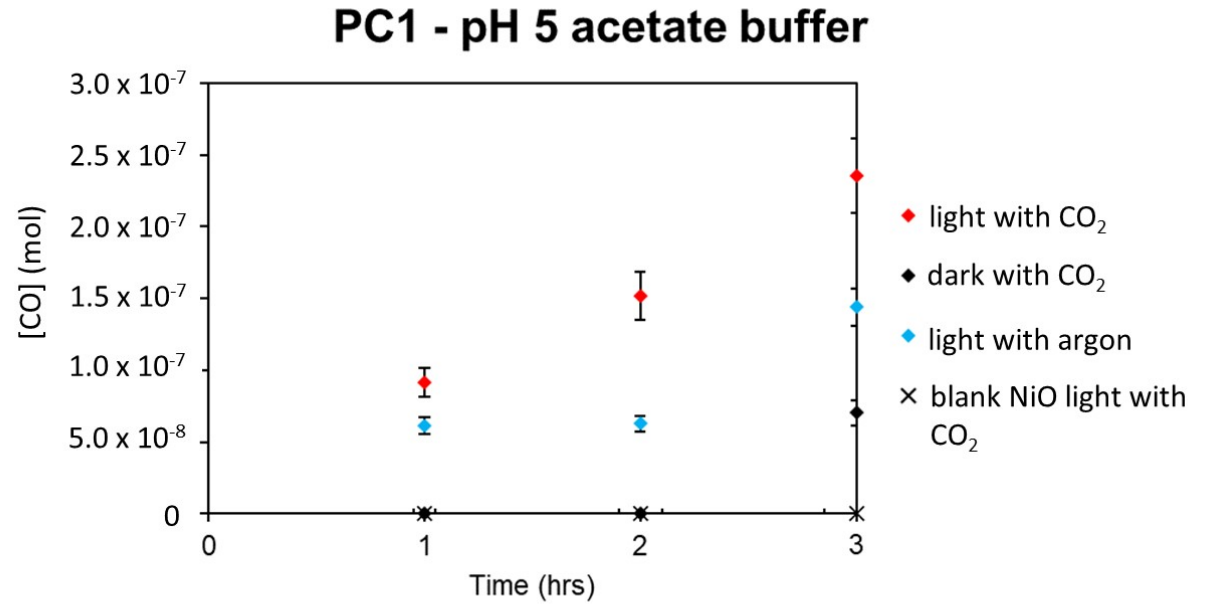

Figure S 74. PC1|NiO thin film evolved CO detected by gas chromatography in 0.1 M pH 5 acetate buffer with an applied bias of -0.5 V vs Ag/AgCl under 1 sun AM 1.5, (100 mW cm^{-2}) irradiation. The experiment in the light under Ar and in the dark did produce a small amount of CO, possibly from the acetate buffer.

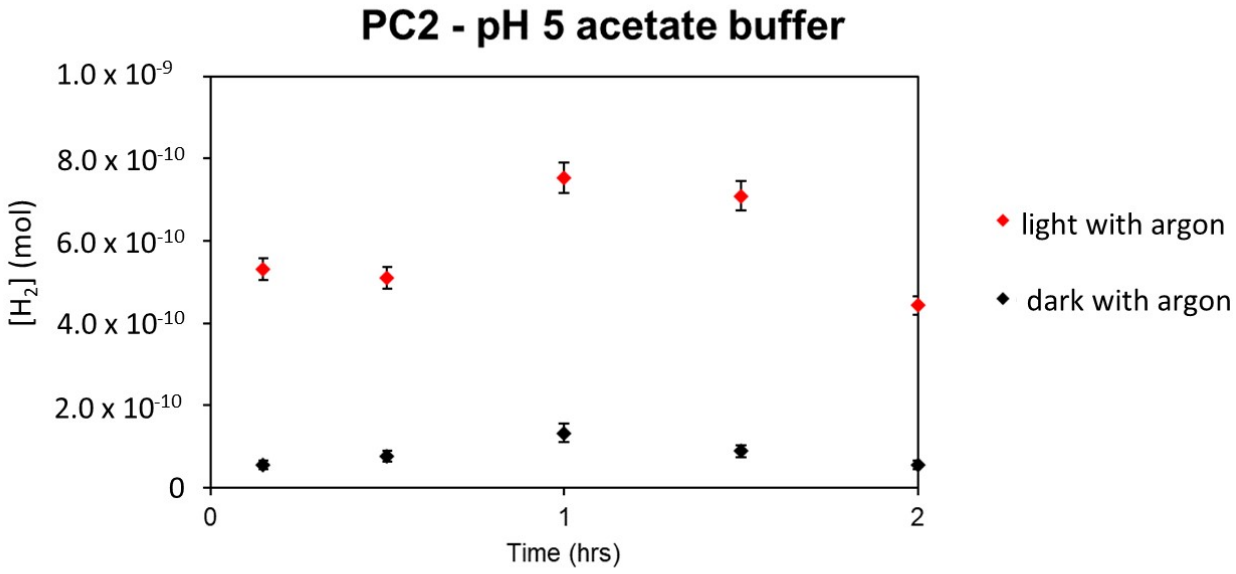

Figure S 75. PC2|NiO thin film evolved CO detected by gas chromatography in 0.1 M pH 5 acetate buffer with an applied bias of -0.5 V vs Ag/AgCl under 1 sun AM 1.5, (100 mW cm^{-2}) irradiation.

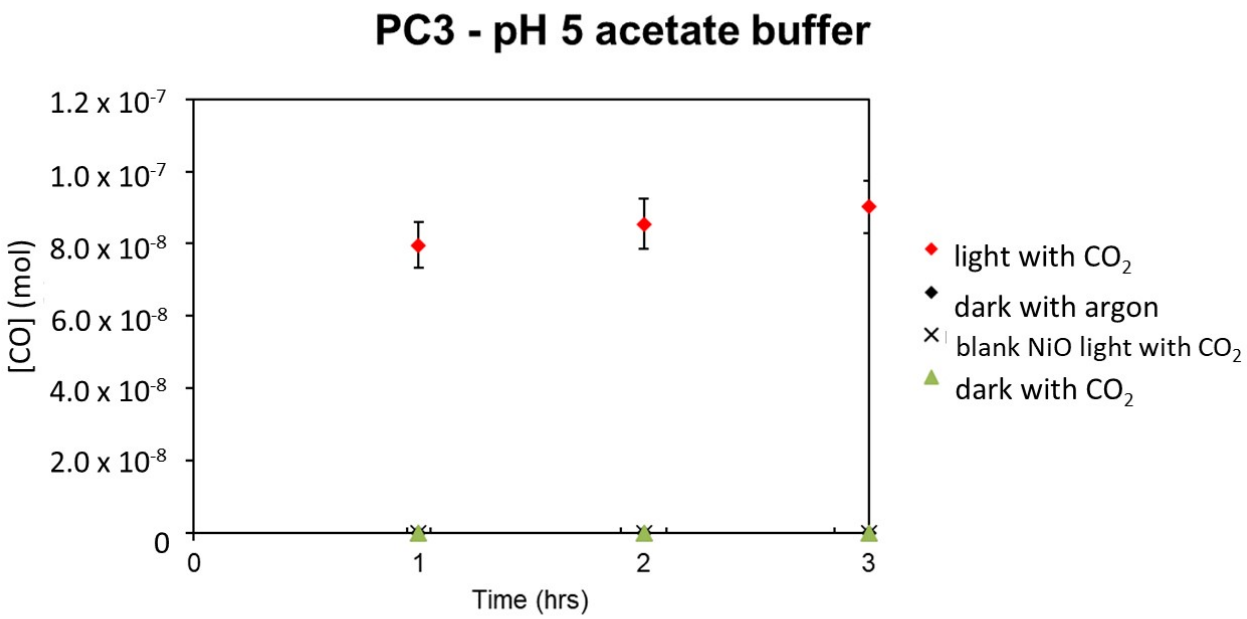

Figure S 76. PC3|NiO thin film evolved CO detected by gas chromatography in 0.1 M pH 5 acetate buffer with an applied bias of -0.5 V vs Ag/AgCl under 1 sun AM 1.5, (100 mW cm^{-2}) irradiation.

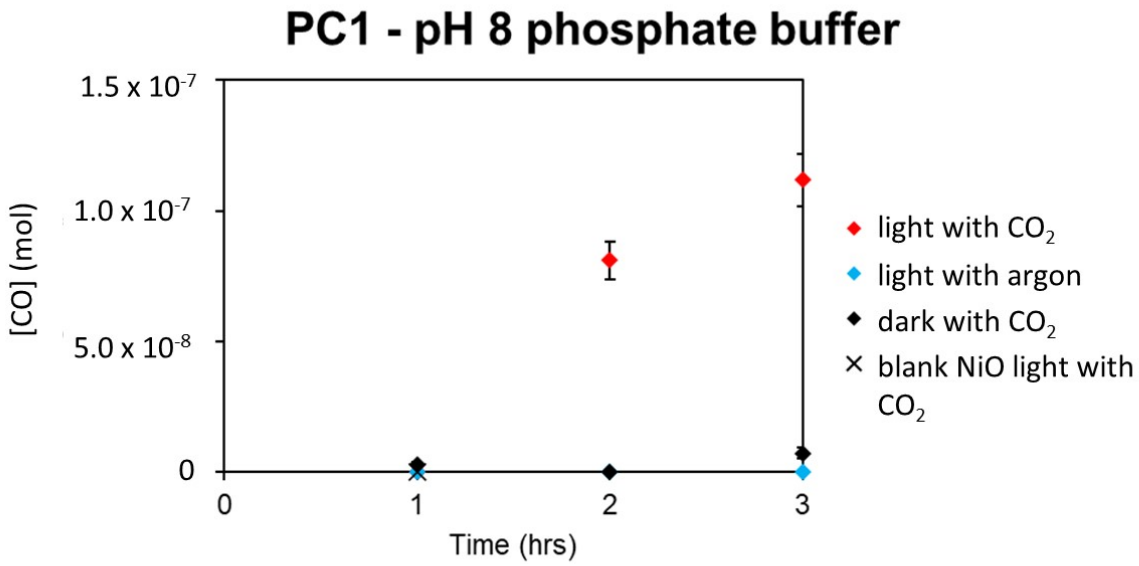

Figure S 77. PC1|NiO thin film evolved CO detected by gas chromatography in 0.1 M pH 8 phosphate buffer with an applied bias of -0.5 V vs Ag/AgCl under 1 sun AM 1.5 (100 mW cm^{-2}) irradiation.

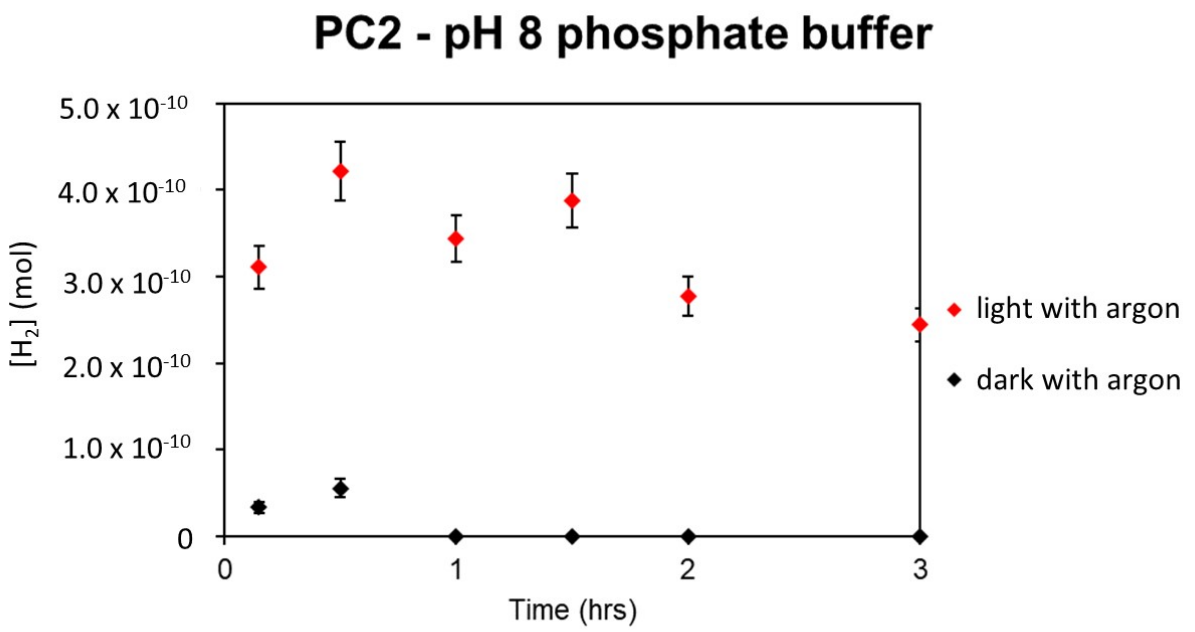

Figure S 78. PC2|NiO thin film evolved hydrogen detected by gas chromatography in 0.1 M pH 8 phosphate buffer with an applied bias of -0.5 V vs Ag/AgCl under 1 sun AM 1.5, (100 mW cm^{-2}) irradiation.

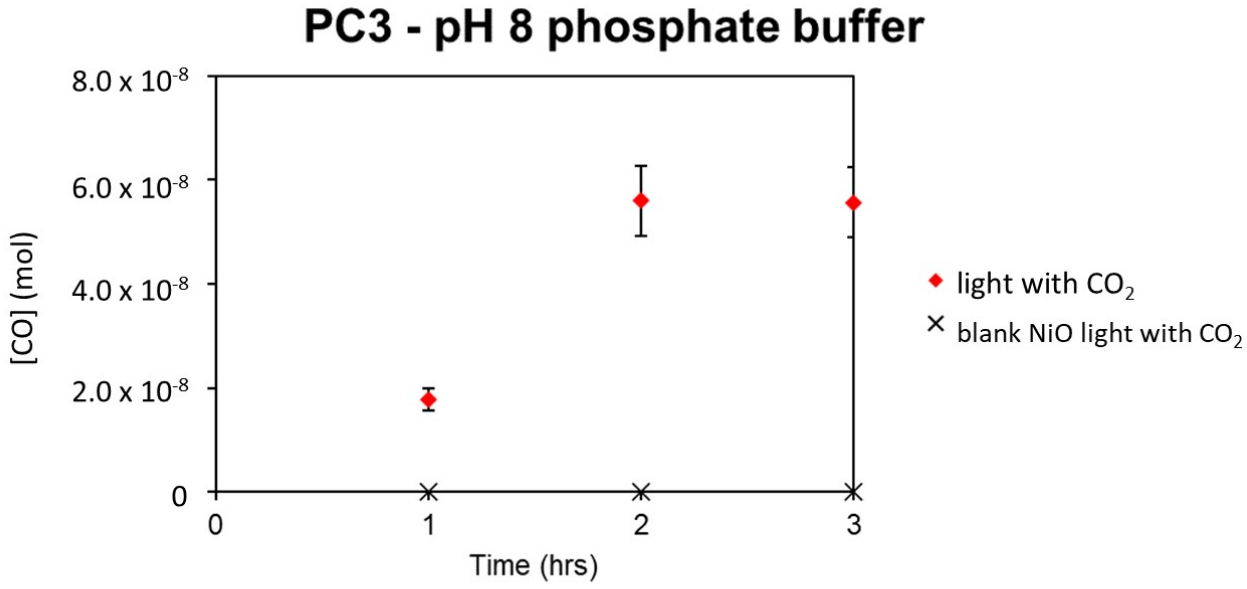

Figure S 79. PC3|NiO thin film evolved CO detected by gas chromatography in 0.1 M pH 8 phosphate buffer with an applied bias of -0.5 V vs Ag/AgCl under 1 sun AM 1.5, (100 mW cm^{-2}) irradiation.

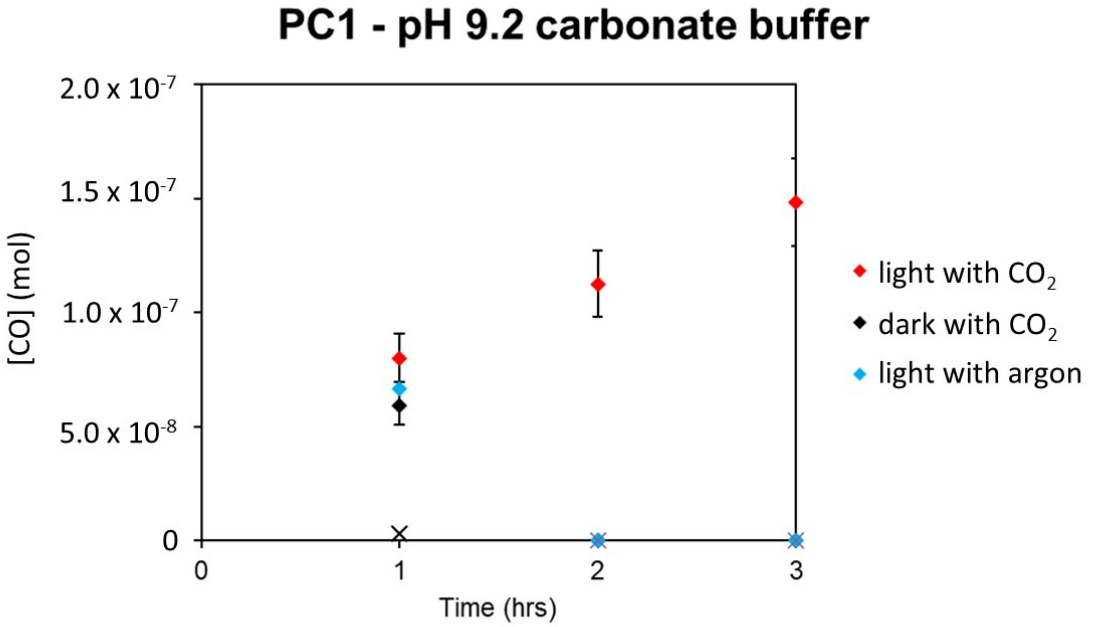

Figure S 80. PC1|NiO thin film evolved CO detected by gas chromatography in 0.1 M pH 9.2 carbonate buffer with an applied bias of -0.5 V vs Ag/AgCl under 1 sun AM 1.5, (100 mW cm^{-2}) irradiation.

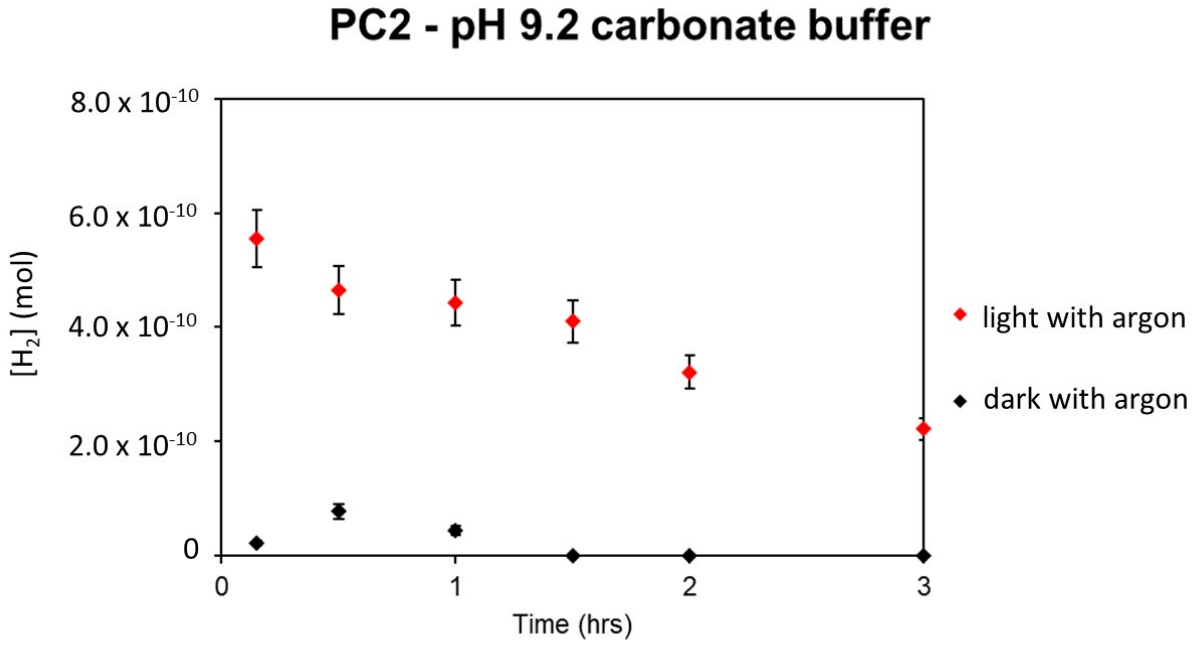

Figure S 81. PC2|NiO thin film evolved hydrogen detected by gas chromatography in 0.1 M pH 9.2 carbonate buffer with an applied bias of -0.5 V vs Ag/AgCl under 1 sun AM 1.5, (100 mW cm^{-2}) irradiation.

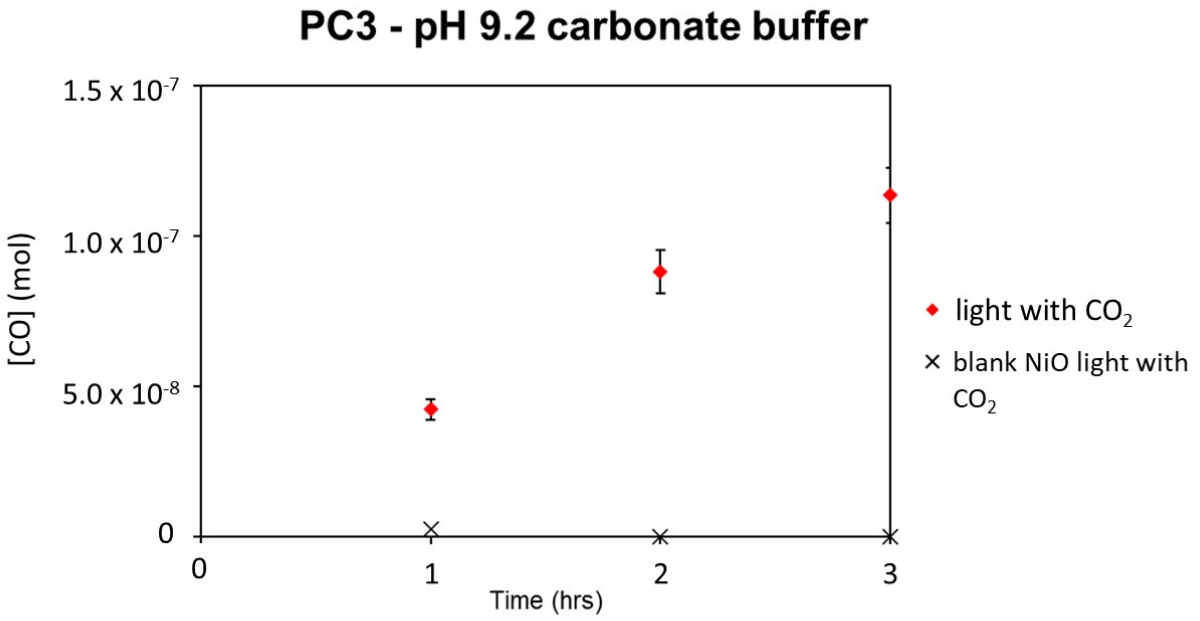

Figure S 82. PC3|NiO thin film evolved CO detected by gas chromatography in 0.1 M pH 9.2 carbonate buffer with an applied bias of -0.5 V vs Ag/AgCl under 1 sun AM 1.5, (100 mW cm^{-2}) irradiation.

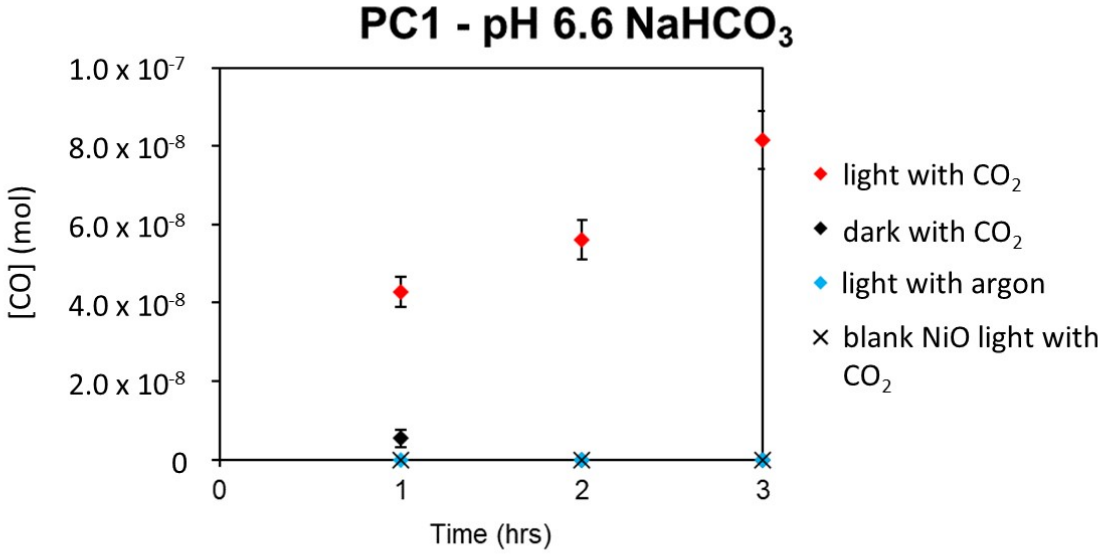

Figure S 83. PC1|NiO thin film evolved CO detected by gas chromatography in 50 mM pH 6.6 $NaHCO_3$ solution with an applied bias of -0.5 V vs Ag/AgCl under 1 sun AM 1.5, (100 mW cm^{-2}) irradiation.

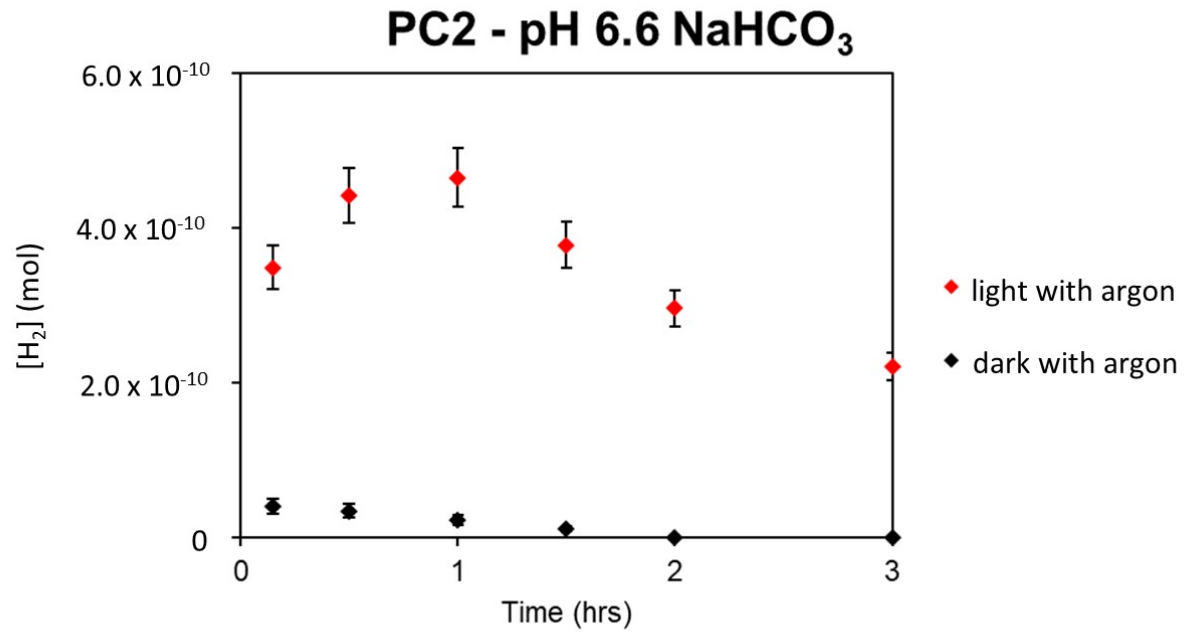

Figure S 84. PC2|NiO thin film evolved hydrogen detected by gas chromatography in 50 μM pH 6.6 $NaHCO_3$ solution with an applied bias of -0.5 V vs Ag/AgCl under 1 sun AM 1.5, (100 mW cm^{-2}) irradiation.

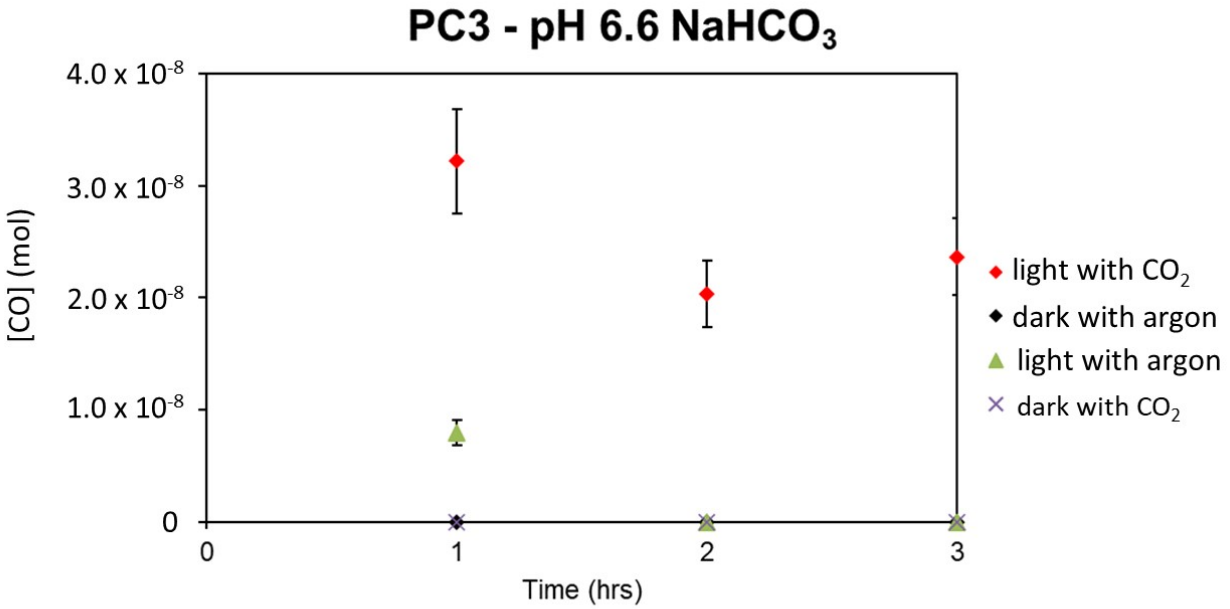

Figure S 85. PC3|NiO thin film evolved CO detected by gas chromatography in 50 mM pH 6.6 $NaHCO_3$ solution with an applied bias of -0.5 V vs Ag/AgCl under 1 sun AM 1.5, (100 mW cm^{-2}) irradiation.

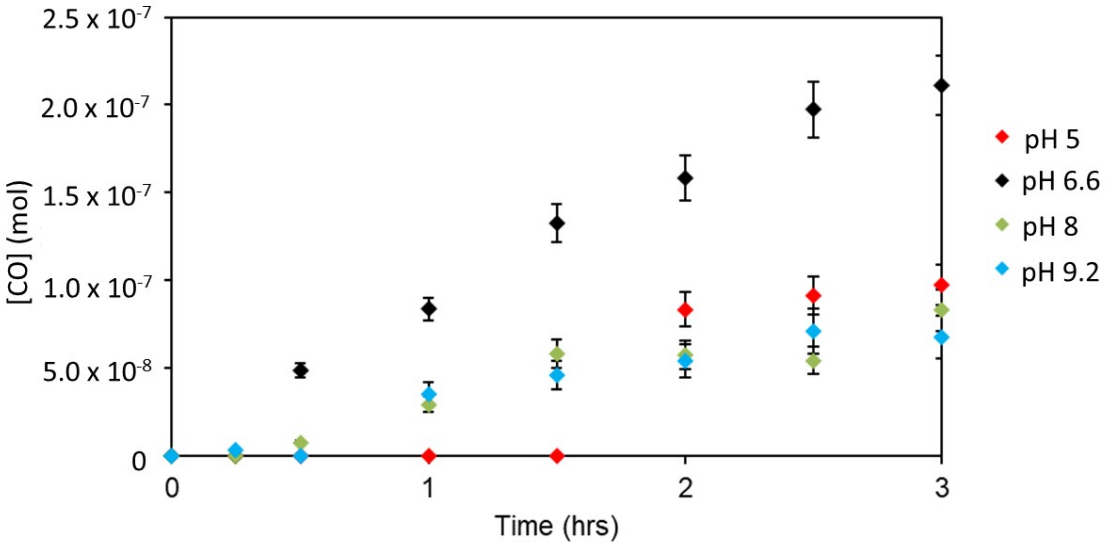

Figure S 86. PC1|NiO thin film evolved CO detected by gas chromatography in with an applied bias of -0.2 V vs Ag/AgCl under 1 sun AM 1.5, (100 mW cm^{-2}) irradiation in various pH buffer solutions as described earlier. Note the pH 6.6 is 50 mM $NaHCO_3$ solution.

	Applied Potential (V) vs Ag/AgCl	Electrolyte	Charge (C)	Electrons (mol)	CO peak (1 hr)	CO peak (2hrs)	CO peak (3hrs)	[CO] 1 hr (mol)	[CO] 2 hrs (mol)	[CO] 3 hrs (mol)	H_2 peak (1hr)	H_2 peak (2hrs)	H_2 peak (3hrs)	$[H_2]$ / mol (1hr)	$[H_2]$ / mol (2hrs)	$[H_2]$ / mol (3hrs)
PC1 (Light)	-0.5	pH 5 (with CO_2)	0.0498	5.16×10^{-7}	3058	5097	7891	9.12×10^{-8}	1.52×10^{-7}	2.36×10^{-7}	481	780	919	5.33×10^{-9}	8.65×10^{-9}	1.02×10^{-8}
PC1 (Light)	-0.5	pH 5 (with argon)	0.0586	6.07×10^{-7}	2056	2102	4831	6.14×10^{-8}	6.27×10^{-8}	1.44×10^{-7}	2	69	142	2.22×10^{-11}	7.65×10^{-10}	1.57×10^{-9}
PC1 (Dark)	-0.5	pH 5 (with CO_2)	0.0264	2.74×10^{-7}	0	0	2353	0	0	7.02×10^{-8}	0	0	66	0	0	7.32×10^{-10}

	Applied Potential (V)	Electrolyte	Charge (C)	Electrons (mol)	H_2 peak (15 mins)	H_2 peak (30 mins)	H_2 peak (1hrs)	H_2 peak (1.5hrs)	H_2 peak (2hrs)	$[H_2]$ / mol (15mins)	$[H_2]$ / mol (30mins)	$[H_2]$ / mol (1hrs)	$[H_2]$ / mol (1.5hrs)	$[H_2]$ / mol (2hrs)		
PC2 (Light)	-0.5	pH 5 (with argon)	0.0180	1.87×10^{-7}	48	46	68	64	40	5.32×10^{-10}	5.1×10^{-10}	7.53×10^{-10}	7.10×10^{-10}	4.44×10^{-10}		
PC2 (Dark)	-0.5	pH 5 (with argon)	0.0070	7.26×10^{-8}	5	7	12	8	5	negligible	-	-	-	-		

	Applied Potential (V) vs Ag/AgCl	Electrolyte	Charge (C)	Electrons (mol)	CO peak (1 hr)	CO peak (2hrs)	CO peak (3hrs)	[CO] 1 hr (mol)	[CO] 2 hrs (mol)	[CO] 3 hrs (mol)	H_2 peak (1hr)	H_2 peak (2hrs)	H_2 peak (3hrs)	$[H_2]$ / mol (1hr)	$[H_2]$ / mol (2hrs)	$[H_2]$ / mol (3hrs)
PC3 (Light)	-0.5	pH 5 (with CO_2)	0.0447	4.63×10^{-7}	2666	2864	3022	7.96×10^{-8}	8.55×10^{-8}	9.02×10^{-8}	278	532	691	3.08×10^{-9}	5.90×10^{-9}	7.66×10^{-9}
PC3 (Dark)	-0.5	pH 5 (with argon)	0.0112	1.16×10^{-7}	0	0	0	0	0	0	0	0	0	0	0	0
PC3 (Light)	-0.5	pH 5 (with argon)	0.0883	9.15×10^{-7}	349	1082	1396	1.04×10^{-8}	3.22×10^{-8}	3.17×10^{-8}	0	0	0	0	0	0
PC3 (Dark)	-0.5	pH 5 (with CO_2)	0.0486	5.03×10^{-7}	0	0	0	0	0	0	0	0	0	0	0	0

NiO Blank Film (Light)	-0.5	pH 5 (with CO_2)	0.0191	1.98×10^{-7}	0	0	0	0	0	0	0	0	0	0	0	0
NiO Blank Film (Dark)	-0.5	pH 5 (with CO_2)	0.0182	1.89×10^{-7}	0	0	0	0	0	0	0	0	0	0	0	0

Table S3. Matrix of GC experiments with the photocatalysts in 0.1 M pH 5 acetate buffer. All light experiments are under simulated 1 sun AM 1.5 light (100 mW cm^{-2}).

	Applied Potential (V)	Electrolyte	Charge (C)	Electrons (mol)	CO peak (1 hr)	CO peak (2 hrs)	CO peak (3 hrs)	[CO] 1 hr (mol)	[CO] 2 hrs (mol)	[CO] 3 hrs (mol)	H_2 peak (1hr)	H_2 peak (2 hrs)	H_2 peak (3 hrs)	[H_2] / mol (1 hr)	[H_2] / mol (2 hrs)	[H_2] / mol (3 hrs)
PC1 (Light)	-0.5	pH 6.6 $NaHCO_3$ (with CO_2)	0.0519	5.38×10^{-7}	2712	3569	5178	4.27×10^{-8}	5.61×10^{-8}	8.15×10^{-8}	9	0	0	5.24×10^{-11}	0	0
PC1 (Light)	-0.5	pH 6.6 $NaHCO_3$ (with argon)	0.0455	4.72×10^{-7}	0	0	0	0	0	0	0	0	0	0	0	0
PC1 (Dark)	-0.5	pH 6.6 $NaHCO_3$ (with CO_2)	0.00766	7.94×10^{-8}	340	0	0	5.35×10^{-9}	0	0	0	0	0	0	0	0

	Applied Potential (V)	Electrolyte	Charge (C)	Electrons (mol)	H_2 peak (15 mins)	H_2 peak (30 mins)	H_2 peak (1 hrs)	H_2 peak (1.5 hrs)	H_2 peak (2 hrs)	H_2 peak (3 hrs)	[H_2] / mol (15 mins)	[H_2] / mol (30 mins)	[H_2] / mol (1 hrs)	[H_2] / mol (1.5 hrs)	[H_2] / mol (2 hrs)	[H_2] / mol (3 hrs)
PC2 (Light)	-0.5	pH 6.6 $NaHCO_3$ (with argon)	0.0345	3.58×10^{-7}	60	76	80	65	51	38	3.49×10^{-10}	4.43×10^{-10}	4.66×10^{-10}	3.78×10^{-10}	2.97×10^{-10}	2.21×10^{-10}
PC2 (Dark)	-0.5	pH 6.6 $NaHCO_3$ (with argon)	0.005	5.18×10^{-8}	7	6	4	2	0	0	4.08×10^{-11}	3.49×10^{-11}	2.33×10^{-11}	1.16×10^{-11}	0	0

	Applied Potential (V)	Electrolyte	Charge (C)	Electrons (mol)	CO peak (1 hr)	CO peak (2hrs)	CO peak (3hrs)	[CO] 1 hr (mol)	[CO] 2 hrs (mol)	[CO] 3 hrs (mol)	H_2 peak (1 hr)	H_2 peak (2 hrs)	H_2 peak (3 hrs)	[H_2] / mol (1 hr)	[H_2] / mol (2 hrs)	[H_2] / mol (3 hrs)
PC3 (Light)	-0.5	pH 6.6 $NaHCO_3$ (with CO_2)	0.0934	9.68×10^{-7}	2045	1294	1502	3.22×10^{-8}	2.04×10^{-8}	2.36×10^{-8}	50	100	23	2.91×10^{-10}	5.82×10^{-10}	1.34×10^{-10}
PC3 (Light)	-0.5	pH 6.6 $NaHCO_3$	0.0765	7.93×10^{-7}	503	0	0	7.91×10^{-9}	0	0	20	0	0	1.16×10^{-10}	0	0

		(with argon)														
PC3 (Dark)	-0.5	pH 6.6 $NaHCO_3$ (with argon)	0.0423	4.38×10^{-7}	0	0	0	0	0	0	0	0	0	0	0	0
PC3 NiO (Dark)	-0.5	pH 6.6 $NaHCO_3$ (with CO_2)	0.0644	6.67×10^{-7}	0	0	0	0	0	0	0	0	0	0	0	0

	Applied Potential (V)	**Electrolyte**	**Charge (C)**	**Electrons (mol)**	**CO peak (1 hr)**	**CO peak (2hrs)**	**CO peak (3hrs)**	**[CO] 1 hr (mol)**	**[CO] 2 hrs (mol)**	**[CO] 3 hrs (mol)**	**H_2 peak (1 hr)**	**H_2 peak (2 hrs)**	**H_2 peak (3 hrs)**	**[H_2] / mol (1 hr)**	**[H_2] / mol (2 hrs)**	**[H_2] / mol (3 hrs)**
NiO Blank Film (Light)	-0.5	pH 6.6 $NaHCO_3$ (with CO_2)	0.0171	1.77×10^{-7}	0	0	0	0	0	0	0	0	0	0	0	0
NiO Blank Film (Dark)	-0.5	pH 6.6 $NaHCO_3$ (with CO_2)	N/A	-	0	0	0	0	0	0	0	0	0	0	0	0

Table S4. Matrix of GC experiments with the photocatalysts in 50 µM pH 6.6 $NaHCO_3$ solution. All light experiments are under simulated 1 sun AM 1.5 light (100 mW cm^{-2}).

	Applied Potential (V) vs Ag/AgCl	**Electrolyte**	**Charge (C)**	**Electrons (mol)**	**CO peak (1 hr)**	**CO peak (2 hrs)**	**CO peak (3 hrs)**	**[CO] 1 hr (mol)**	**[CO] 2 hrs (mol)**	**[CO] 3 hrs (mol)**	**H_2 peak (1hr)**	**H_2 peak (2 hrs)**	**H_2 peak (3 hrs)**	**[H_2] / mol (1 hr)**	**[H_2] / mol (2 hrs)**	**[H_2] / mol (3 hrs)**
PC1 (Light)	-0.5	pH 8 (with CO_2)	0.0350	3.63×10^{-7}	0	5023	6941	0	8.09×10^{-8}	1.12×10^{-7}	63	259	279	3.61×10^{-10}	1.48×10^{-9}	1.60×10^{-9}
PC1 (Light)	-0.5	pH 8 (with argon)	0.0237	2.46×10^{-7}	0	0	0	0	0	0	89	0	0	5.09×10^{-10}	0	0
PC1 (Dark)	-0.5	pH 8 (with CO_2)	0.0136	1.41×10^{-7}	187	0	451	3.01×10^{-9}	0	7.26×10^{-9}	0	0	0	0	0	0

	Applied Potential (V)	**Electrolyte**	**Charge (C)**	**Electrons (mol)**	**H_2 peak (15 mins)**	**H_2 peak (30 mins)**	**H_2 peak (1 hrs)**	**H_2 peak (1.5 hrs)**	**H_2 peak (2 hrs)**	**[H_2] / mol (15 mins)**	**[H_2] / mol (30 mins)**	**[H_2] / mol (1 hrs)**	**[H_2] / mol (1.5 hrs)**	**[H_2] / mol (2 hrs)**		

PC2 (Light)	-0.5	pH 8 (with argon)	0.2300	2.39×10^{-6}	28	38	31	35	25	3.10×10^{-10}	4.21×10^{-10}	3.44×10^{-10}	3.88×10^{-10}	2.77×10^{-10}		
PC2 (Dark)	-0.5	pH 8 (with argon)	0.0234	2.43×10^{-7}	3	5	0	0	0	negligible	-	-	-	-		

	Applied Potential (V) vs Ag/AgCl	**Electrolyte**	**Charge (C)**	**Electrons (mol)**	**CO peak (1 hr)**	**CO peak (2 hrs)**	**CO peak (3 hrs)**	**[CO] 1 hr (mol)**	**[CO] 2 hrs (mol)**	**[CO] 3 hrs (mol)**	**H_2 peak (1 hr)**	**H_2 peak (2 hrs)**	**H_2 peak (3 hrs)**	**[H_2] / mol (1 hr)**	**[H_2] / mol (2 hrs)**	**[H_2] / mol (3 hrs)**
PC3 (Light)	-0.5	pH 8 (with CO_2)	0.0383	3.70×10^{-7}	1106	3481	3457	1.78×10^{-8}	5.61×10^{-8}	5.57×10^{-8}	170	402	275	9.73×10^{-10}	2.31×10^{-9}	1.57×10^{-9}
PC3 (Dark)	-0.5	pH 8 (with CO_2)	0.0108	1.12×10^{-7}	0	0	0	0	0	0	0	0	0	0	0	0
PC3 (Light)	-0.5	pH 8 (with argon)	0.0293	3.04×10^{-7}	186	50	0	3.00×10^{-9}	8.05×10^{-10}	0	0	0	0	0	0	0
PC3 (Dark)	-0.5	pH 8 (with argon)	0.0093	9.63×10^{-8}	0	0	0	0	0	0	0	0	0	0	0	0

NiO Blank Film (Light)	-0.5	pH 8 (with CO_2)	0.0270	2.80×10^{-7}	0	0	0	0	0	0
NiO Blank Film (Dark)	-0.5	pH 8 (with CO_2)	N/A	N/A	-	-	-	-	-	-

Table S5. Matrix of GC experiments with the photocatalysts in 0.1 M pH 8 phosphate buffer. All light experiments are under simulated 1 sun AM 1.5 light (100 mW cm^{-2}).

	Applied Potential (V) vs Ag/AgCl	**Electrolyte**	**Charge (C)**	**Electrons (mol)**	**CO peak (1 hr)**	**CO peak (2hrs)**	**CO peak (3hrs)**	**[CO] 1 hr (mol)**	**[CO] 2 hrs (mol)**	**[CO] 3 hrs (mol)**	**H_2 peak (1hr)**	**H_2 peak (2hrs)**	**H_2 peak (3hrs)**	**[H_2] / mol (1hr)**	**[H_2] / mol (2hrs)**	**[H_2] / mol (3hrs)**
PC1 (Light)	-0.5	pH 9.2 (with CO_2)	0.0329	3.41×10^{-7}	5010	7035	9277	8.01×10^{-8}	1.1×10^{-7}	1.48×10^{-7}	87	253	256	5.25×10^{-10}	1.53×10^{-9}	1.54×10^{-9}
PC1 (Light)	-0.5	pH 9.2 (with argon)	0.0256	2.65×10^{-7}	416	0	0	6.65×10^{-8}	0	0	0	0	0	0	0	0

PC1 (Dark)	-0.5	pH 9.2 (with CO_2)	0.0092	9.52×10^{-8}	369	**0**	0	5.90×10^{-8}	0	0	0	0	0	0	0	0

	Applied Potential (V)	**Electrolyte**	**Charge (C)**	**Electrons (mol)**	**H_2 peak (15 mins)**	**H_2 peak (30 mins)**	**H_2 peak (1 hrs)**	**H_2 peak (1.5 hrs)**	**H_2 peak (2 hrs)**	**$[H_2]$ / mol (15 mins)**	**$[H_2]$ / mol (30 mins)**	**$[H_2]$ / mol (1 hrs)**	**$[H_2]$ / mol (1.5 hrs)**	**$[H_2]$ / mol (2 hrs)**		
PC2 (Light)	-0.5	pH 9.2 (with argon)	0.0120	1.24×10^{-7}	50	42	40	37	29	5.54×10^{-10}	4.66×10^{-10}	4.43×10^{-10}	4.10×10^{-10}	3.21×10^{-10}		
PC2 (Dark)	-0.5	pH 9.2 (with argon)	0.0070	7.25×10^{-8}	2	7	4	0	0	Negligible	-	-	-	-		

	Applied Potential (V) vs Ag/AgCl	**Electrolyte**	**Charge (C)**	**Electrons (mol)**	**CO peak (1 hr)**	**CO peak (2 hrs)**	**CO peak (3 hrs)**	**[CO] 1 hr (mol)**	**[CO] 2 hrs (mol)**	**[CO] 3 hrs (mol)**	**H_2 peak (1 hr)**	**H_2 peak (2 hrs)**	**H_2 peak (3 hrs)**	**$[H_2]$ / mol (1 hr)**	**$[H_2]$ / mol (2 hrs)**	**$[H_2]$ / mol (3 hrs)**
PC3 (Light)	-0.5	pH 9.2 (with CO_2)	0.0460	4.77×10^{-7}	2649	5515	7108	4.23×10^{-8}	8.8×10^{-8}	1.14×10^{-7}	136	218	301	8.2×10^{-10}	1.31×10^{-9}	1.81×10^{-9}
PC3 (Dark)	-0.5	pH 9.2 (with CO_2)	0.0200	2.17E x 10^{-7}	0	0	0	0	0	0	0	0	0	0	0	0
PC3 (Light)	-0.5	pH 9.2 (with argon)	0.0207	2.157E x 10^{-7}	76	0	0	0	0	1.22×10^{-9}	0	0	0	0	0	0
PC3 (Dark)	-0.5	pH 9.2 (with argon)	0.0080	8.29E x 10^{-8}	0	0	0	0	0	0	0	0	0	0	0	0

NiO Blank (Light)	-0.5	pH 9.2 (with CO_2)	0.0210	2.18E x 10^{-7}	157	0	0	2.51 x 10^{-9}	0	0
NiO Blank (Dark)	-0.5	pH 9.2 (with CO_2)	N/A	N/A	-	-	-	-	-	-

Table S6. Matrix of GC experiments with the photocatalysts in 0.1 M pH 9.2 carbonate buffer. All light experiments are under simulated 1 sun AM 1.5 light (100 mW cm^{-2}).

	PC1 (under CO_2)	PC2 (under Ar)	PC3 (under CO_2)
η_{Far}/% (CO)	91	-	39
η_{Far}/% (H_2)	2.0	0.24	1.7
[CO]/μmol h^{-1} cm^{-2}	0.1 (± 0.011)	-	0.038 (±0.003)
[H_2]/nmol h^{-1} cm^{-2}	4.3 (± 0.473)	0.95 (± 0.0475)	3.2 (±0.256)
TOF (CO) h^{-1}	1.8	-	0.8
TON (H_2) h^{-1}	0.08	0.007	0.07

Table S7. Faradaic efficiencies (η_{Far}/%), and turnovers per hour per catalytic centre (TOF) for CO and H_2 production during photoelectrocatalysis for the photocatalysts in 0.1 M pH 5 acetate buffer under 1 sun AM1.5 illumination (100 mW cm^{-2}). The applied bias to these systems was -0.5 V vs Ag/AgCl.

	PC1 (under CO_2)	PC2 (under Ar)	PC3 (under CO_2)
η_{Far}/% (CO)	30	-	4.9
η_{Far}/% (H_2)	nil	<0.1	<0.1
[CO]/μmol h^{-1} cm^{-2}	0.035 (± 0.0031)	-	0.01 (± 0.00145)
[H_2]/nmol h^{-1} cm^{-2}	Nil	Very low	Very low
TOF (CO) h^{-1}	0.63	Nil	0.21
TOF (H_2) h^{-1}	Nil	Nil	Nil

Table S8. Faradaic efficiencies (η_{Far}/%), and turnovers per catalyst per hour (TOF) for CO and H_2 production during photoelectrocatalysis for the photocatalysts in 50 μM pH 6.6 $NaHCO_3$ solution under 1 sun AM1.5 illumination (100 mW cm^{-2}). The applied bias to these systems was -0.5 V vs Ag/AgCl.

	PC1 (under CO_2)	PC2 (under Ar)	PC3 (under CO_2)
η_{Far}/% (CO)	61.6	-	28.1
η_{Far}/% (H_2)	0.44	<0.1	0.4
[CO]/μmol h^{-1} cm^{-2}	0.047 (± 0.0042)	-	0.024 (± 0.0028)
[H_2]/nmol h^{-1} cm^{-2}	0.67 (± 0.060)	0.18 (± 0.014)	0.66 (± 0.079)
TOF (CO) h^{-1}	0.86	-	0.50
TOF (H_2) h^{-1}	0.013	0.003	0.013

Table S9. Faradaic efficiencies (η_{Far}/%), and turnovers per catalyst per hour (TOF) for CO and H_2 production during photoelectrocatalysis for the photocatalysts in 0.1 M pH 8 phosphate buffer under 1 sun AM1.5 illumination (100 mW cm^{-2}). The applied bias to these systems was -0.5 V vs Ag/AgCl.

	PC1 (under CO_2)	PC2 (under Ar)	PC3 (under CO_2)
η_{Far}/% (CO)	87.0	-	47.6
η_{Far}/% (H_2)	0.45	0.2	0.38
[CO_2]/µmol h^{-1} cm^{-2}	0.062 (± 0.080)	-	0.048 (± 0.004)
[H_2]/nmol h^{-1} cm^{-2}	0.065 (± 0.008)	0.2 (± 0.018)	0.077 (± 0.006)
TOF (CO) h^{-1}	1.14	-	1.02
TOF (H_2) h^{-1}	0.013	0.003	0.017

Table S10. Faradaic efficiencies (η_{Far}/%), and turnovers per catalyst per hour (TOF) for CO and H_2 production during photoelectrocatalysis for the photocatalysts in 0.1 M pH 9.2 carbonate buffer under 1 sun AM1.5 illumination (100 mW cm^{-2}). The applied bias to these systems was -0.5 V vs Ag/AgCl.

Calibration of Gas Chromatography Measurements

The main gaseous products of interest in this study were carbon monoxide and hydrogen. Calibration of the gas chromatograph's flame ionization detector (FID) and thermal conductivity detector (TCD) was accomplished by dosing known mixtures of a certified standard gas (BOC) containing 5,000 ppm propylene, 5,000 ppm methane, 5,000 ppm ethylene, 5,000 ppm methane, 10,000 ppm carbon monoxide, 10,000 ppm hydrogen and the balance carbon dioxide.

Calibration was done by taking the glass reaction cell described in earlier in the manuscript and injecting known amounts of the standard gas into the headspace with each electrolyte present. The gas is allowed to equilibrate for 5 mins, then a headspace sample of 0.5 ml is withdrawn as one would do during the photoelectrocatalysis experiments.

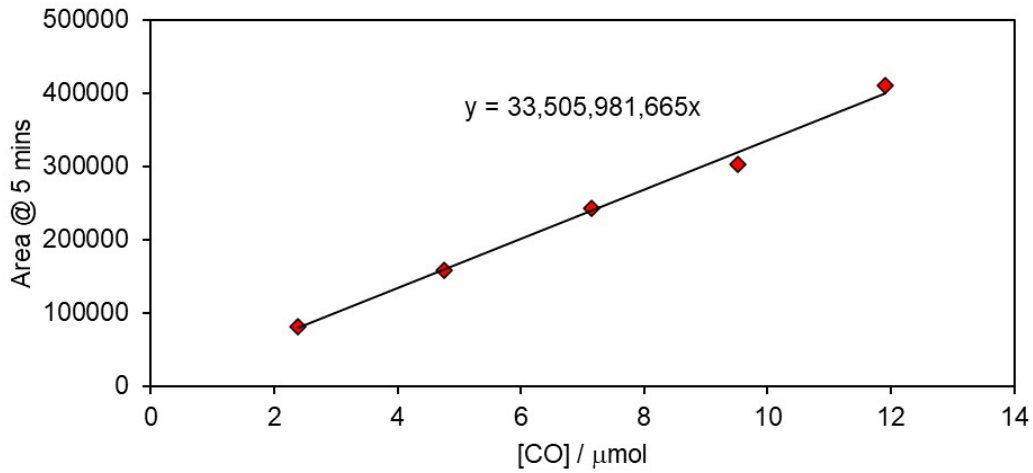

Figure S 87. Calibration chart for carbon monoxide concentration measured by gas chromatography using a flame ionization detector. Sampling was from the PEC cell headspace containing pH 5 acetate buffer.

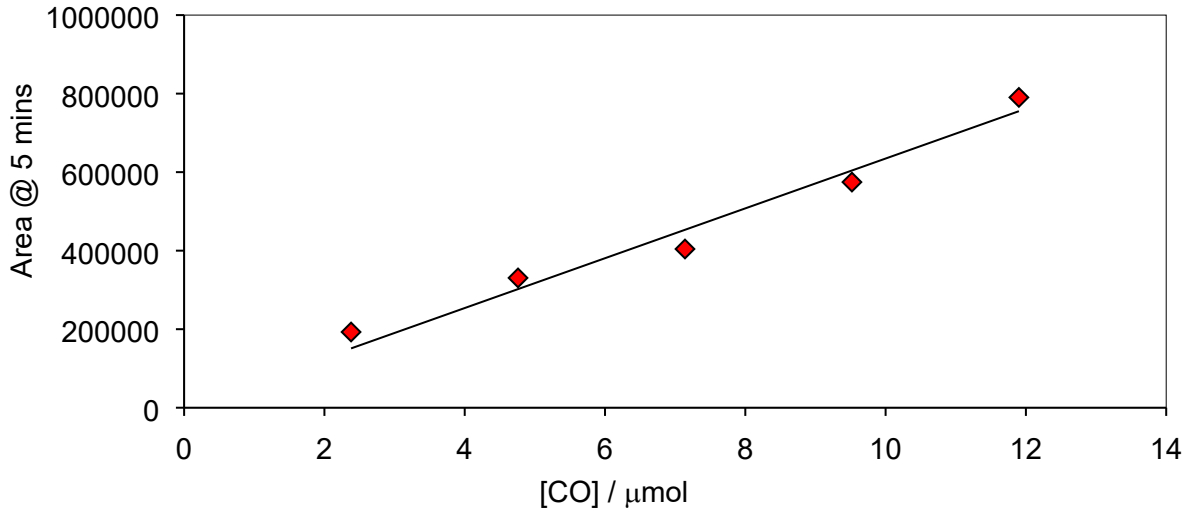

Figure S 88. Calibration chart for carbon monoxide concentration measured by gas chromatography using a flame ionization detector. Sampling was from the PEC cell headspace containing 50 μM pH 6.6 $NaHCO_3$ solution.

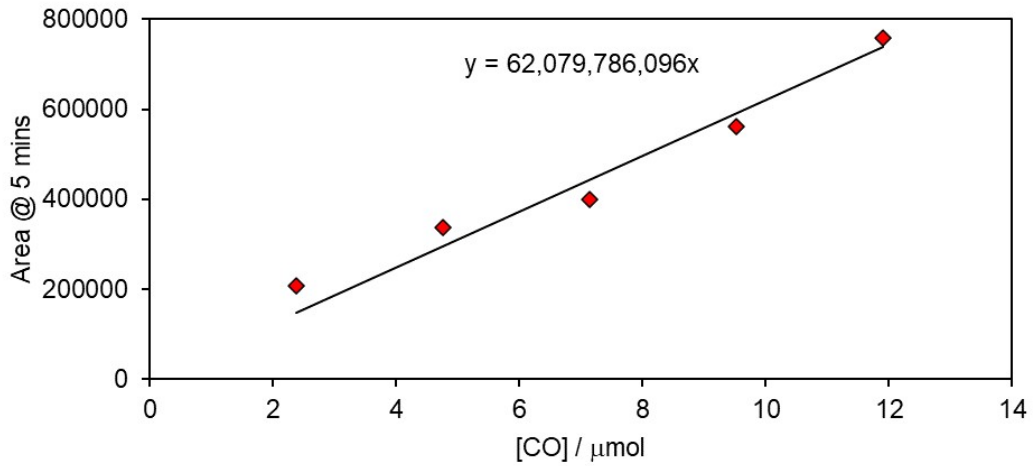

Figure S 89. Calibration chart for carbon monoxide concentration measured by gas chromatography using a flame ionization detector. Sampling was from the PEC cell headspace containing pH 8 phosphate buffer.

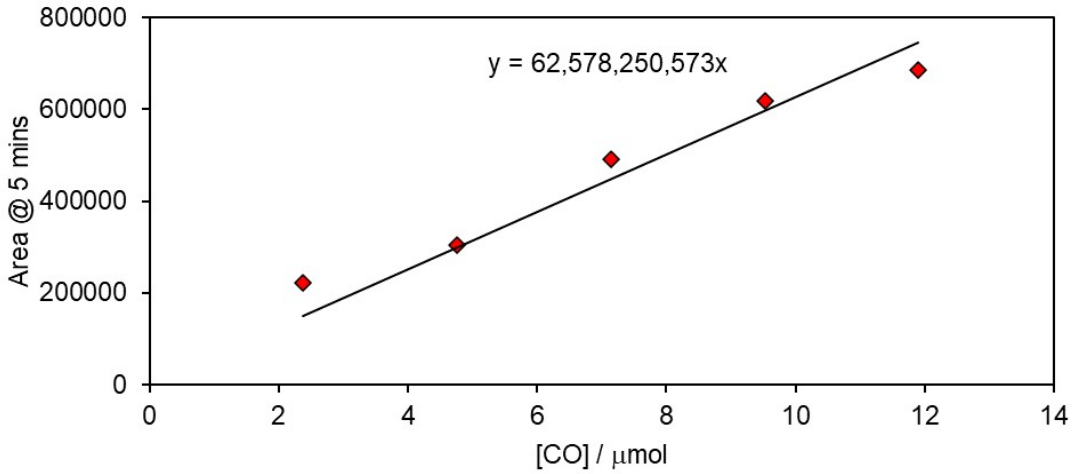

Figure S 90. Calibration chart for carbon monoxide concentration measured by gas chromatography using a flame ionization detector. Sampling was from the PEC cell headspace containing pH 9.2 carbonate buffer.

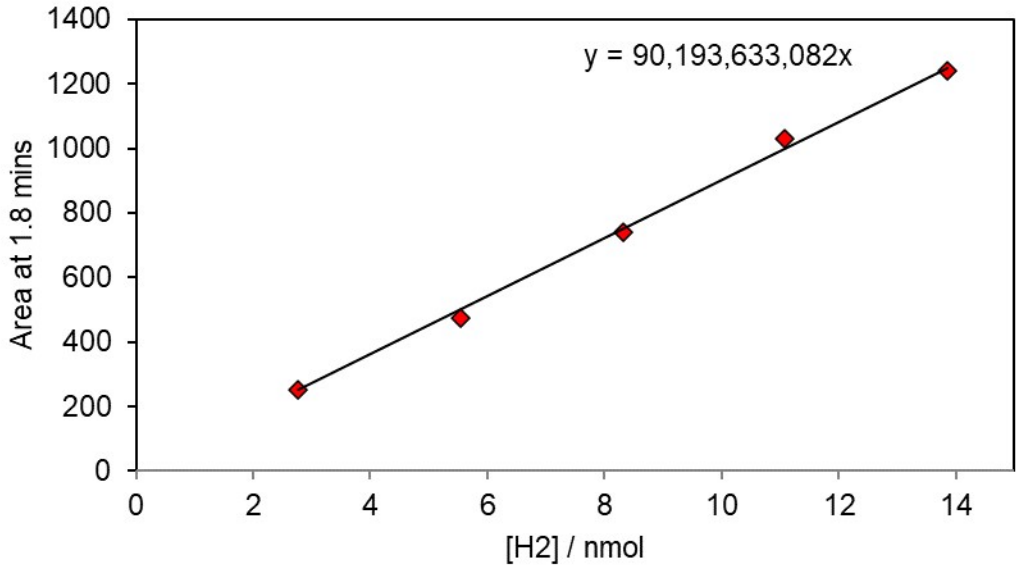

Figure S 91. Calibration chart for hydrogen concentration measured by gas chromatography using a thermal conductivity detector. Sampling was from the PEC cell headspace containing pH 5 acetate buffer.

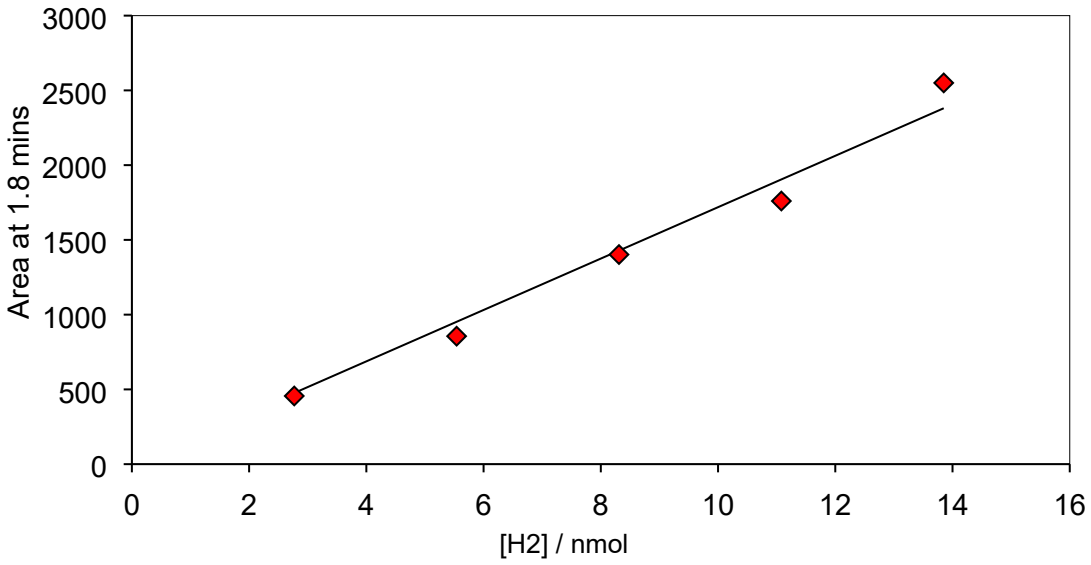

Figure S 92. Calibration chart for hydrogen concentration measured by gas chromatography using a thermal conductivity detector. Sampling was from the PEC cell headspace containing 50 μM pH 6.6 $NaHCO_3$ solution.

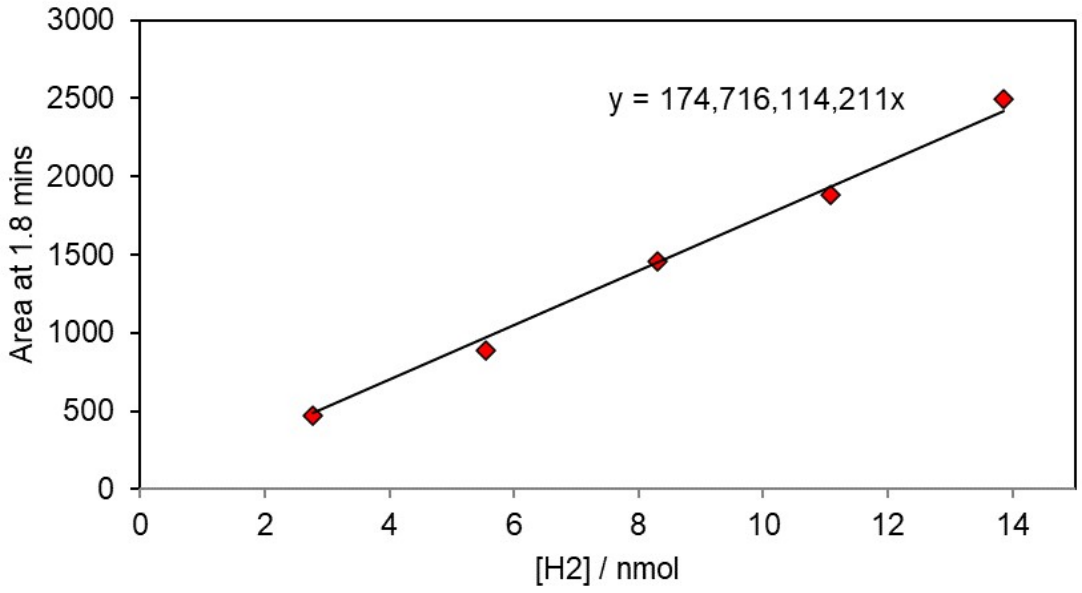

Figure S 93. Calibration chart for hydrogen concentration measured by gas chromatography using a thermal conductivity detector. Sampling was from the PEC cell headspace containing pH 8 phosphate buffer.

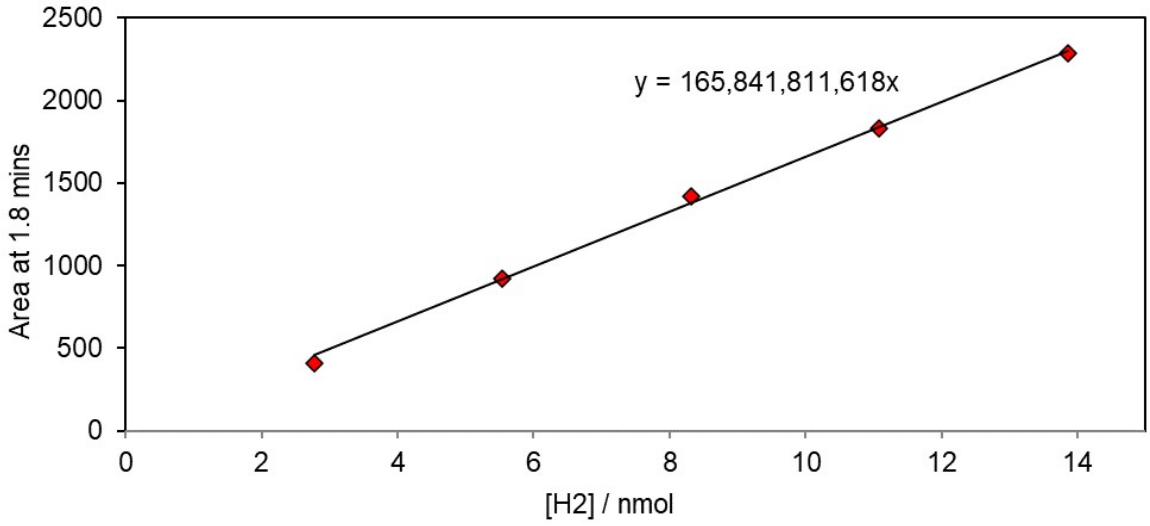

Figure S 94. Calibration chart for hydrogen concentration measured by gas chromatography using a thermal conductivity detector. Sampling was from the PEC cell headspace containing pH 9.2 carbonate buffer.

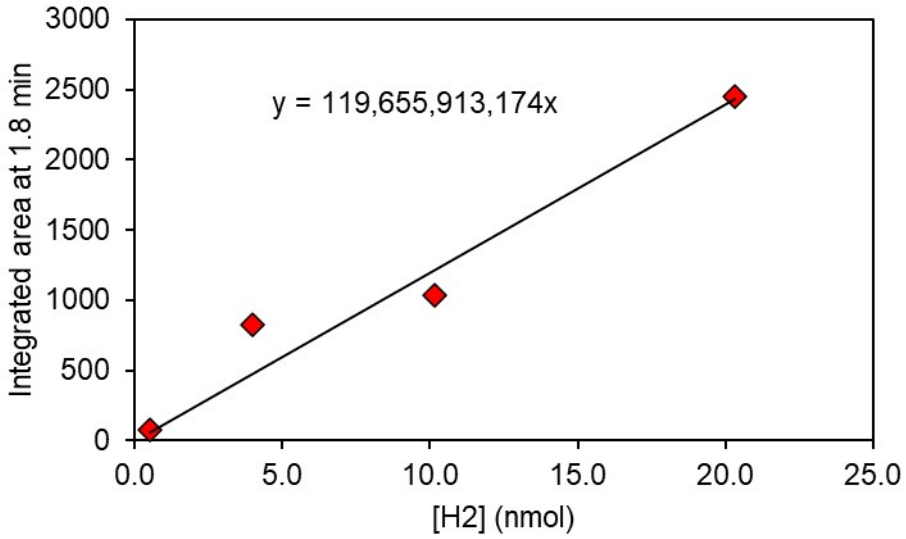

Figure S 95. Calibration chart for hydrogen concentration measured by gas chromatography using a thermal conductivity detector. Here, low concentration calibrated H_2 gas standard mixtures of H_2/N_2 were injected from a gas bag.

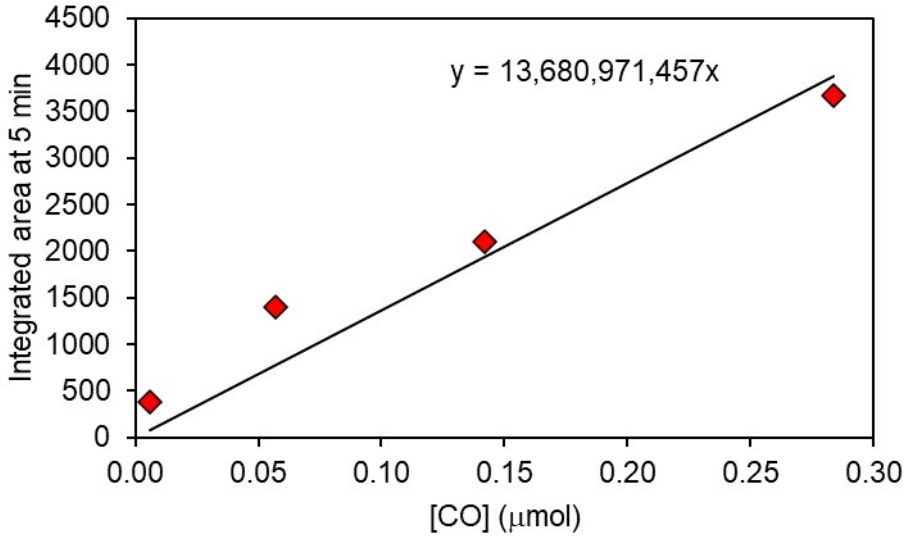

Figure S 96. Calibration chart for carbon monoxide concentrations measured by gas chromatography using a flame ionization. Here, low concentration calibrated CO gas standard mixtures of H_2/N_2 were injected from a gas bag.

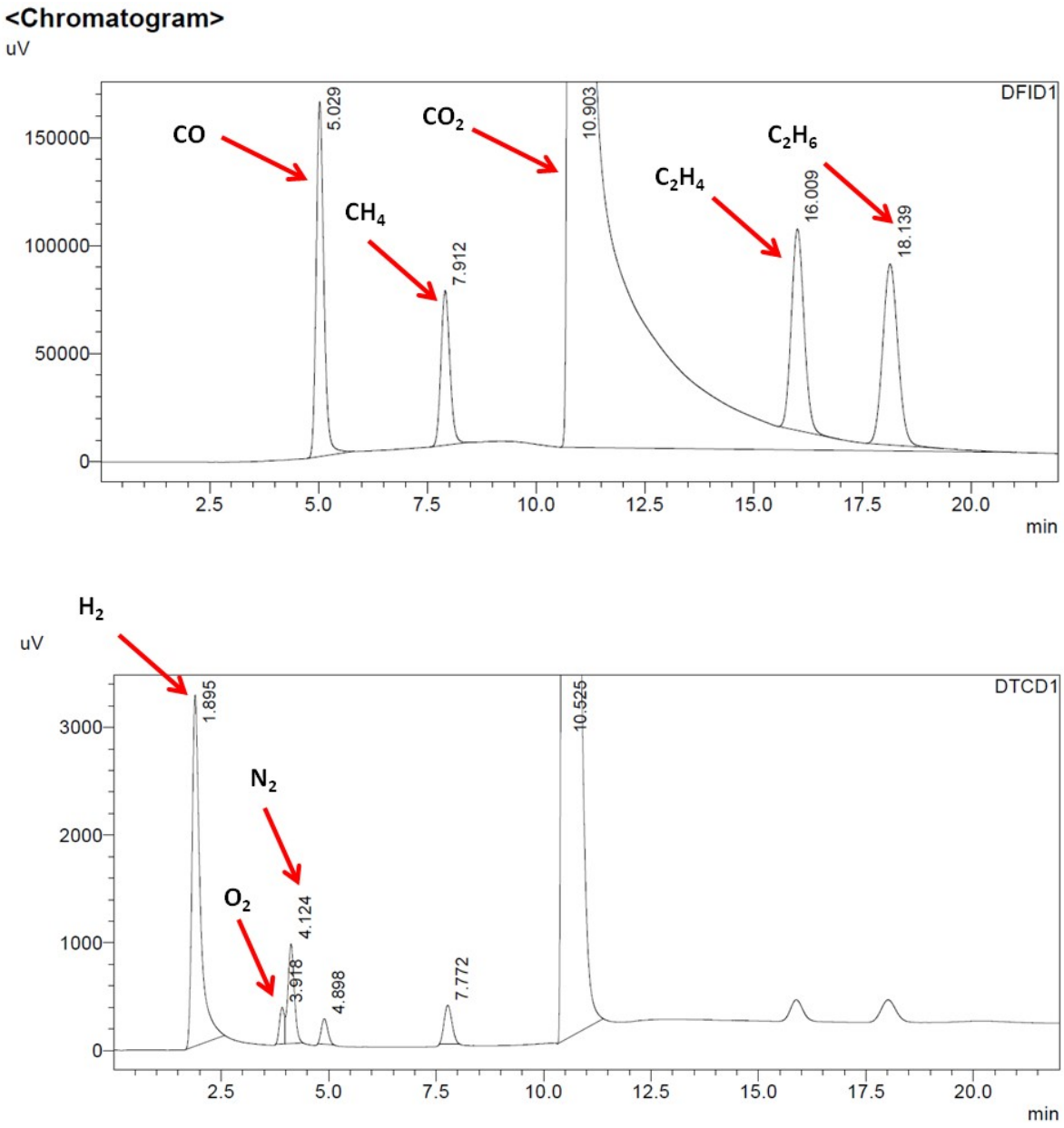

Figure S 97. Representative gas chromatogram traces from calibration of carbon monoxide from a standard mixture. The upper panel shows a trace from the flame-ionization detector, the bottom panel displays the output from the thermal conductivity detector. Major components of the gas mixture have been identified by comparing with manufacturers specifications of the column used (Restek ShinCarbon Restek ShinCarbon ST 80/100).

^{13}CO2 Isotope Labelled Gas Analysis of Products from PC1|NiO

In order to establish the true origin of carbon products evolved from the system PC1|NiO the regular CO_2 feedstock was substituted for $^{13}CO_2$, and gaseous products monitored with GC-MS analysis. The assumption was that any CO produced by photoelectrocatalysis would be isotopic ^{13}CO and other products due to degradation of the photocatalyst would be ^{12}C. The

photocatalysis experiment performed with $^{13}CO_2$, feedstock was PC1 in pH 5 acetate buffer with an applied bias of –0.5 V and –0.2 V vs Ag/AgCl. The conclusion of the data tabulated below is that there is a mixture of genuine photocatalysis and some ^{12}C due to impurities in the gas stream and potential degradation of the photocatalyst, consistent with the UV-vis and XPS studies.

GC-MS analysis details

*Instrument: Agilent 8890 GC system with 5977B GC/MSD mass spec

*Column: HP-PLOT-Q

For experiment at -0.2 V

*Injection: 400 microlitres manual injection with gas tight syringe

*Oven: 50 degrees for 2 mins then increase 10 degrees per minute to 100 degrees and hold 3 mins. Solvent delay 0.5 min.

*Inlet temp 100 degree, flow 1 ml per min, transfer line 280 degrees, injection volume 1 microlitre, carrier gas helium. SIM and scan mode used, range of mass 1.6 to 150, ions monitored 44, 45, 28, 29, 12C, 13C.

For the experiment at -0.5 V vs Ag/AgCl

*Injection: 40 microlitres manual injection with gas tight syringe

*Oven: 40 degrees for 10 mins then increase 40 degrees per minute to 120 degrees and hold 5 mins. Solvent delay 0.5 min.

*Inlet temp 100 degree, flow 1 ml per min, transfer line 230 degrees, injection volume 1 microlitre, carrier gas helium. SIM and scan mode used, range of mass 1.6 to 150, ions monitored 44, 45, 28, 29, 12C, 13C.

Note that with the above GC-MS method it was not possible to effectively separate carbon monoxide from residual air in the reaction vessel. This presents a challenge in distinguishing between N_2 in air (m/z 28), ^{12}CO (m/z 28) and ^{13}CO (m/z 29). We could not obtain clear chromatographic separation of the gases due to the column that was available. To separate the ^{13}CO from ^{12}CO and N_2 we used the extracted ion chromatogram (EIC) by plotting the intensity of the signal observed at 12, 13, 28 and 29 ions separately. To separate the ^{13}CO from ^{12}CO and nitrogen, we used an extracted ion chromatogram (EIC) and plotted the area of the signal observed at 12, 13, 28 and 29 ions separately. The main evidence that we were

producing ^{13}CO was that the area of the ^{13}CO peak increases against the ^{12}CO peak (from EIC, example below), while the portion of air was constant.

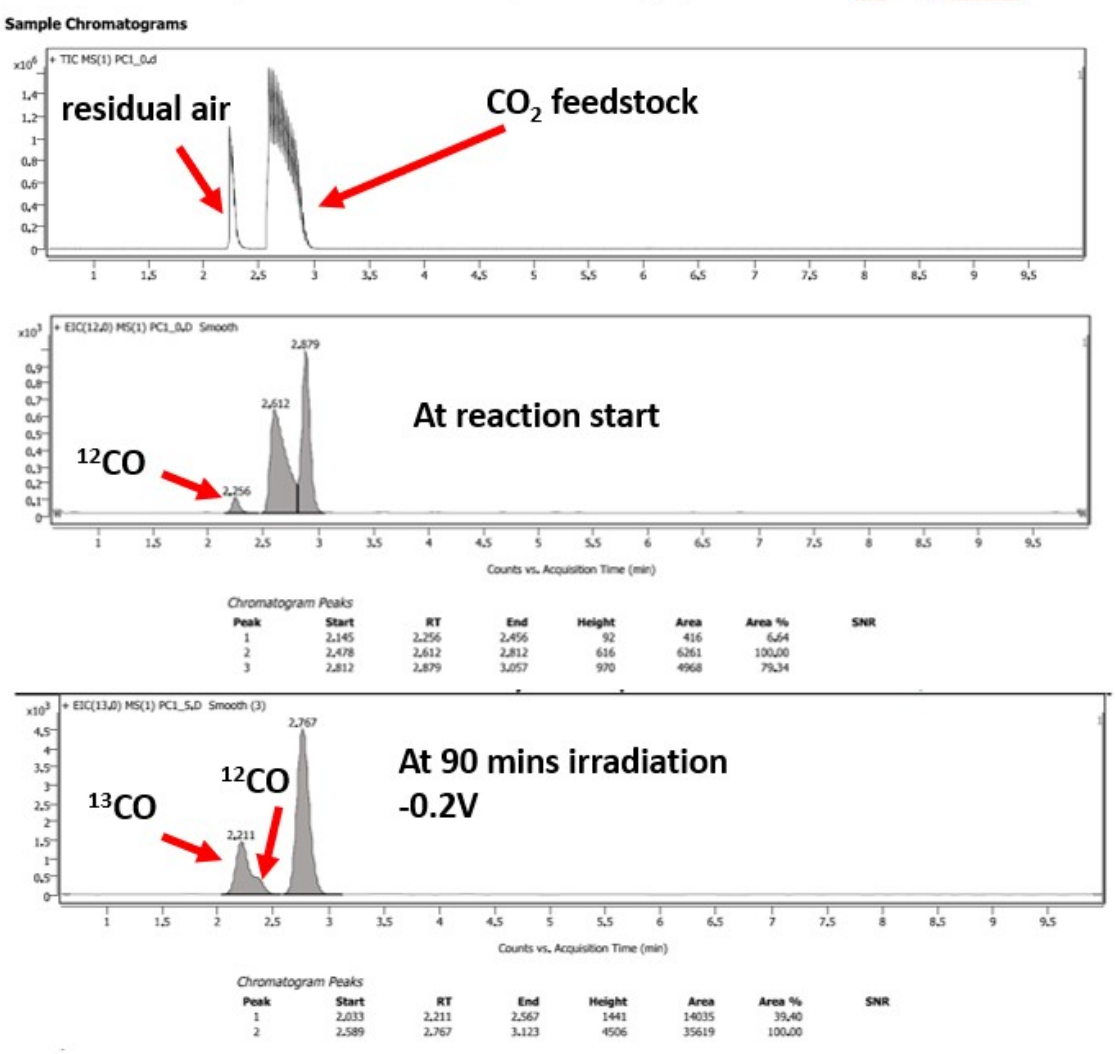

Figure S 98. Example of GC-MS Analysis PC1 @ pH 5 -0.2 V vs Ag/AgCl.

PC1 @ pH 5 -0.5 V vs Ag/AgCl	^{12}CO	^{13}CO	$^{13}CO/^{12}CO$
0 min	10905	60985	5.59
30 min	20049	96587	4.82
60 min	30799	148363	4.82
90 min	39593	81318	2.05
120 min	19980	95012	4.76

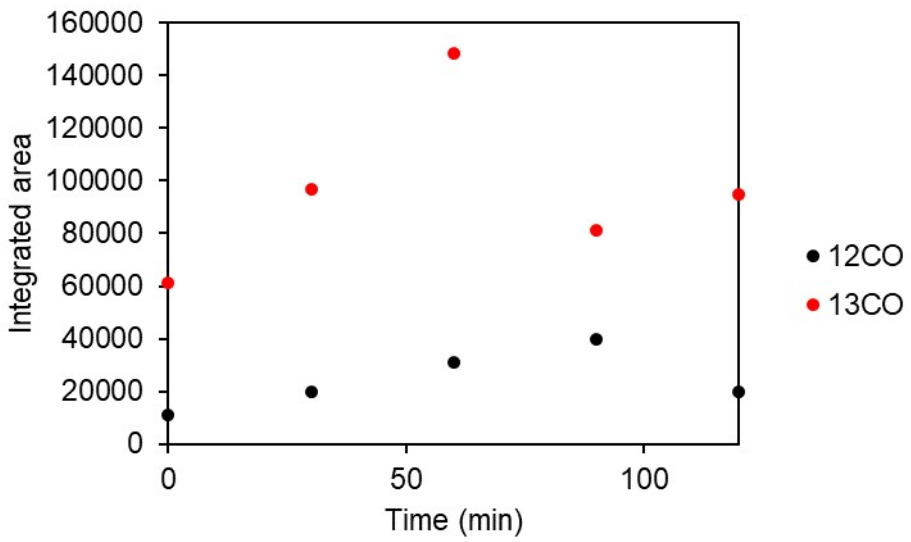

Figure S 99. Evolution of ^{13}CO vs ^{12}CO evolved from photoelectrocatalysis reaction of PC1 in pH 5 acetate buffer under 1 sun AM 1.5 irradiation and an applied external bias of –0.5 V vs Ag/AgCl as monitored by GC-MS.

PC1 @ pH 5 -0.2 V vs Ag/AgCl	**^{12}CO**	**^{13}CO**	**$^{13}CO/^{12}CO$**
0 min	415	4127	9.95
15 min	1578	6563	4.16
30 min	1934	8978	4.64
60 min	1948	9621	4.94
90 min	2665	14035	5.27
120 min	2725	9737	3.57

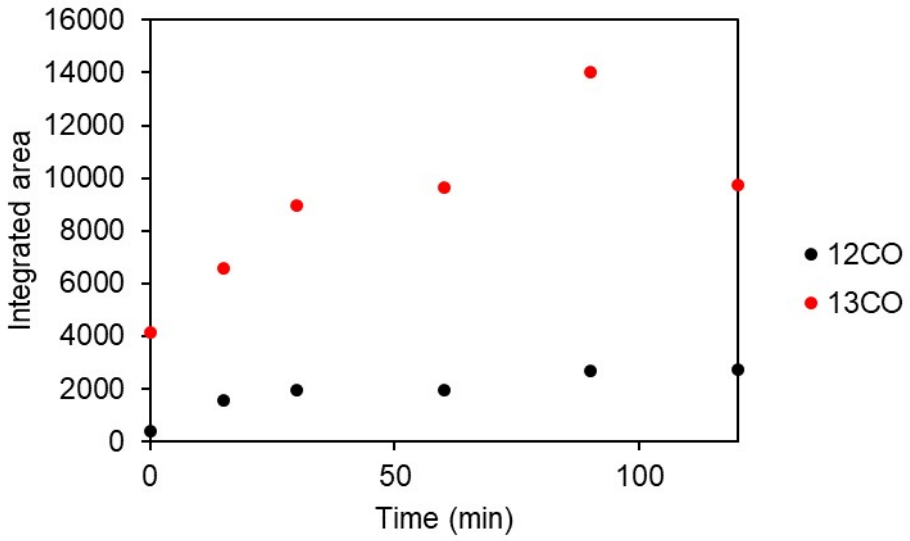

Figure S 100. Evolution of ^{13}CO vs ^{12}CO evolved from photoelectrocatalysis reaction of PC1 in pH 5 acetate buffer under 1 sun AM 1.5 irradiation and an applied external bias of –0.2 V vs Ag/AgCl as monitored by GC-MS.

PC1 @ pH 8 -0.2 V vs Ag/AgCl	**^{12}CO**	**^{13}CO**	**$^{13}CO/^{12}CO$**
0 min	238	1811	7.61
15 min	523	3405	6.51
30 min	663	4626	6.98
60 min	1024	5686	5.55
90 min	989	7225	7.30
120 min	1073	6257	5.83
180 min	1455	6287	4.32

Feedstock gas ($^{13}CO_2$)	**^{12}CO**	**^{13}CO**	**$^{13}CO/^{12}CO$**	**$^{13}CO2$**

pure				
repeat 1	3282	17430	5.31	295300000
repeat 2	2684	14410	5.37	292500000
repeat 3	2183	10351	4.74	292900000

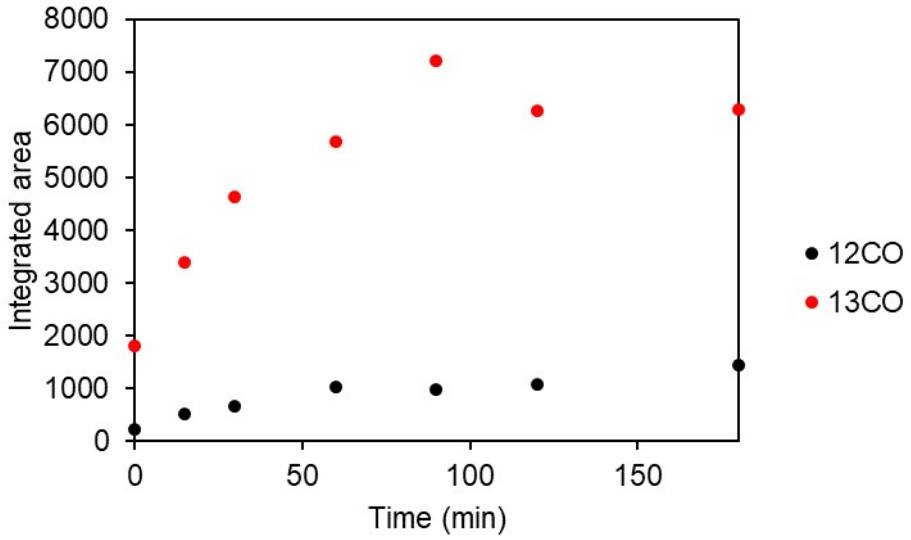

Figure S 101. Evolution of ^{13}CO vs ^{12}CO evolved from photoelectrocatalysis reaction of PC1 in pH 8 phosphate buffer under 1 sun AM 1.5 irradiation and an applied external bias of –0.2 V vs Ag/AgCl as monitored by GC-MS.

S6. X-Ray Photoelectron Spectroscopy

X-ray photoelectron spectroscopy (XPS) measurements were obtained for the photocatalysts on NiO both before and after photoelectrocatalysis experiments as described in the main manuscript. The films had been irradiated with 1 sun intensity illumination AM 1.5 light for 1000 seconds under chopped light conditions in 0.1 M pH 5 acetate buffer with an applied bias of -0.2 V vs Ag/AgCl. The adventitious carbon signal located at 284.8 eV was used to calibrate samples.

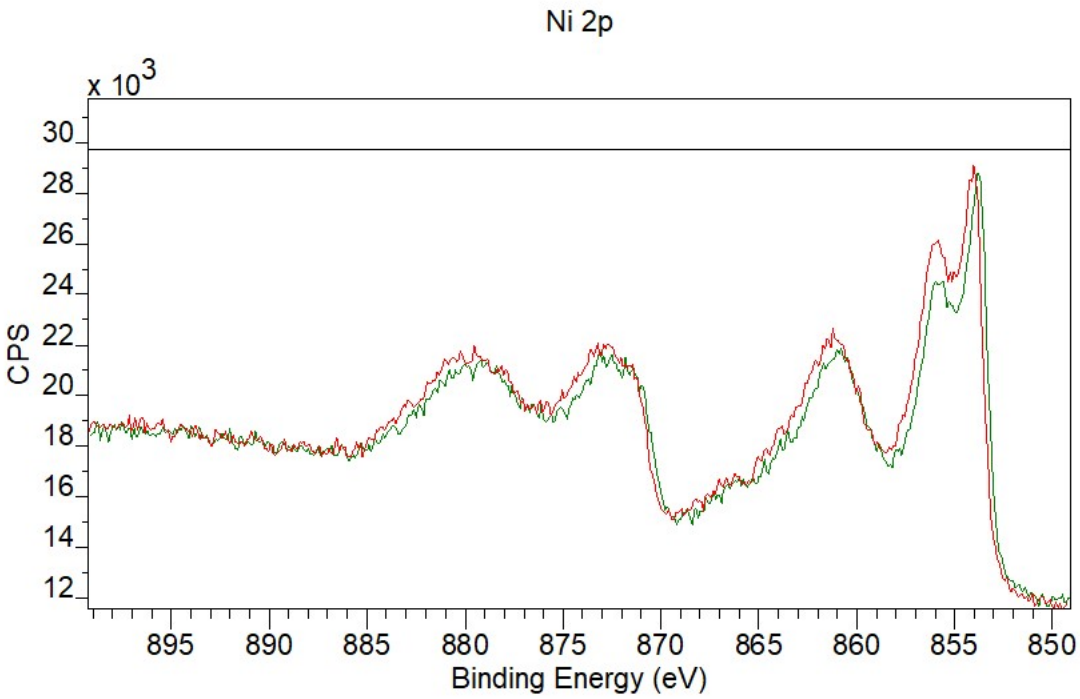

Figure S 102. Unsensitized NiO thin film nickel 2p region before photoelectrocatalysis (red trace), after photoelectrocatalysis (green trace) in 0.1 M pH 5 acetate buffer with an applied bias of -0.2 V vs Ag/AgCl under 1 sun AM 1.5, (100 mW cm^{-2}) irradiation.

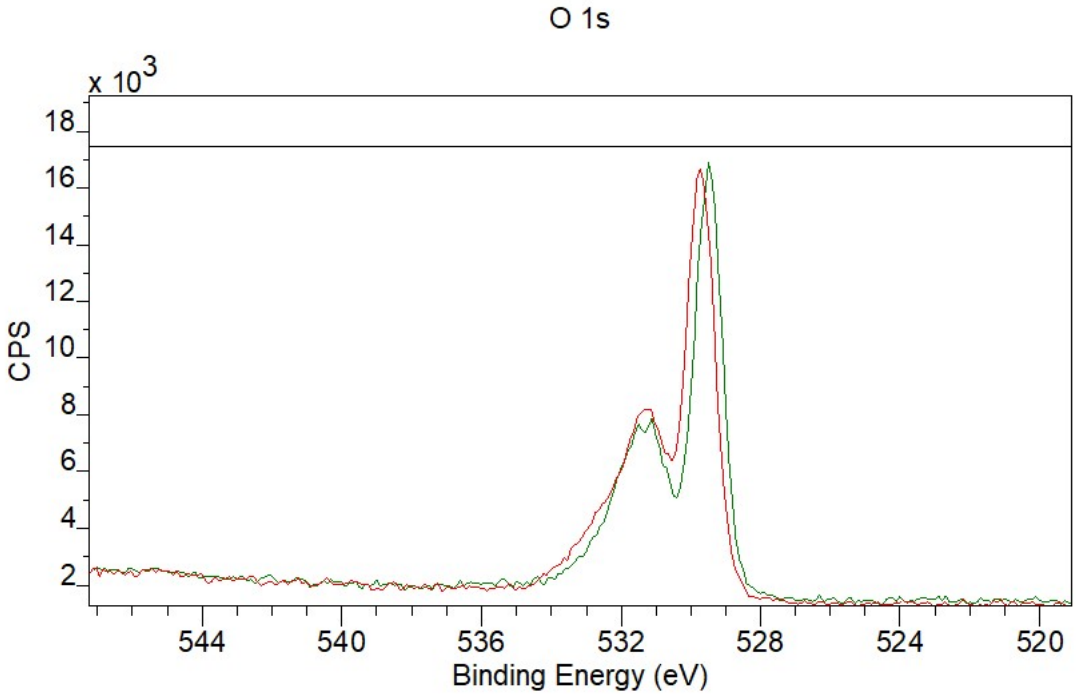

Figure S 103. Unsensitized NiO thin film oxygen 1s region before photoelectrocatalysis (red trace), after photoelectrocatalysis (green trace) in 0.1 M pH 5 acetate buffer with an applied bias of -0.2 V vs Ag/AgCl under 1 sun AM 1.5, (100 mW cm^{-2}) irradiation.

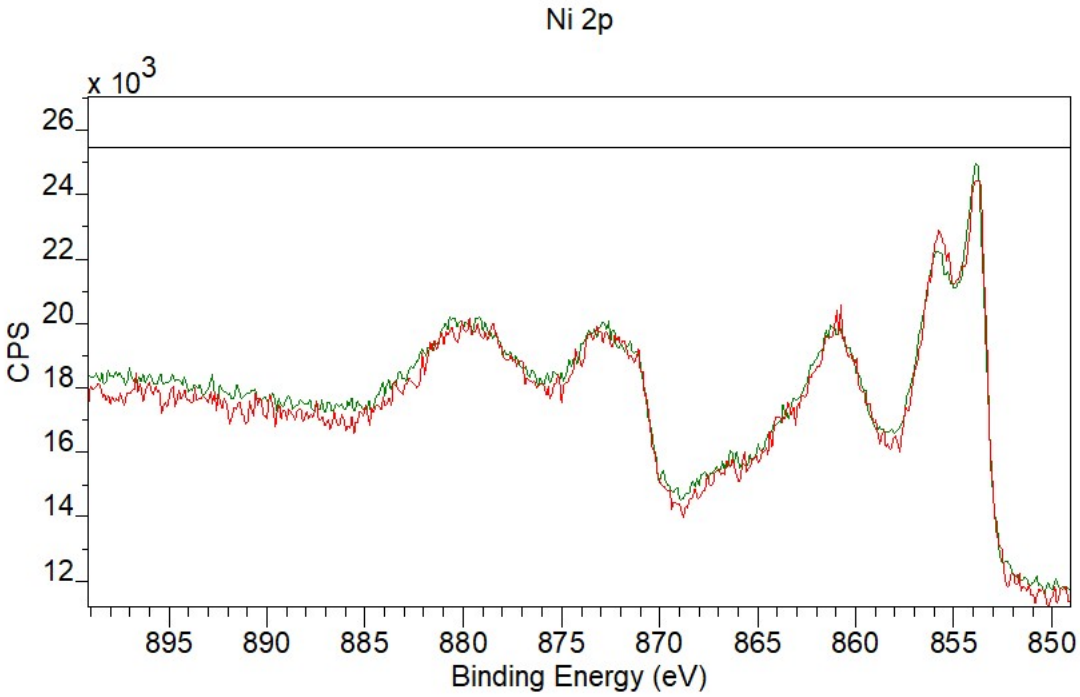

Figure S 104. PC1|NiO thin film nickel 2p region before photoelectrocatalysis (red trace), after photoelectrocatalysis (green trace) in 0.1 M pH 5 acetate buffer with an applied bias of -0.2 V vs Ag/AgCl under 1 sun AM 1.5, (100 mW cm^{-2}) irradiation.

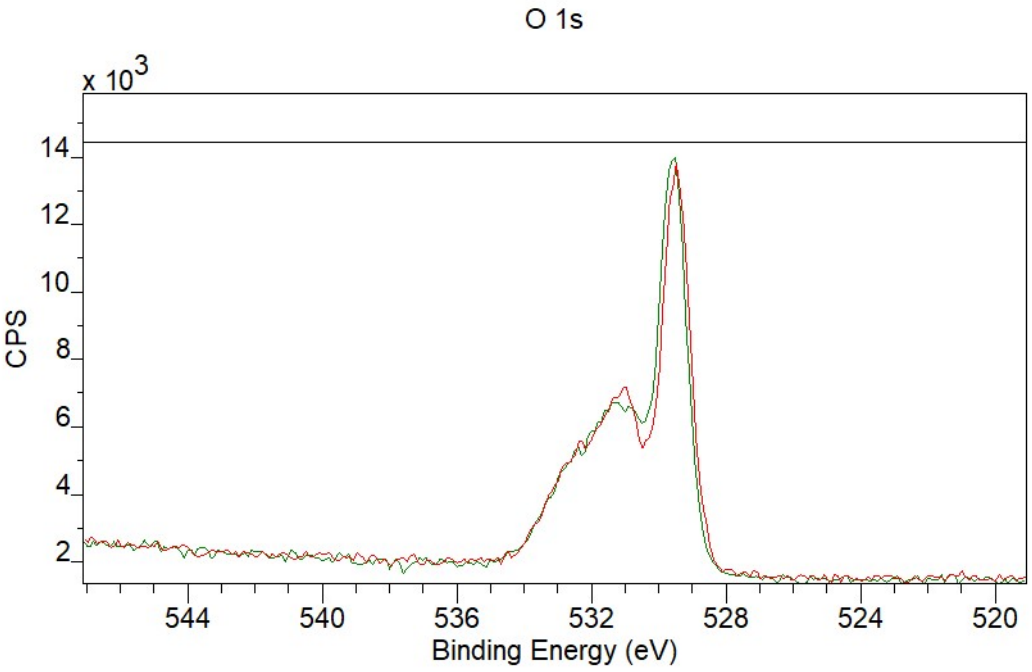

Figure S 105. PC1|NiO thin film oxygen 1s region before photoelectrocatalysis (red trace), after photoelectrocatalysis (green trace) in 0.1 M pH 5 acetate buffer with an applied bias of -0.2 V vs Ag/AgCl under 1 sun AM 1.5, (100 mW cm^{-2}) irradiation.

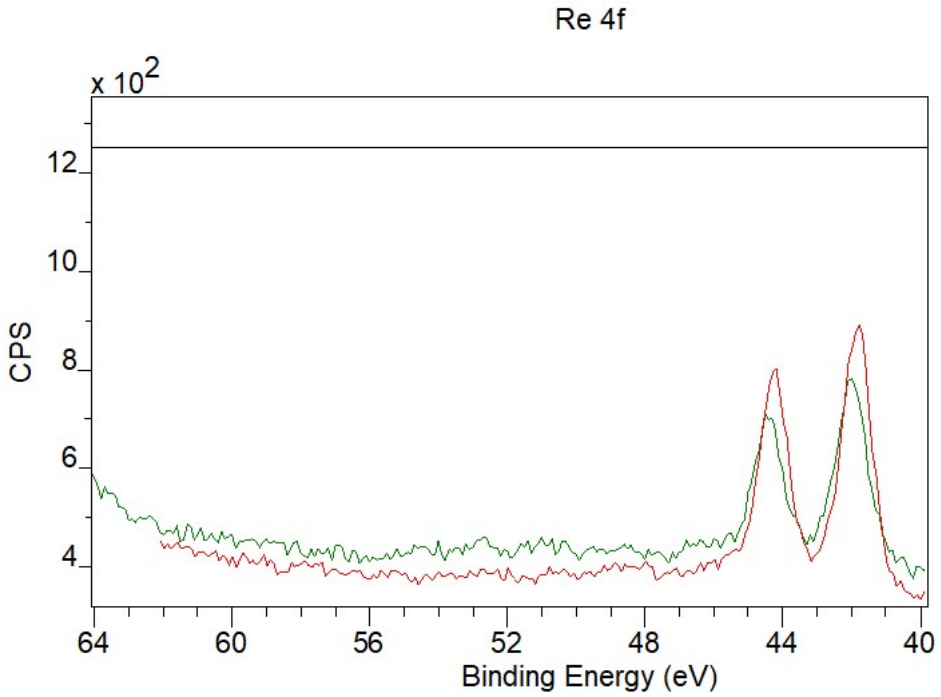

Figure S 106. PC1|NiO thin film rhenium 4f region before photoelectrocatalysis (red trace), after photoelectrocatalysis (green trace) in 0.1 M pH 5 acetate buffer with an applied bias of -0.2 V vs Ag/AgCl under 1 sun AM 1.5, (100 mW cm^{-2}) irradiation.

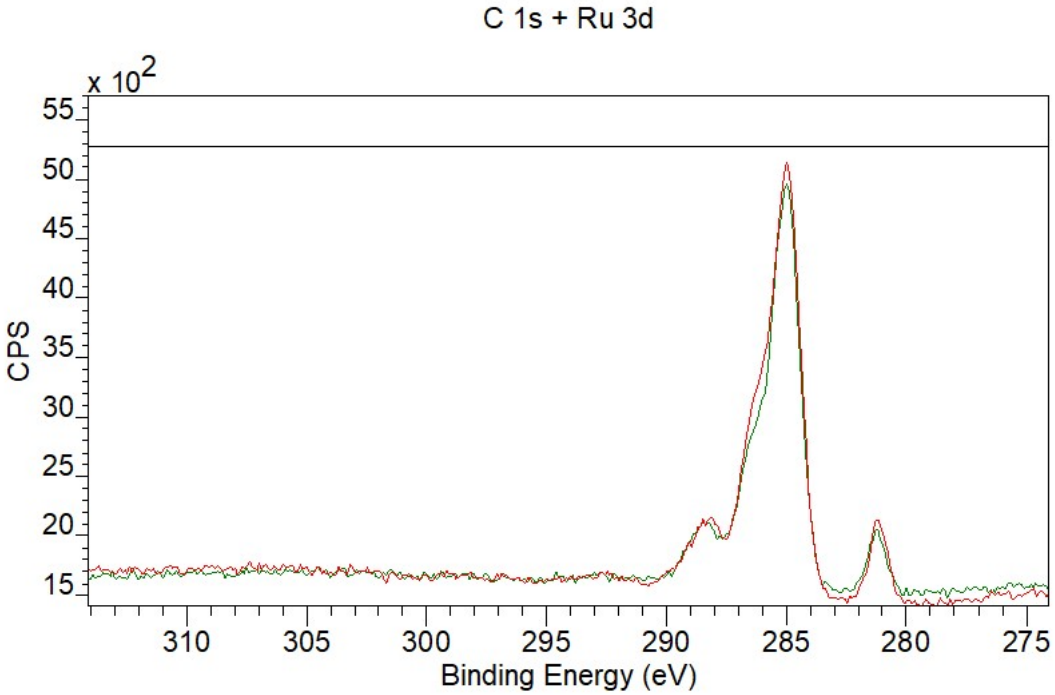

Figure S 107. PC1|NiO thin film carbon 1s and ruthenium 3d regions before photoelectrocatalysis (red trace), after photoelectrocatalysis (green trace) in 0.1 M pH 5

acetate buffer with an applied bias of -0.2 V vs Ag/AgCl under 1 sun AM 1.5, (100 mW cm^{-2}) irradiation.

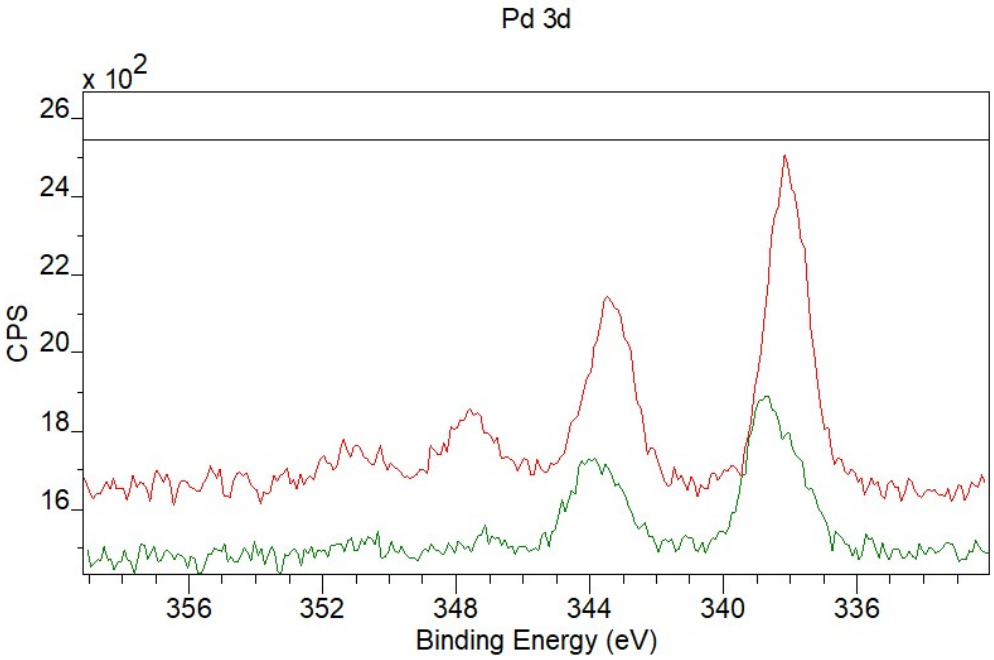

Figure S 108. PC2|NiO palladium 3d region before photoelectrocatalysis (red trace), after photoelectrocatalysis (green trace) in 0.1 M pH 5 acetate buffer with an applied bias of -0.2 V vs Ag/AgCl under 1 sun AM 1.5, (100 mW cm^{-2}) irradiation.

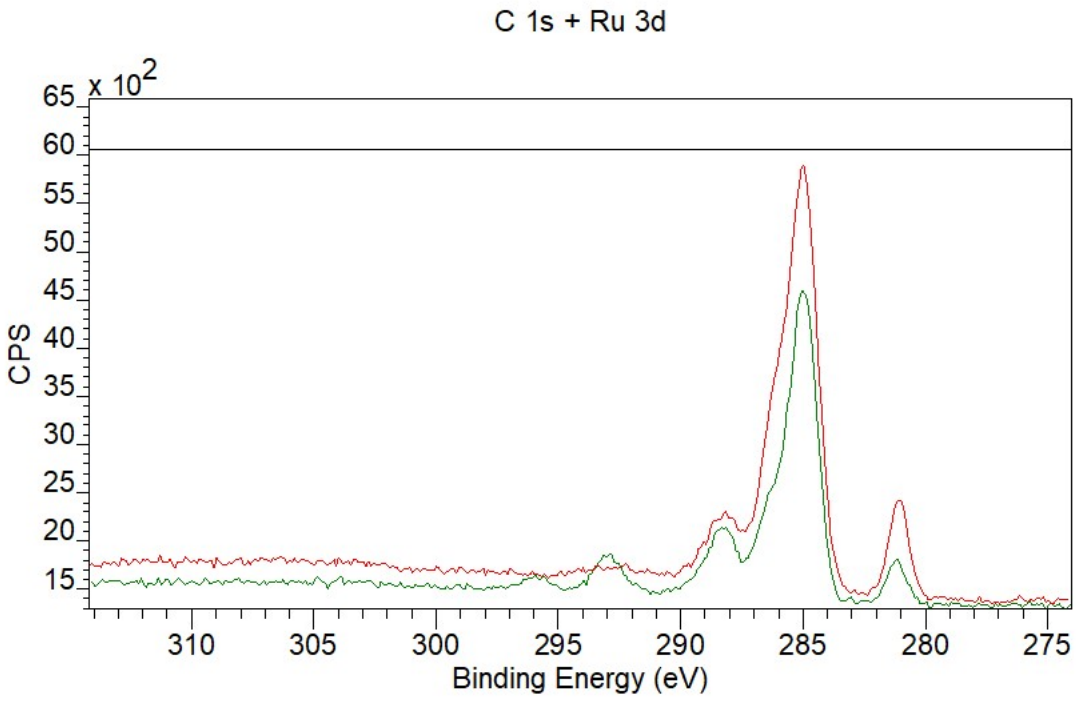

Figure S 109. PC2|NiO carbon 1s and ruthenium 3d regions before photoelectrocatalysis (red trace), after photoelectrocatalysis (green trace) in 0.1 M pH 5 acetate buffer with an applied bias of -0.2 V vs Ag/AgCl under 1 sun AM 1.5, (100 mW cm^{-2}) irradiation.

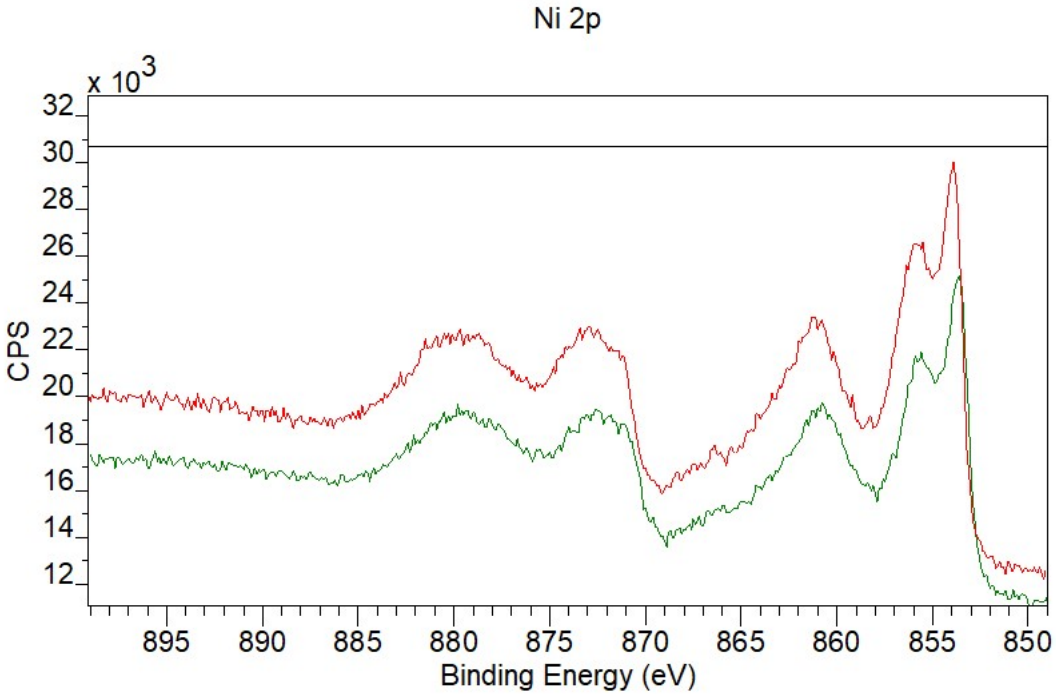

Figur

e S 110. PC2|NiO nickel 2p region before photoelectrocatalysis (red trace), after photoelectrocatalysis (green trace) in 0.1 M pH 5 acetate buffer with an applied bias of -0.2 V vs Ag/AgCl under 1 sun AM 1.5, (100 mW cm^{-2}) irradiation.

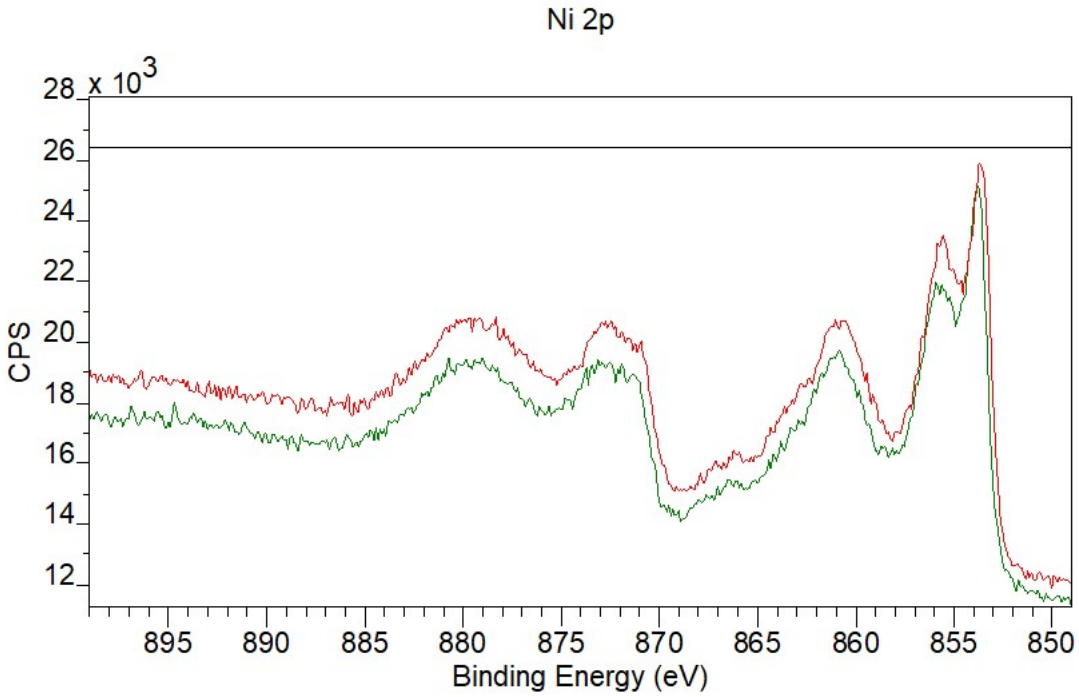

Figure S 111. PC3|NiO thin film nickel 2p region before photoelectrocatalysis (red trace), after photoelectrocatalysis (green trace) in 0.1 M pH 5 acetate buffer with an applied bias of -0.2 V vs Ag/AgCl under 1 sun AM 1.5, (100 mW cm^{-2}) irradiation.

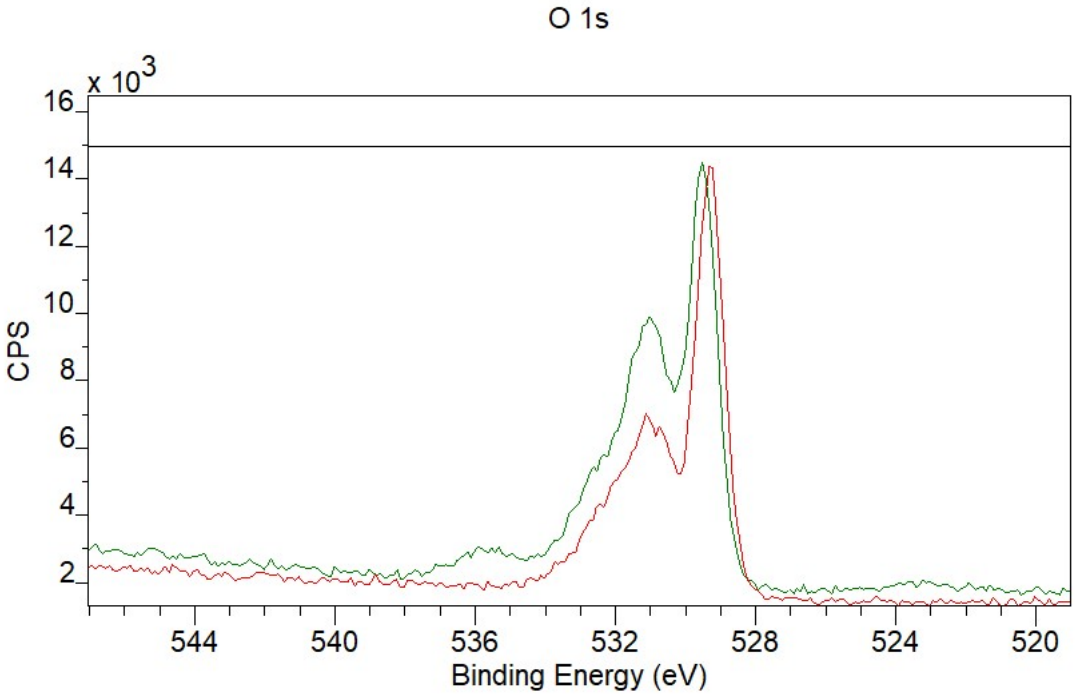

Figure S 112. PC3|NiO thin film oxygen 1s region before photoelectrocatalysis (red trace), after photoelectrocatalysis (green trace) in 0.1 M pH 5 acetate buffer with an applied bias of -0.2 V vs Ag/AgCl under 1 sun AM 1.5, (100 mW cm^{-2}) irradiation.

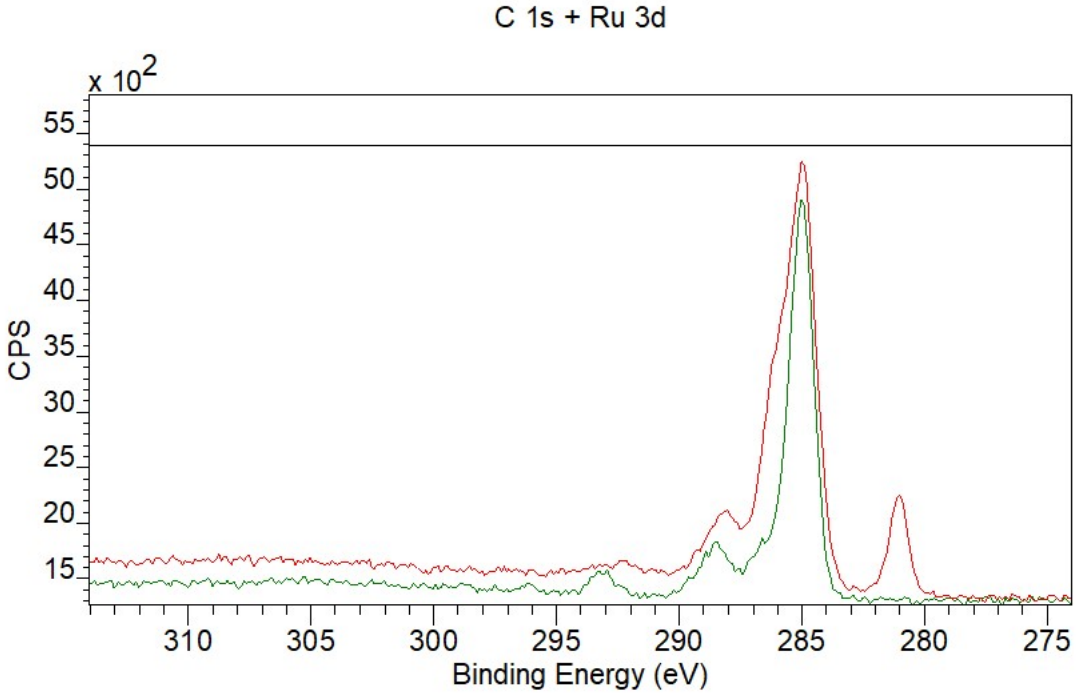

Figure S 113. PC3|NiO thin film carbon 1s and ruthenium 3d regions before photoelectrocatalysis (red trace), after photoelectrocatalysis (green trace) in 0.1 M pH 5 acetate buffer with an applied bias of -0.2 V vs Ag/AgCl under 1 sun AM 1.5, (100 mW cm^{-2}) irradiation.

References

1 J. F. Geldard and F. Lions, *J. Org. Chem.*, 1965, **30**, 318–319.

2 L. Hammarström, T. Norrby, G. Stenhagen, J. Mårtensson, B. Åkermark and M. Almgren, *Journal of Physical Chemistry B*, 1997, **101**, 7494–7504.

3 I. Bratsos and E. Alessio, in *Inorganic Syntheses*, Wiley Blackwell, 2010, vol. 35, pp. 148–163.

4 M. Toyama, T. Takizawa, I. Morita, N. Nagao, Y. Kuramochi and H. Ishida, *Chemistry - A European Journal*, 2019, **25**, 16582–16590.

5 S. Sumikura, S. Mori, S. Shimizu, H. Usami and E. Suzuki, *J Photochem Photobiol A Chem*, 2008, **199**, 1–7.

6 C. Slavov, H. Hartmann and J. Wachtveitl, *Anal Chem*, 2015, **87**, 2328–2336.